Gold Nanoparticles and Their Applications in Engineering

Edited by Safaa Najah Saud Al-Humairi

Gold Nanoparticles and Their Applications in Engineering

Edited by Safaa Najah Saud Al-Humairi

Notice

Statements and opinions expressed in the chapters are these of the individual contributors and not necessarily those of the editors or publisher. No responsibility is accepted for the accuracy of information contained in the published chapters. The publisher assumes no responsibility for any damage or injury to persons or property arising out of the use of any materials, instructions, methods or ideas contained in the book.

We are IntechOpen,
the world's leading publisher of Open Access books
Built by scientists, for scientists

6,300+
Open access books available

172,000+
International authors and editors

190M+
Downloads

156
Countries delivered to

Our authors are among the
Top 1%
most cited scientists

12.2%
Contributors from top 500 universities

CLARIVATE ANALYTICS
BOOK CITATION INDEX
INDEXED

WEB OF SCIENCE™

Selection of our books indexed in the Book Citation Index
in Web of Science™ Core Collection (BKCI)

Interested in publishing with us?
Contact book.department@intechopen.com

Numbers displayed above are based on latest data collected.
For more information visit www.intechopen.com

Meet the editor

Dr. Safaa Najah Saud Al-Humairi is a postdoctoral and Ph.D. graduate in Mechanical/Biomaterials Engineering from the University of Teknologi Malaysia. His research focuses on the design and development of novel biomaterials and their related applications. Currently, he is an associate professor and program coordinator at the Management and Science University, Shah Alam, Malaysia. Dr. Safaa is a registered professional engineer in numerous engineering associations and societies and has more than 12 years of experience in material engineering, manufacturing, and design. He is the author of more than 120 journal research articles. He has also been awarded several special, gold, silver, and bronze medals in many innovations and innovative national and international engineering and technology exhibitions. He is also an editor and reviewer for several well-known journals and publishers.

Contents

Preface

Gold Nanoparticles and Their Applications in Engineering provides an overview of recent research into gold nanoparticles (AuNPs), covering their preparation, characterization, fabrication, and potential optical and biological applications. New, exciting research in this area has attracted much attention over the past few decades, and with excellent purpose. This book discusses a variety of complex subjects related to the optical, physical, medical, and biological uses of AuNPs. The advancement of nanotechnology draws researchers' attention to synthesizing environmentally acceptable, safe, non-toxic applications that may be employed in mass production. The self-assembly of AuNPs may be obtained using these straightforward, low-cost, stable, long-lasting, and repeatable aqueous room-temperature synthesis methods. Research and development using AuNP materials in aqueous or non-aqueous phases in completely modified or unmodified states as hybrids are essential to improve their mechanical and biological applications. The innovative functional uses of AuNPs may be influenced by nanotechnology and nanoscience to control substances at the nanoscale, where they typically exist at the level of a few nanometers. This book examines methods of AuNP preparation and characterization as well as the potential applications of AuNPs worldwide.

Chapter 1 provides an introduction to AuNPs, including scientific background and potential horizons. Chapter 2 presents a strategy for enhancing gas sensitivity and chemical stability via electrode engineering. Chapter 3 discusses the global market for AuNPs and challenges in the post-pandemic economy. Chapter 4 examines the effect of gold seed layer annealing on surface roughness and nanostructure growth. Chapter 5 reviews microbial fuel cells formulated from nanocomposites. Finally, Chapter 6 presents a study of enhanced infrared absorption spectroscopy by AuNPs.

This book is ideal for advanced-level students and researchers who wish to expand their understanding of AuNPs.

Dr. Safaa Najah Saud Al-Humairi
Associate Professor,
Faculty of Information Sciences and Engineering,
Management and Science University,
Selangor, Malaysia

Introductory Chapter: Gold Nanoparticles – Scientific Background and Potential Horizons

Safaa Najah Saud Al-Humairi

1. Introduction

Gold was discovered quite early and has been studied and used for at least a few thousand years. Gold follows copper and silver in importance on the periodic table, placing it in Group 11. Because of its flexible face-centered cubic (F.C.C.) structure, gold has a metallic radius comparable to that of silver [1]. Particles of Au have a lower single-bond covalent radius compared to Ag. Gold's combination of chemical and physical properties is unique, and this is true in both its microscopic and macroscopic phases. Its macroscopic chemical stability, strong redox potential, and bright yellow color make it easily recognizable. Its electrical structure can be comprehended by applying concepts from quantum mechanics and Einstein's theory of relativity. It has been observed that the conductivity, electrical structure, reactivity, melting temperature, and mechanical properties of particles will change at the nanoscale if the particles are reduced in size to a point smaller than the minimum permissible size [2]. Nanomaterial particles (nm) are considered important because of their physical and chemical properties, and they are being studied for applications in various fields. It has the potential to revolutionize many different fields in order to increase productivity [3]. Organic photovoltaics, sensory probes, therapeutic agents, drug administration in biological and medical applications, electronic conductors, and catalysis are a few of the cutting-edge uses that have been investigated and implemented in recent years. Recently, a new class of materials known as nanomaterials has evolved. Nanomaterials are those whose fundamental unit, roughly corresponding to the size of 10–100 atoms, is closely packed within a three-dimensional region with a dimension on the nanometer scale (0.1–100 nm) [4]). Nanomaterials, such as nanoparticles, have been under development the longest and are the most advanced technology. Various fields, including medicine, biology, physics, chemistry, and the senses, use nanoparticles and nanotechnology extensively because of their unique features [5]. Nanoparticles made of noble metals, including copper, mercury, silver, platinum, and gold, have recently received more attention from scientists. Gold nanoparticles' optical and electrical properties can be tuned by adjusting their size, shape, surface chemistry, or aggregation state [6]. As a result, gold nanoparticles have become a popular choice for use in various applications. Their exceptional physical qualities account for this. Surface plasmon oscillations, for instance, may be used for sensing, imaging, and labeling. As a result, gold nanoparticles are often employed in medicinal applications rather than potentially harmful metals like platinum. Making nanoparticles of gold

makes it possible to utilize previously inaccessible places, opening up exciting new avenues of research and development.

2. Gold nanoparticle properties and their various applications and activities

Gold nanoparticles are a versatile material that can be used in a wide range of applications. This is because their electronic and physical properties are well understood, thanks to well-developed ways to make them. Their surface chemistry is also easy to change. Because of these qualities, gold nanoparticles are one of the most commonly used nanomaterials in academic research and are a key part of many medical devices and industrial products around the world. Gold nanoparticle utilization has several practical benefits, in this case, gold nanoparticles' diameter of 5 nm or less are ideal for use as catalysts [7]. Toxic air pollutants may be converted into far safer molecules. In addition, this gold nanoparticle can potentially be employed in treating tumors and cancer [8]. It's also applicable to other molecules, including those used in medicine. Moreover, gold nanoparticles have the fantastic and practical capacity to transform specific wavelengths of light into heat [9]. Gold nanoparticles, in particular, have shown great promise in improving the performance of solar cells, which absorb sunlight and convert it into electricity [10]. Gold nanoparticles have recently been discovered to be useful in various scientific disciplines. Optical coding in many colors for biological experiments is one example of how glasses may be coated to alter their characteristics. These gold nanoparticles have also been employed to improve organic light-emitting diodes' quantum and electroluminescence efficiency. Detecting minute concentrations of analytes is now possible with novel sensors made possible by nanoparticle materials—for instance, a few parts per million (ppm) of chemical vapors. In addition, these gold nanoparticles have traditionally been used in the textile dyeing process. Another fascinating use for these nanoparticles is in high-density data storage and the provision of sustainable energy through solar cells [11]. For a better industrial clean processes, less pollution, and purified water are just a few of the many critical environmental issues that may be addressed using technologies based on gold nanoparticles [12]. Similarly resistant to oxidation, gold is, in reality, one of the most stable metals. In addition to catalyzing the electrochemical redox oxidation and reduction of CO and $CH3OH$, the hydrogenation of unsaturated substrates, and CO oxidation, functional thiolate-stabilized gold nanoparticles may also catalyze the hydrogenation of unsaturated substrates [13]. As part of nanotechnology, gold nanoparticles may regulate and detect mercury. In theory, gold nanoparticles may be very effective as mercury oxidation catalysts. One of the best applications of gold nanoparticles is improving environmental quality. Carbon monoxide is a poisonous gas with no taste or smell, yet it may kill a person within minutes [14]. The solution can be found simply in gold nanoparticles. Gold nanoparticles transform carbon monoxide (CO) into carbon dioxide (CO_2), a far safer chemical [15]. In recent years, noble metal nanoparticles have become more popular for water purification and contaminant detection. Gold nanoparticles have also been shown to be efficient adsorbents for filtering out high levels of mercury in the water supply. Contrarily, AuNPs possess a variety of features that make them excellent bionanotechnology instruments. These systems are useful for imaging because of the large variety of surface functions and bioconjugates that may be attached to AuNPs and their exceptional physical characteristics. And by modifying the monolayer on

the surface of the analyte, a highly sensitive and selective diagnostic system may be developed. Therapeutic potential has also been seen for AuNP-based delivery vectors, owing to their high surface loading of medication and genes and their tuneable release of the payloads. Collectively, AuNPs are very adaptable materials for future biological and bioengineering uses.

Author details

Safaa Najah Saud Al-Humairi
Faculty of Information Sciences and Engineering, Management and Science University, Selangor, Malaysia

*Address all correspondence to: safaaengineer@gmail.com

IntechOpen

References

[1] Patterson CC. Native copper, silver, and gold accessible to early metallurgists. American Antiquity. 1971;**36**(3):286-321

[2] Daniel M-C, Astruc D. Gold nanoparticles: Assembly, supramolecular chemistry, quantum-size-related properties, and applications toward biology, catalysis, and nanotechnology. Chemical Reviews. 2004;**104**(1):293-346

[3] Gwinn MR, Vallyathan V. Nanoparticles: Health effects—Pros and cons. Environmental Health Perspectives. 2006;**114**(12):1818-1825

[4] Akinsete TO, Adebayo-Tayo BC, Adekanmbi AO. The phytochemical and antimicrobial potentials of the crude extracts of Bridelia ferruginea and the extracellular biosynthesized silver nanoparticles. JAMPS. 2017;**14**(3):1-13

[5] Ramalingam V. Multifunctionality of gold nanoparticles: Plausible and convincing properties. Advances in Colloid and Interface Science. 2019;**271**:101989

[6] Jiang Z, Hu M, Fan L, Pan Y, Tang W, Zhai G, et al. Combining visible light and infrared imaging for efficient detection of respiratory infections such as COVID-19 on portable device. 2020. arXiv preprint arXiv:2004.06912

[7] Hvolbæk B, Janssens TV, Clausen BS, Falsig H, Christensen CH, Nørskov JK. Catalytic activity of Au nanoparticles. Nano Today. 2007;**2**(4):14-18

[8] Kennedy LC, Bickford LR, Lewinski NA, Coughlin AJ, Hu Y, Day ES, et al. A new era for cancer treatment: Gold-nanoparticle-mediated thermal therapies. Small. 2011;**7**(2):169-183

[9] Taheri-Ledari R, Ahghari MR, Ansari F, Forouzandeh-Malati M, Mirmohammadi SS, Zarei-Shokat S, et al. Synergies in antimicrobial treatment by a levofloxacin-loaded halloysite and gold nanoparticles with a conjugation to a cell-penetrating peptide. Nanoscale Advances. 2022;**4**(20):4418-4433

[10] Zhang C, Luo Q, Shi J, Yue L, Wang Z, Chen X, et al. Efficient perovskite solar cells by combination use of Au nanoparticles and insulating metal oxide. Nanoscale. 2017;**9**(8):2852-2864

[11] Diallo MS, Fromer NA, Jhon MS. Nanotechnology for sustainable development: Retrospective and outlook. In: Nanotechnology for Sustainable Development. New York City, USA: Springer; 2013. pp. 1-16

[12] Khan S, Naushad M, Al-Gheethi A, Iqbal J. Engineered nanoparticles for removal of pollutants from wastewater: Current status and future prospects of nanotechnology for remediation strategies. Journal of Environmental Chemical Engineering. 2021;**9**(5):106160

[13] Zhang Y, Cui X, Shi F, Deng Y. Nano-gold catalysis in fine chemical synthesis. Chemical Reviews. 2012;**112**(4):2467-2505

[14] Gozubuyuk AA, Dag H, Kaçar A, Karakurt Y, Arica V. Epidemiology, pathophysiology, clinical evaluation, and treatment of carbon monoxide poisoning in child, infant, and fetus. Northern Clinics of Istanbul. 2017;**4**(1):100

[15] Rabiee H, Ge L, Zhang X, Hu S, Li M, Yuan Z. Gas diffusion electrodes (GDEs) for electrochemical reduction of carbon dioxide, carbon monoxide, and dinitrogen to value-added products: A review. Energy & Environmental Science. 2021;**14**(4):1959-2008

Chapter 2

Converting Silver Electrodes into Porous Gold Counterparts: A Strategy to Enhance Gas Sensor Sensitivity and Chemical Stability *via* Electrode Engineering

Yunnan Fang

Abstract

This chapter describes a strategy for sensitivity and chemical stability enhancement of chemiresistive gas sensors *via* electrode engineering. In this strategy, flexible chemiresistive gas sensors were fabricated by uniformly depositing functionalized semiconducting carbon nanotubes (CNTs) on a polyimide substrate *via* a novel layer-by-layer wet chemical method, followed by inkjet printing fine-featured silver interdigitated electrodes (IDEs) on the substrate. The electrode engineering was realized by converting the inkjet-printed IDEs into their highly porous and chemically stable gold counterparts *via* a mild and facile two-step process, with the substrate-IDE adhesion retained. As a proof-of-concept demonstration, a diethyl ethylphosphonate (DEEP, a simulant of the nerve agent sarin) sensor equipped with inkjet-printed dense silver IDEs was converted into its counterpart equipped with highly porous gold IDEs. The resulting gold-electrode gas sensor exhibited sensitivity to DEEP of at least fivefold higher than a similar sensor electrode with the dense silver IDEs. The sensitivity enhancement was probably due to the catalytic activity of the resulting gold IDEs, as well as the creation of the nano−/micro-scale pores in the gold IDEs that increased the Schottky contacts between the gold IDEs and the semiconducting CNTs.

Keywords: sensitivity enhancement, chemical stability enhancement, inkjet printing, porous gold electrode, Schottky contact

1. Introduction

Metal nanoparticle-based inkjet inks have been formulated from a number of metals such as silver [1], gold [2, 3], copper [4, 5], and nickel [6]. Among these metals silver is the best heat and electricity conductor [7] and silver nanoparticle (SNP)-based inks not only are the most commonly used with a well-settled technology but also show the most commercial significance, as indicated by their highest

sales volume among all metal-based inks [8]. However, due to some pollutants such as carbonyl sulfide (OCS) and hydrogen sulfide (H$_2$S) presented in air, silver (especially silver nanoparticles) tarnishes under ambient and even dry conditions [9, 10], resulting in significantly reduced conductivity [11]. Particularly, the concerns on poor conductivity of inkjet-printed silver traces in an electrochemical device are severe when used in aqueous environments, due to their oxidation and degradation under an applied electrical potential [3]. To prevent/minimize such oxidation−/degradation-based tarnishing, some passivation treatments, such as coating the silver structures with nickel [12] or polymers [13], have been successfully attempted.

In contrast to silver, gold is one of the most stable and inert chemical elements, the most ductile and malleable of all metals, and in the meantime an excellent electricity conductor. Accordingly, gold is preferable to silver for a number of applications. For instance, gold is preferred to silver to make printed circuit board electrodes for medical use (such as electrodes for high-resolution gastrointestinal electrical mapping), due to the fact that the oxidizing agents used to sterilize the electrodes at a low temperature, such as hydrogen peroxide and ozone, would oxidize silver but not gold [14, 15]. As another reported example, gold prevailed over silver as the electrode material for zinc oxide-based chemiresistive CO and NO$_2$ sensors for high sensitivity and short recovery time, due to that fact that gold was resistant to the poisoning or oxidizing of the target gases but silver was not [16].

Increasing evidence has shown that the device performance can be changed significantly by the contact geometry between the metal electrodes and the semiconducting materials. The sensor performance can sometimes be radically affected by the contact resistance formed in the electrode-semiconductor interface [17, 18], which has been conventionally ignored [19]. It has been shown that a Schottky barrier was formed in the contacts of semiconducting carbon nanotubes (CNTs) with gold [20] and that an increase in the Schottky contact area between semiconducting CNTs and gold/chromium electrodes resulted in a radical increase in the sensitivity of some biosensors [21].

Gold nanoparticle-based inks, however, have not been used as commonly as SNP inks. Compared with silver nanoparticles, gold nanoparticles are extremely expensive. Meanwhile, the relative immature techniques for preparing and inkjet printing gold nanoparticle-based inks are also a concern. Additionally, due to the fact that some of the most commonly used flexible substrates (such as polyethylene, terephthalate, and polyethylene naphthalate films and a number of papers such as copy, filter, and photo papers) have a relatively low maximum working temperature, the high sintering temperature (>190°C) needed for gold nanoparticle-based inks has restrained their applications in printing of flexible electronic devices. In contrast, a temperature of as low as 120°C can be used to sinter SNP-based inks, which is well suitable for most commonly-used flexible substrates.

In order to inkjet-print reliable, low-cost and high-performing flexible electronic devices, it is desirable to make use of the exceptional chemical stability of gold nanoparticles, as well as the well-developed formulation technology and low sintering temperature of SNP inks. In addition, compared with their dense counterparts, highly porous gold electrodes create much more Schottky contacts with a semiconducting sensing material (such as semiconducting CNTs), which drastically benefits sensing applications. To meet all these desires, one way that can be done is to inkjet-print an SNP ink, followed by sintering the resulting silver traces at a low temperature (e.g., 120°C) for desired conductivity, and finally chemically converting the resulting dense silver traces into their porous gold counterparts. Some one-step processes to

chemically convert silver structures into their gold counterparts have been reported [22–24]. These processes, however, were not only performed under relatively harsh conditions (at 100°C and in an aqueous solution) but also not able to enhance porosity in the resulting gold components. For applications in printed electronic devices, a serious concern arises on whether the adhesion between the silver patterns and the substrate can survive the harsh conversion conditions. As a matter of fact, for inkjet-printed devices/structures, the trace substrate adhesion has always been a constant concern, especially when they use a smooth-surfaced substrate (polyimide, PET and PEN films, silicon wafer, and glass plates.), and/or have to work in relatively harsh environments (such as high humidity, water- or organic solvent-based solutions, elevated temperatures, vibration, and bending). Surprisingly, as shown in a recent report, even buffers were able to kill the adhesion between a plastic substrate (PET or PEN) and inkjet-printed silver interdigitated electrodes (IDEs) [3], let alone chemically turning silver patterns printed on a plastic substrate to their gold counterparts in an aqueous solution at a high temperature.

Among the most commonly used flexible substrates for inkjet-printed electronic devices, Kapton® films exhibit excellent flexibility and mechanical robustness, as well as exceptional thermal and chemical stability. Some types of Kapton® films, such as Kapton® HN and HA films, have a slip additive incorporated in the polyimide matrix [25] to enhance their mechanical properties and reduce their resistance to sliding over themselves or parts of converting equipment. For example, a Kapton® 500 HN polyimide film (**Figure 1a**) has a slip additive, which has been identified as $CaCO_3$ particles [1]. The additive particles in a 500 HN film made its surface look granular under an optical microscope (**Figure 1b**), which seemingly contributed to increased surface roughness. However, as shown in **Figure 1c**, the surface of a Kapton® 500 HN film was actually very smooth, with an arithmetic (Ra) and quadratic (Rq) mean surface roughnesses of 0.67 and 0.89 nm, respectively [1].

Apparently, one solution to ensure the IDE-substrate adhesion to survive the silver-to-gold conversion is to reduce the harshness of the conversion conditions and/or enhance the adhesion by performing surface modification to the substrate prior to inkjet printing.

This chapter describes a strategy to enhance the adhesion between the Kapton® 500 HN polyimide substrate and inkjet-printed silver IDEs by chemically surface-modifying the substrate prior to inkjet printing, and promote the sensitivity and the chemical stability of flexible chemiresistive gas sensors through altering the material
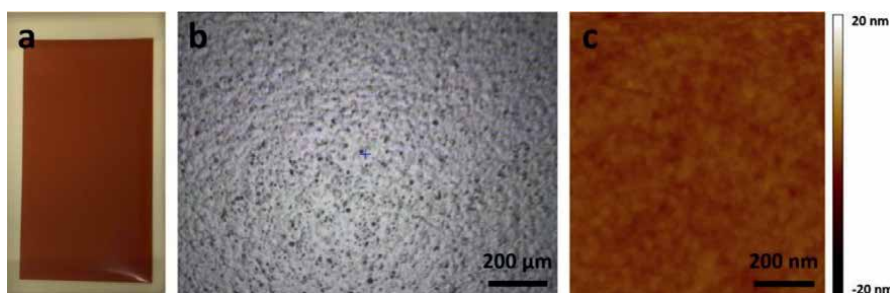

Figure 1.
Optical (a), optical microscopic (b) [26]), and atomic force microscopic (c) [1]) images of a blank Kapton® 500 HN polyimide film (panels b) and c) were licensed under creative commons attribution 4.0 international license and with permission from the Royal Society of Chemistry, respectively).

and the porosity of their electrodes. To begin with, semiconducting single-wall carbon nanotubes (SWCNTs) complexed with a chemoselective compound (selector), which functioned as the sensing material of the sensors, were chemically deposited, in a layer-by-layer fashion, on a piece of Kapton® 500 HN polyimide film with a home-developed chemical process. Secondly, an array of chemiresistive gas sensors was fabricated by inkjet printing fine-featured silver IDEs on the resulting CNT-terminated polyimide substrate. Finally, the silver IDEs were chemically converted into their highly porous and chemically stable gold counterparts under ambient conditions *via* a mild two-step process, without losing the IDE-substrate adhesion. After these processes, the chemical stability of the sensor IDEs and the contact area of the IDEs with the sensing element were drastically enhanced. Additionally, due to the fact the sensing material (i.e., the selector-functionalized CNTs) was chemically and uniformly deposited on the substrate, the individual difference among all the sensors fabricated on the same piece of substrate was minimized, thus allowing for a subsequent fair performance comparison between a sensor with the original dense silver electrodes and one with the converted highly porous gold electrodes.

To exhibit the utility of the strategy mentioned above, two sensors of different types, one electrode with the original inkjet-printed dense silver electrodes, and the other with the converted porous gold electrodes, were placed side by side in a sensor box and exposed to the vapor of diethyl ethylphosphonate (DEEP) generated from a well-calibrated gas generator. The sensing profiles of the two sensors were then compared. DEEP is a simulant of sarin (a G-type nerve agent with a military designation of GB). Sarin is one of the most toxic of the known chemical warfare agents and has been used multiple times by terrorist organizations and rogue states to attack civilians and military troops, resulting in severe mass casualties [27–29]. Exposure to sarin can cause death in minutes. Detecting sarin or its simulants to provide early warnings is becoming more and more of a concern for both civilian and military personnel. This work demonstrated that a sensor with the converted highly porous gold electrodes was at least fivefold more sensitive to DEEP than its counterpart with the original inkjet-printed dense silver electrodes. The possible mechanism responsible for the sensitivity enhancement is discussed.

2. Fabrication of chemiresistive sensors

2.1 Functionalization of semiconducting SWCNTs

Functionalization of SWCNTs with a selector was realized by immobilizing a hexafluoroisopropanol group-containing compound to semiconducting SWCNTs (a hexafluoroisopropanol group has been shown to absorb the target analyte DEEP *via* hydrogen bonding [1]). Specifically, a small sheet of semiconducting SWCNTs was immersed in dimethylformamide (DMF) solvent, followed by a gentle sonication with a probe sonicator to break the sheet into small pieces. A short centrifugation (4, 500 x g, 1 min) was conducted, and the resulting SWCNT pellets were collected and then incubated for 2 hours in an incubator shaker (25°C, 90 rpm) with a selector solution (5 mg/ml solution of 2-(2-hydroxy-1, 1, 1, 3, 3, 3-hexafluoropropyl)-1-naphthol in DMF). This incubation process allowed for the binding of the selector molecules to the SWCNTs *via* π-π interaction. A centrifugation (4500 x g, 5 min) was performed and the supernatant (i.e., unbound selector in DMF) was removed. The pellets were collected, washed three times with DMF solvent (with a 4500 x g/5 min

centrifugation between each wash), and finally re-suspended in DMF. The suspension was further sonicated multiple times with the probe sonicator until a homogeneous solution was obtained.

2.2 Functionalization of substrate

A Kapton® 500 HN polyimide sheet was cleaned by sonication first with an aqueous suspension of powdered precision cleaner for 10 minutes and then with acetone for 10 minutes in an ultrasonic cleaner. A layer-by-layer wet chemical process, which consisted of multiple steps as shown in **Figure 2**, was then used to deposit the SWCNT-selector particles (i.e., SWCNTs functionalized with the selector 2-(2-hydroxy-1, 1, 1, 3, 3, 3-hexafluoropropyl)-1-naphthol) on the cleaned polyimide substrate under ambient conditions. In brief, the following steps were performed with three rinses with DMF after each step: (1). The cleaned polyimide was exposed to a solution of 10 wt% tris (2-aminoethyl) amine in DMF for 1 hour (step (a) in **Figure 2**) to introduce $-NH_2$ groups to the substrate surface. (2). The resulting amine-functionalized substrate was exposed to a solution of 5 mg/ml 1-pyrenebutyric acid N-hydroxysuccinimide ester (PBSE) in DMF for 1 hour (step (b) in **Figure 2**) to allow for the covalent bonding of PBSE to the polyimide *via* the nucleophilic attack reaction depicted in **Figure 3**, resulting in pyrene-terminated polyimide substrate. (3). The pyrene-terminated substrate was exposed to the
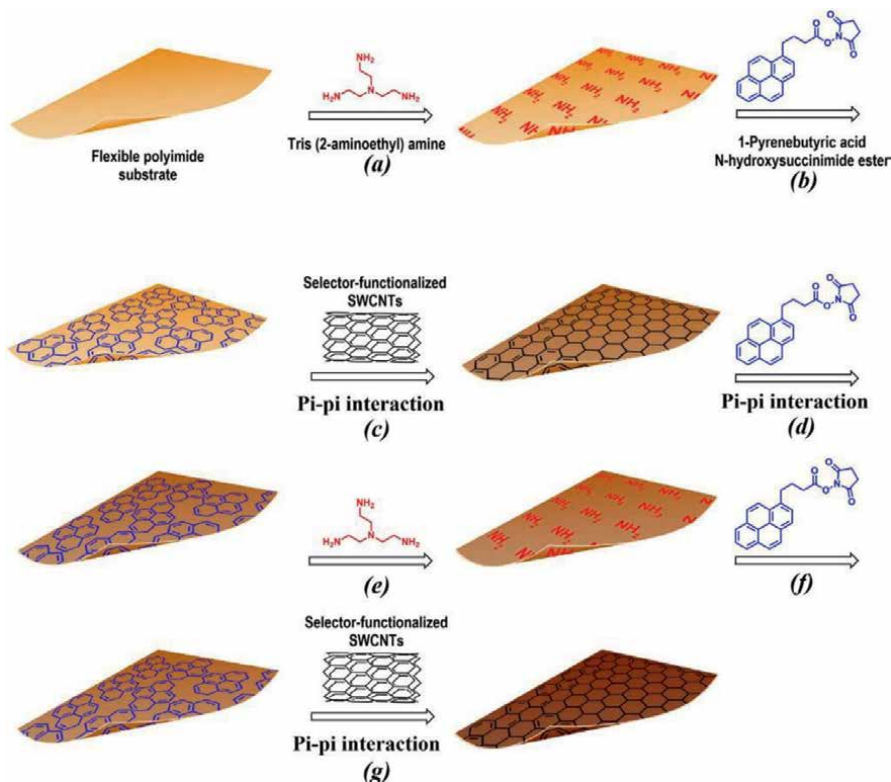
Figure 2.
Schematic of layer-by-layer deposition of the SWCNT-selector particles on a flexible Kapton® 500 HN polyimide substrate [30] (licensed under creative commons attribution 4.0 international license).
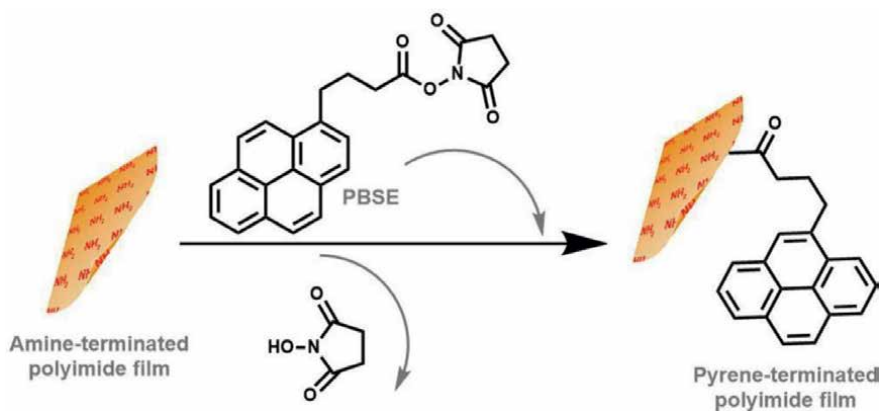
Figure 3.
Reaction of 1-pyrenebutyric acid N-hydroxysuccinimide ester (PBSE) with the amine groups on the amine-functionalized Kapton® 500 HN polyimide substrate, which resulted in pyrene-terminated polyimide substrate.
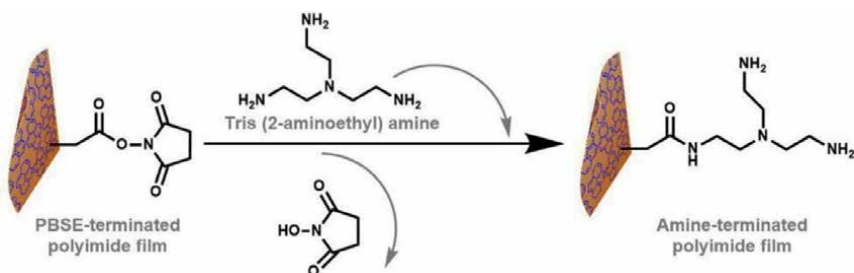
Figure 4.
Schematic of the reaction of tris (2-aminoethyl) amine with PBSE-terminated polyimide substrate, which resulted in amine-terminated polyimide substrate.

DMF-based SWCNT-selector solution for 1 hour (step (c) in **Figure 2**) to allow for the binding of SWCNT-selector particles to the polyimide substrate *via* the π-π interaction between the SWCNTs and the pyrene groups on the substrate (this step deposited the first layer of SWCNT-selector particles on the polyimide substrate). (4). The resulting structure was exposed to the PBSE solution for 1 hour (step (d) in **Figure 2**) to immobilize PBSE to the substrate *via* the π-π interaction between the SWCNTs and the pyrene groups in PBSE. (5). The resulting PBSE-functionalized structure was then exposed to a DMF-based 10 wt% solution of tris (2-aminoethyl) amine for 1 hour (step (e) in **Figure 2**) to introduce –NH$_2$ groups to the substrate *via* the nucleophilic attack reaction between the –NH$_2$ group (s) in tris (2-amino-ethyl) amine and the succinimidyl ester end of PBSE (as depicted in **Figure 4**). (6). The resulting amine-terminated structure was then incubated with the PBSE solution for 1 (step (f) in **Figure 2**) to allow for the introduction of pyrene groups to the substrate surface. (7). The resulting structure was then exposed to the SWCNT-selector solution for 1 hour (step (g) in **Figure 2**) to allow for the binding of the second layer of the SWCNT-selector particles to the substrate. 8). Steps (d), (e), (f), and (g) in **Figure 2** were repeated eight times to deposit more layers of SWCNT-selector particles on the substrate.

2.3 Inkjet printing of silver-based interdigitated electrodes and chemical conversion of dense silver electrodes into porous gold counterparts

Silver-based IDEs were inkjet-printed with a drop-on-demand piezoelectric inkjet printer (DMP-2831, Fujifilm Dimatix, Inc., Santa Clara, CA, USA) for five passes on the functionalized polyimide substrate with a commercial silver nanoparticle-based ink, followed by a 120°C/3 h sintering process. Both the IDE finger width and the spacing between two adjacent fingers were 100 μm.

The conversion of inkjet-printed dense silver electrodes of a sensor into their porous gold counterparts was conducted under ambient conditions with a two-step process. In the first step, the sensor was incubated with a 3 wt% solution of gold(III) chloride in diluted HCl for 1 hour in an incubator shaker with a temperature of 25°C and a speed of 90 rpm, followed by rinsing three times with DI water. In the second step, the resulting structures were exposed overnight to an aqueous saturated solution of sodium chloride in the incubator shaker (25°C/90 rpm), followed by rinsing with DI water and drying with flowing air.

Figure 5a shows an optical image of an array of inkjet-printed sensors on a piece of functionalized Kapton® polyimide substrate, while **Figure 5b** shows a scanned image of one of the sensors in the array. The electrodes after the two-step conversion (**Figure 5c**) were morphologically similar to those before the conversion (**Figure 5b**). However, the electrodes before and after the two-step conversion exhibited the typical silver and gold colors, respectively.

Scanning electron microscopy (SEM) images of an inkjet-printed sensor (before the silver-to-gold conversion), and the energy-dispersive X-ray spectroscopy (EDX) pattern of its silver IDEs are shown in **Figure 6**. Under the scanning electron microscope, the silver nanoparticles were densely packed and virtually spherical in shape

Figure 5.
Optical and scanned images of inkjet-printed sensors before and after the two-step wet chemical conversion of the silver IDEs into their porous gold counterparts. (a) Optical image of an array of sensors before the conversion. (b) and (c) scanned images of a single sensor before and after, respectively, of the conversion [30] (licensed under creative commons attribution 4.0 international license).
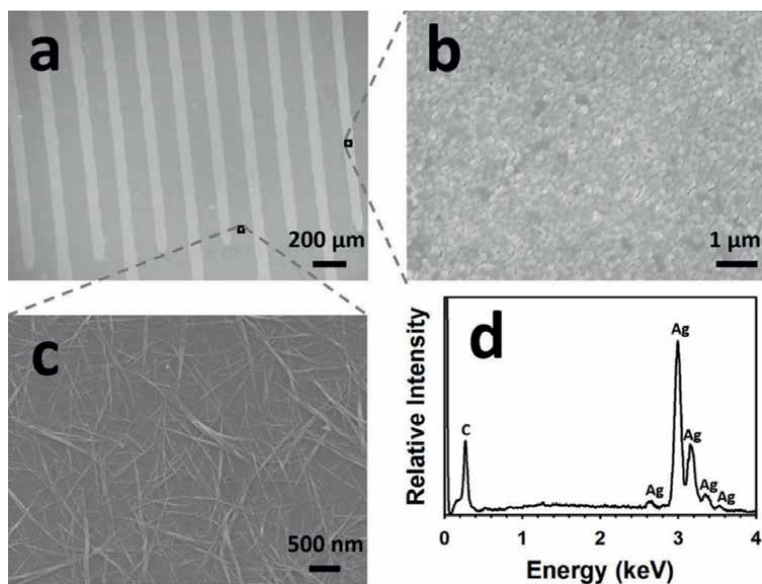
Figure 6.
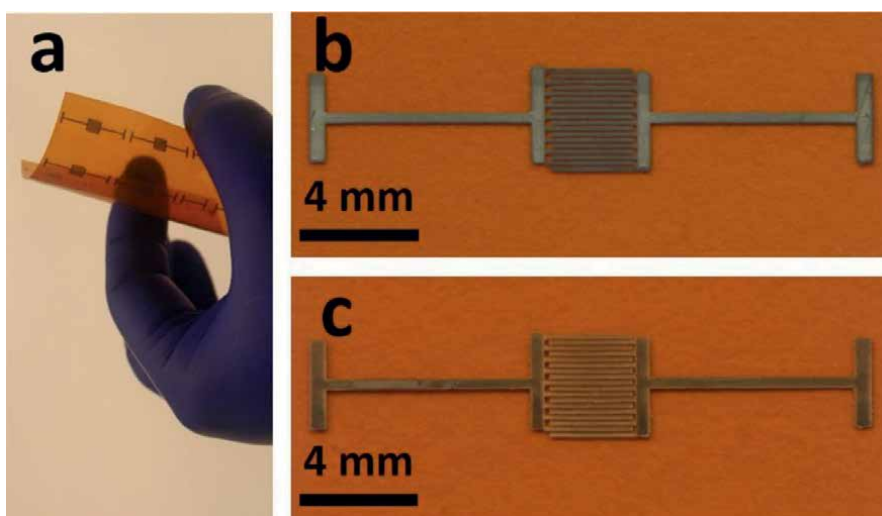*SEM and EDX analyses of a sensor with inkjet-printed silver-based IDEs. (a) Low magnification SEM image of the sensor. (b) High magnification SEM image focusing on the silver nanoparticles in an IDE finger. (c) High magnification SEM image focusing on the individual SWCNT-selector particles between two adjacent fingers. (d) EDX pattern of the specimen shown in panel b) [30] (licensed under creative commons attribution 4.0 international license).*

with a diameter of ~150 nm after a 120°C/3 hour annealing process (**Figure 6b**). The SWCNT-selector particles between two adjacent IDE fingers were randomly and virtually evenly distributed on the surface of the polyimide substrate (**Figure 6c**). The EDX analyses on the silver IDEs show the presence of the elements silver and carbon (**Figure 6d**). It is worth mentioning that the carbon peak in the **Figure 6d** originated from the carbon-containing functionalized polyimide substrate and the carbon film that was sputter-coated on the sensor to make the sample conductive prior to the SEM and EDX analyses, not from the silver IDEs.

The incubation of an inkjet-printed sensor with the gold(III) chloride solution brought in a drastic change in the morphology of its IDEs. That is, the particles turned irregular in shape and much larger than the starting silver nanoparticles (**Figure 7a**). The elements gold, silver, and chlorine were detected in the resulting IDEs (**Figure 7c**). The subsequent incubation with a saturated sodium chloride solution brought in another drastic change in the morphology of the IDEs, the particles became significantly shrank in size and much more loosely packed, resulting in highly porous IDEs (**Figure 7b**). Elemental analyses of the porous IDEs showed that, compared with the elemental composition of the starting silver-based IDEs (**Figure 6d**), the elements silver and chlorine disappeared but gold was retained (**Figure 7d**), which means that the incubation with the saturated sodium chloride solution and the subsequent rinsing selectively removed the side product(s) of the silver-to-gold converting reaction. Again, the carbon peak in **Figure 7d** came from the functionalized polyimide substrate and the sputter-coated carbon film on the porous IDEs.
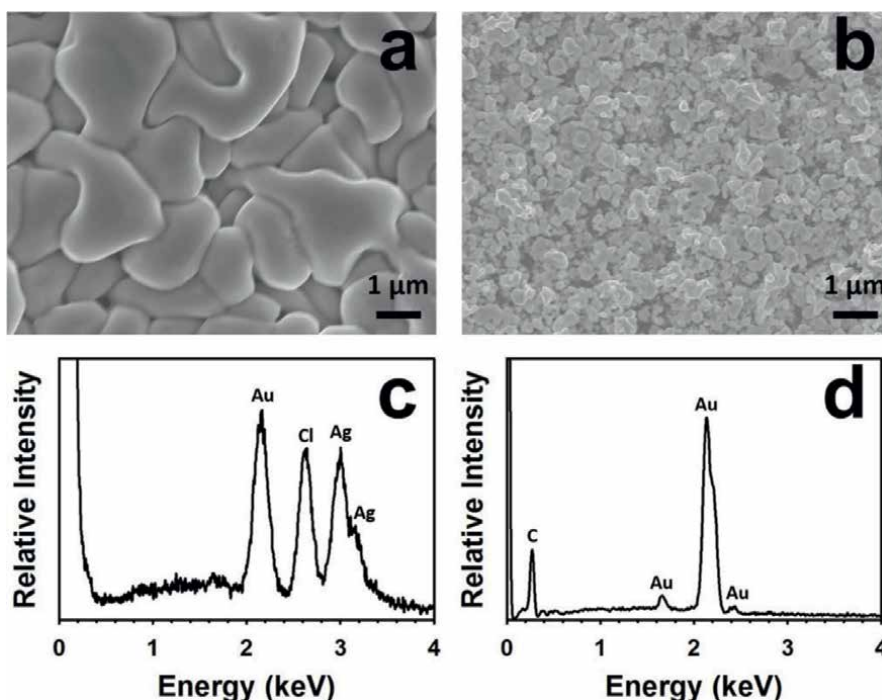
Figure 7.
SEM and EDX analyses of the sensor IDEs at their different stages after the silver-to-gold conversion. (a) SEM image of the IDEs after the silver-to-gold conversion but before the selective removal of the side product(s). (b) SEM image of the IDEs after both the silver-to-gold conversion and the side product removal. (c) and (d) EDX analyses of the specimens shown in a) and b), respectively [30] (licensed under creative commons attribution 4.0 international license).

Figure 8 shows the X-ray diffraction (XRD) patterns of a sensor at its different fabrication stages. Unfortunately, the XRD peaks of gold and silver overlapped in the 2θ range scanned in this work (i.e., 20° - 50°) [31, 32], and accordingly, XRD analyses performed on the sensor were unable to differentiate silver from gold. Fortunately, EDX analyses can easily distinguish the two elements. The following conclusions can be reached when combining the information drawn from the EDX (**Figures 6d, 7c**, and **d**) and XRD (**Figure 8**) analyses of sensor IDEs:

1. The inkjet-printed IDEs (before the silver-to-gold conversion) were made of silver (as shown in **Figures 6d** and **8b**).

2. The gold(III) chloride solution converted silver into gold and a side product, silver chloride (as shown in **Figures 7c** and **8c**).

3. The saturated sodium chloride solution selectively dissolved silver chloride, leaving porous gold behind (**Figures 7d** and **8d**).

With these characterization results, it can be concluded that the starting inkjet-printed dense silver IDEs were converted into their porous gold counterparts by the two-step process under ambient conditions.
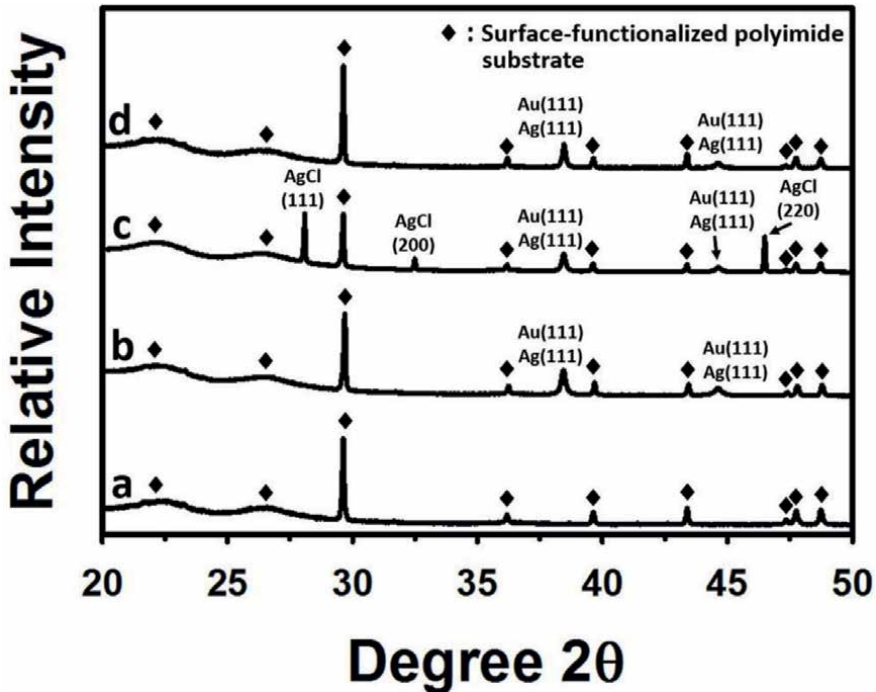
Figure 8.
XRD analyses of (a) the polyimide substrate functionalized with SWCNT-selector particles. (b) the functionalized polyimide substrate with inkjet-printed IDEs that have been subjected to the 120°C/3 hour annealing process. (c) the functionalized polyimide substrate with inkjet-printed IDEs that have been subjected to the 120°C/3 hour annealing process and the silver-to-gold conversion process. (d) the functionalized polyimide substrate with IDEs that have been subjected to the 120°C/3 hour annealing process, the silver-to-gold conversion process, and the side product removal process [30] (licensed under creative commons attribution 4.0 international license).

3. Characterization of chemiresistive sensors

3.1 Assessments of IDE-substrate adhesion

Visual inspection and Scotch®-tape peel testing were utilized to assess the adhesion between the metal traces (dense silver or porous gold IDEs) and the functionalized polyimide substrate. Visual inspection was performed from different angles while slowly finger-bending a sensor to a radius of curvature of ~1 cm, first in tension and then in compression. The strength of the adhesion of the silver or gold IDEs to the functionalized polyimide substrate was assessed by Scotch®-tape peel testing. Briefly, the back of a sensor was glued or taped to a smooth- and flat-surfaced plastic piece, and then the adhesive side of a piece of Scotch® magic tape (3 M company) was finger-pressed firmly against the front of the sensor (**Figure 9a** and **c**). Finally, the tape was peeled off slowly from the sensor at an angle of ~90°.

By visual inspection, no detachment was observed between the functionalized polyimide substrate and the dense silver or the porous gold IDEs, which was an indication that the adhesion between the inkjet-printed silver IDEs and the polyimide substrate survived the silver-to-gold conversion and the subsequent removal of the side product silver chloride. For Scotch®-tape peel testing, as shown in **Figure 9b**, with the tape taken off, the dense Ag IDEs on the polyimide substrate were essentially unimpaired (there was only one very small silver particle with a diameter of ~0.2 mm
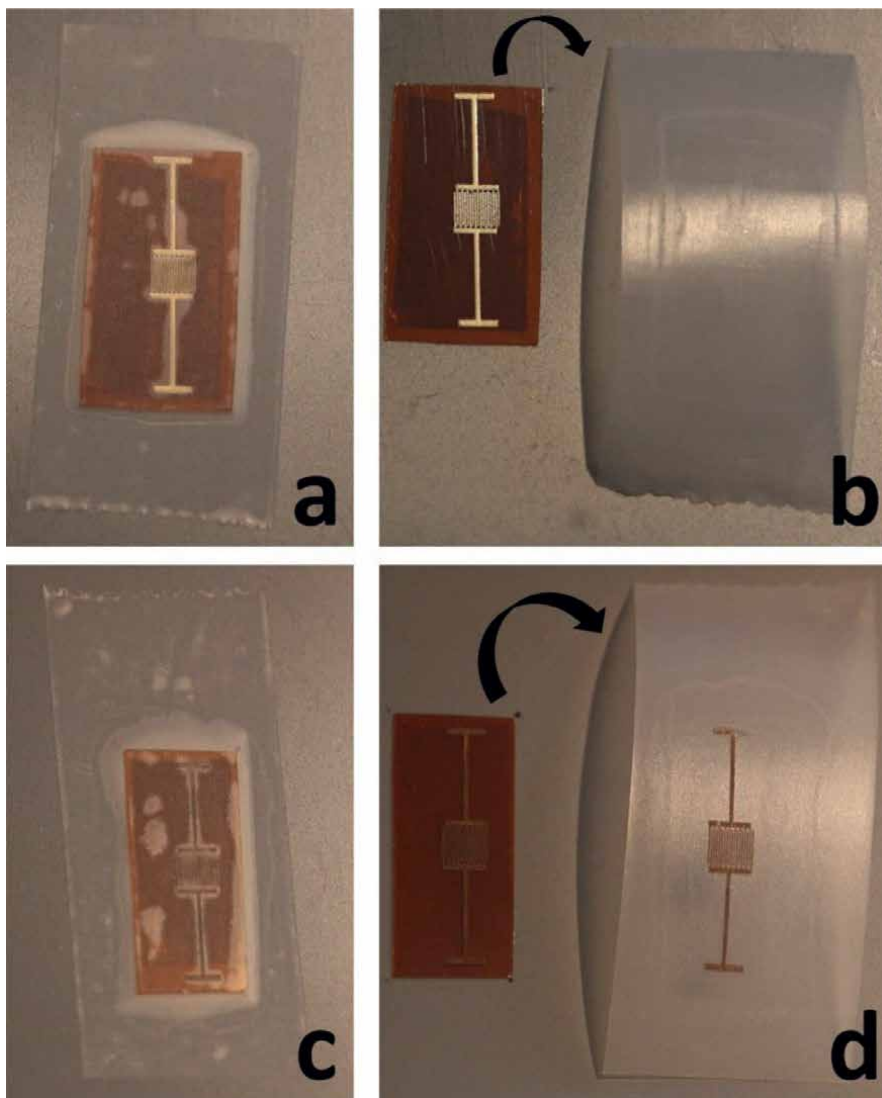
Figure 9.
Scotch®-tape peel testing on the sensors with the starting dense silver IDEs and with the porous gold IDEs. (a) and (c) optical images of the sensors with the dense silver IDEs and with the porous gold IDEs, respectively, that have been firmly stuck to a piece of scotch® magic tape. (b) and (d) optical images of the sensors with the silver IDEs and with the porous gold IDEs, respectively, after the removal of the tape [30] (licensed under creative commons attribution 4.0 international license).

taken by the tape). By contrast, the porous gold IDEs seemed to be delaminated by the removal of the type. This is, quite a number of top layer gold residues originally on the polyimide substrate were taken by the tape, with the gold nanoparticles that remained on the polyimide substrate still forming an essentially intact IDE pattern (**Figure 9d**).

3.2 Gas sensing

A DEEP permeation tube (KIN-TEK Laboratories, Inc.), a FlexStream™ Gas Standards Generator (KIN-TEK Laboratories, Inc.), and nitrogen gas with a flow
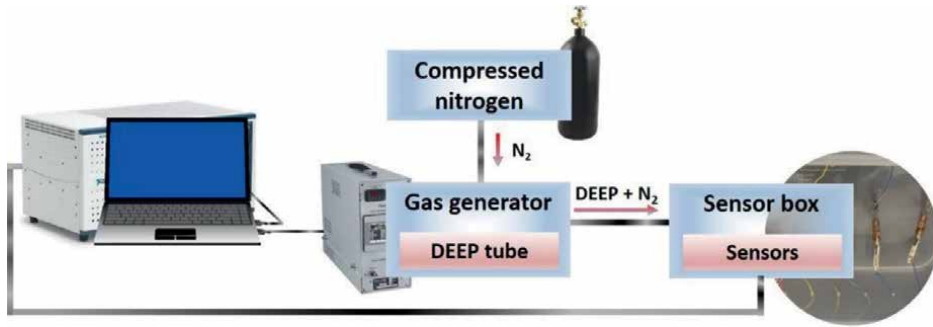
Figure 10.
Schematic diagram of the setup for the sensing of DEEP vapor.

rate of 500 sccm were used to generate the 2.0 ppm DEEP vapor stream. A home-developed sensing system automated with LabVIEW-based programs was used to monitor the real-time changes in the electrical resistance of the sensors in the sensor box. A schematic diagram of the gas sensing setup is shown in **Figure 10**. In a typical sensing trial, two sensors, one with inkjet-printed dense silver IDEs and the other with porous gold IDEs, were accommodated side by side in the sensor box. Upon exposing the sensors to either the carrier gas nitrogen or the 2.0 ppm DEEP balanced with nitrogen, their electrical resistance changes with time were automatically recorded by the system.

As revealed by **Figure 11**, neither the sensor electrode with the original dense silver IDEs nor the sensor electrode with the porous gold IDEs was responsive to the carrier gas nitrogen (0–10 min time range) that was launched prior to the onset of the DEEP vapor. Upon launching the 2.0 ppm DEEP vapor, the electrical resistance of both sensors began to increase and continued increasing until the DEEP release was stopped. During the duration of DEEP release (10–73 min time range), there was a much faster increase in the electrical resistance of the sensor electrode with the porous gold IDEs than its counterpart with the dense silver IDEs. At the end of the DEEP release, the relative sensitivity (S) of the sensor with the porous gold IDEs reached ~47% (**Figure 11** solid line), compared to only ~9% for the sensor with the dense silver IDEs (**Figure 11** dash-dot line). That is to say, the conversion of the dense silver IDEs of a sensor into their porous gold counterparts enhanced the sensitivity of the sensor by more than fivefold. The relative sensitivity S is defined as

$$S = \frac{R - R_0}{R_0} \tag{1}$$

where R_0 and R denoting the electrical resistances of a sensor right before and at a particular time after, respectively, the sensor was exposed to the DEEP vapor. Once the release of the DEEP vapor was stopped, the electrical resistance of both sensors began to decrease slowly, indicating the slow and partial recovery of the sensors.
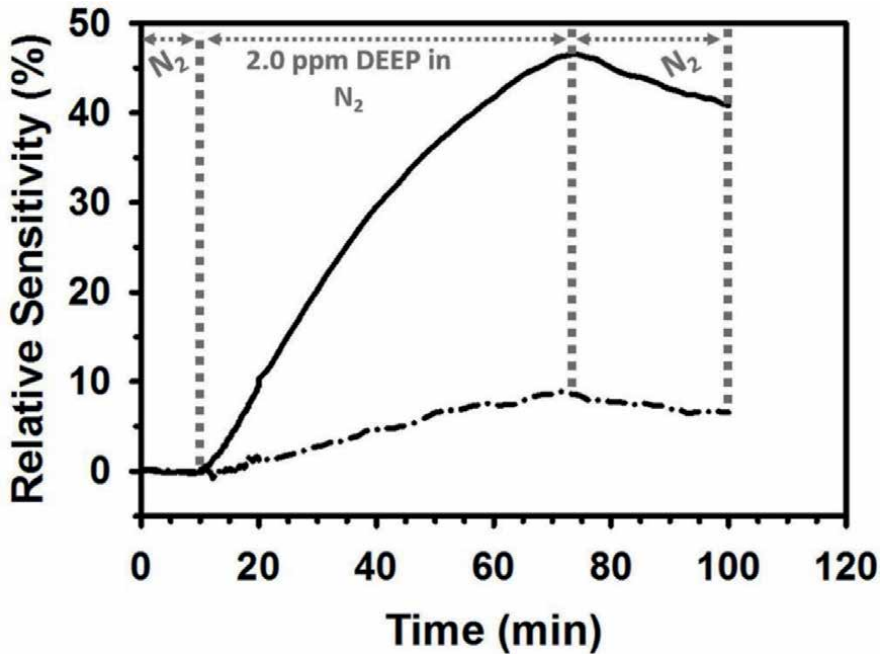
Figure 11.
Typical sensing profiles of the SWCNT-based sensors with the inkjet-printed dense silver IDEs (dash-dot line) and with the porous gold IDEs (solid line) upon exposure to the carrier gas nitrogen (0–10 min and 73–100 min) and the 2.0 ppm DEEP vapor (10–73 min).

4. Discussion

It has been reported that the following chemical reaction (Eq. (2)) took place during a one-step conversion of silver nanostructures into their gold counterparts (with no extra pores created) at an elevated temperature of 100°C [22–24]:

$$3Ag(s) + HAuCl_4(aq) => Au(s) + 3AgCl(aq) + HCl(aq) \tag{2}$$
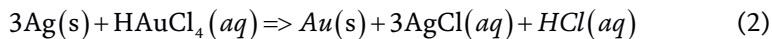
where the silver chloride formed in the reaction was completely dissolved under the experimental conditions. Different from these previous reports, in the current work the silver-to-gold conversion was performed at room temperature. Based on the EDX (**Figures 6d, 7c, and d**) and XRD (**Figure 8**) analyses of the IDEs at different stages, it can be concluded that at room temperature, a silver-to-gold converting reaction similar to the one presented in Eq. (2) took place, but the silver chloride was produced in solid form. That is to say, in the current work the following reaction (Eq. (3)) was responsible for the room temperature silver-to-gold conversion:

$$3Ag(s) + HAuCl_4(aq) => Au(s) + 3AgCl(s) + HCl(aq) \tag{3}$$
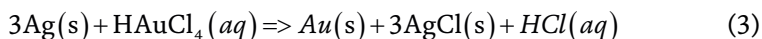
The fact that the silver chloride in Eq. (3) was in solid form and incorporated in the gold matrix turned out to be beneficiary for sensitivity enhancement since the nano−/micro-scale pores in the gold IDEs were mainly created by the selective dissolution of the silver chloride that was performed following the silver-to-gold conversion. In addition to the silver chloride dissolution, the size difference between silver and a gold atom, which had a Van der Waals radius of 172 and 166 pm, respectively, also contributed to the pore creation in the gold IDEs, since a slight shrinkage occurred in the atomic size when a silver atom was converted into a gold atom. It was difficult, however, to experimentally determine the porosity of the porous gold IDEs, since the gold IDEs were not free-standing but on a polyimide film. Nevertheless, a rough estimation of the porosity of the gold IDEs can be calculated theoretically based on Eq. (3) and some inherent properties of the elements gold and silver. Assuming the starting inkjet-printed silver IDEs were fully dense, the total pore volume of the porous gold IDEs is the sum of the pore volumes created by the dissolution of the silver chloride and by the atomic shrinkage when three moles of silver was chemically converted into one mole of gold (based on the stoichiometry of Eq. (3)). With the densities of gold and silver being 19.32 and 10.49 g/cm^3, respectively and their atomic masses 196.97 and 107.87, respectively, the porosity of the porous gold IDEs was calculated to be about 67%.

The Scotch®-tape peel testing delaminated the porous gold IDEs, but the adhesion between the substrate and the porous gold IDE seemed unimpaired by the peeling-off of the tape. This means the creation of nano−/micro-scale pores in the gold IDEs weakened the connection between the gold nanoparticles.

The mechanism for the sensitivity enhancement due to the change in the electrode material, and geometry is still not well understood. Based on the experimental observations described in this work and some relevant literature, it is speculated that the "electrode effects" and the "porosity effects" were responsible for the significant sensitivity enhancement. The "electrode effects" refer to the fact that the catalytic activity of the gold electrodes contributes to the enhanced sensitivity, even though such effects are not conventionally considered to contribute to the electrical resistance change of chemiresistive sensors [33]. An unequivocal agreement has not been reached so far regarding how the sensing behavior of a chemiresistive sensor is affected by the material that its electrodes are made of [34], but more and more evidence shows that different electrode metals react with an target analyte differently [16, 35, 36]. Sensor electrodes that are made of a noble metal (such as palladium and gold) can act as catalysts and contribute to the overall electrical conductance and the sensor sensitivity [35, 37–40]. "Porosity effects" refer to the fact that increased number of nano−/micro-scale pores in the electrodes lead to increased Schottky contacts that contribute to the enhanced sensitivity. In the current work, the Schottky contacts between the porous gold electrodes and the semiconducting SWCNTs probably contributed more to the overall electrical resistance change of a sensor than the bulk SWCNTs. As a matter of fact, there has been increasing evidence indicating that the interface between metal electrodes and semiconducting CNTs might contribute significantly to the performance of electronic devices such as gas sensors [18] and transistors [41].

There are only a small number of reports in the literature on DEEP detection. Most of these reports utilized mass spectrometry, which featured high sensitivity and selectivity, to detect DEEP. For example, active capillary plasma ionization coupled to an ion trap mass spectrometer [42] and selected ion flow tube mass spectrometry (SIFT-MS) [43] have been used to detect DEEP, with a detection limit of 0.15 ppb and

45 pptv, respectively. Additionally, DEEP vapor of 135 ppm has been detected with optical reflectivity spectroscopy [44]. Reports on detection of DEEP vapor with a chemiresistive sensor have been very scarce. As an example, a flexible chemiresistive sensor based on non-functionalized reduced graphene oxide has been used to sense 2.0 ppm DEEP vapor with a low relative sensitivity of 5.2% [1]. In terms of sensitivity to DEEP vapor, chemiresistive sensors are apparently not as good as mass spectrometry. Nevertheless, mass spectrometry is associated with tedious sample preparation, solvent management, and bulky equipment. In contrast, chemiresistive sensors described in this work are ultra-lightweight, flexible, miniature-sized, and wearable, do not require sample preparation or solvents, and can be readily integrated into wireless sensing platforms to realize wireless detection.

Based on the generic nature of the facile and mild method described in this work to increase the electrode chemical stability and Schottky contacts of a sensor, the method can be readily applied to other semiconductor-based chemiresistive sensors for the purpose of sensitivity and chemical stability enhancement.

5. Conclusions

Functionalized SWCNTs were virtually evenly deposited on a polyimide film through a novel layer-by-layer wet chemical method. Flexible chemiresistive sensors were then fabricated by inkjet printing fine-featured silver IDEs on the resulting functionalized substrate. Sensors with highly porous (with a calculated porosity of ~67%) and chemically stable gold IDEs were fabricated *via* a facile and ambient condition two-step wet chemical process. The adhesion between the inkjet-printed silver IDEs and the substrate survived the two-step dense silver to porous gold conversion process, but the creation of the nano−/micro-scale pores in the resulting gold IDEs weakened the connection between gold nanoparticles.

The dense silver to porous gold conversion turned to be very efficient in enhancing the sensitivity of the sensors to DEEP (a simulant of the nerve agent sarin). A sensor equipped with the converted porous gold IDEs exhibited a sensitivity to DEEP of more than five times higher than a similar sensor equipped with the original dense silver IDEs. The drastic sensitivity increase was probably due to the catalytic activity of the gold IDEs and the increased Schottky contacts between the porous gold electrodes and the semiconducting SWCNTs.

The electrode engineering idea described in this work is generic and readily applicable to other semiconductor-based chemiresistive sensors to enhance their sensitivity and chemical stability.

Conflict of interest

The author declares no conflict of interest.

Author details

Yunnan Fang
School of Electrical and Computer Engineering, Georgia Institute of Technology,
Atlanta, Georgia, USA

*Address all correspondence to: yunnan.fang@mse.gatech.edu

IntechOpen

References

[1] Fang YN, Hester JGD, deGlee B, Tuan CC, Brooke PD, Le TR, et al. A novel, facile, layer-by-layer substrate surface modification for the fabrication of all-inkjet-printed flexible electronic devices on Kapton. Journal of Materials Chemistry C. 2016;**4**(29):7052-7060. DOI: 10.1039/c6tc01066k

[2] Jensen GC, Krause CE, Sotzing GA, Rusling JF. Inkjet-printed gold nanoparticle electrochemical arrays on plastic. Application to immunodetection of a cancer biomarker protein. Physical Chemistry Chemical Physics. 2011;**13**(11):4888-4894. DOI: 10.1039/c0cp01755h

[3] Pavinatto FJ, Paschoal CWA, Arias AC. Printed and flexible biosensor for antioxidants using interdigitated inkjetted electrodes and gravure-deposited active layer. Biosensors & Bioelectronics. 2015;**67**:553-559. DOI: 10.1016/j.bios.2014.09.039

[4] Abhinav KV, Rao RVK, Karthik PS, Singh SP. Copper conductive inks: Synthesis and utilization in flexible electronics. RSC Advances. 2015;**5**(79):63985-64030. DOI: 10.1039/c5ra08205f

[5] Sipila E, Ren YN, Virkki J, Sydanheimo L, Tentzeris MM, Ukkonen L. Parametric optimization of inkjet printing and optical sintering of nanoparticle inks. In: 2015 9th European Conference on Antennas and Propagation (EuCAP). New York: IEEE; 2015

[6] Tseng WJ, Chen CN. Dispersion and rheology of nickel nanoparticle inks. Journal of Materials Science. 2006;**41**(4):1213-1219. DOI: 10.1007/s10853-005-3659-z

[7] Spellman FR. Chemistry for Nonchemists: Principles and Applications for Environmental Practitioners. Lanham, Maryland: Government Institutes; 2006. p. 352

[8] Rajan K, Roppolo I, Chiappone A, Bocchini S, Perrone D, Chiolerio A. Silver nanoparticle ink technology: State of the art. Nanotechnology, Science and Applications. 2016;**9**:1-13. DOI: 10.2147/nsa.s68080

[9] Ankersmit HA, Tennent NH, Watts SF. Hydrogen sulfide and carbonyl sulfide in the museum environment - part 1. Atmospheric Environment. 2005;**39**(4):695-707. DOI: 10.1016/j.atmosenv.2004.10.013

[10] Franey JP, Kammlott GW, Graedel TE. The corrosion of silver by atmospheric sulfurous gases. Corrosion Science. 1985;**25**(2):133-143. DOI: 10.1016/0010-938x(85)90104-0

[11] Russ GJ. Electrical characteristics of contacts contaminated with silver sulfide film. IEEE Transactions on Parts, Hybrids, and Packaging. 1970;**PMP6**(4):129. DOI: 10.1109/tpmp.1970.1136268

[12] Molina-Lopez F, Briand D, de Rooij NF. All additive inkjet printed humidity sensors on plastic substrate. Sensors and Actuators B: Chemical. 2012;**166**:212-222. DOI: 10.1016/j.snb.2012.02.042

[13] Altenberend U, Molina-Lopez F, Oprea A, Briand D, Barsan N, de Rooij NF, et al. Towards fully printed capacitive gas sensors on flexible PET substrates based on Ag interdigitated transducers with increased stability. Sensors and Actuators B: Chemical.

2013;**187**:280-287. DOI: 10.1016/j. snb.2012.11.025

[14] Baumgartner HJ, Hood GC, Monger JM, Roberts RM, Sanborn CE. Decomposition of concentrated hydrogen peroxide on silver. I. Low temperature reaction and kinetics. Journal of Catalysis. 1963;**2**(5):405-414. DOI: 10.1016/0021-9517(63)90105-2

[15] Waterhouse GIN, Bowmaker GA, Metson JB. Oxidation of a polycrystalline silver foil by reaction with ozone. Applied Surface Science. 2001;**183**(3-4):191-204. DOI: 10.1016/s0169-4332(01)00561-x

[16] Lin HM, Tzeng SJ, Hsiau PJ, Tsai WL. Electrode effects on gas sensing properties of nanocrystalline zinc oxide. Nanostructured Materials. 1998;**10**(3):465-477. DOI: 10.1016/s0965-9773(98)00087-7

[17] Faglia G, Comini E, Sberveglieri G, Rella R, Siciliano P, Vasanelli L. Square and collinear four probe array and hall measurements on metal oxide thin film gas sensors. Sensors and Actuators B: Chemical. 1998;**53**(1-2):69-75. DOI: 10.1016/s0925-4005(98)00290-1

[18] Suehiro J, Imakiire H, Hidaka S, Ding WD, Zhou GB, Imasaka K, et al. Schottky-type response of carbon nanotube NO2 gas sensor fabricated onto aluminum electrodes by dielectrophoresis. Sensors and Actuators B: Chemical. 2006;**114**(2):943-949. DOI: 10.1016/j.snb.2005.08.043

[19] Saukko S, Lantto V. Influence of electrode material on properties of SnO2-based gas sensor. Thin Solid Films. 2003;**436**(1):137-140. DOI: 10.1016/s0040-6090(03)00509-1

[20] Zhang JB, Xi N, Lai KWC. Performance evaluation and analysis

for carbon nanotube (CNT) based IR detectors - art. no. 65421N. In: Andresen BF, Fulop GF, Norton PR, Editors. Infrared Technology and Applications XXXIII. Proceedings of the Society of Photo-Optical Instrumentation Engineers (Spie). Bellingham: SPIE; 2007. pp. N5421

[21] Byon HR, Choi HC. Network single-walled carbon nanotube-field effect transistors (SWNT-FETs) with increased Schottky contact area for highly sensitive biosensor applications. Journal of the American Chemical Society. 2006;**128**(7):2188-2189. DOI: 10.1021/ja056897n

[22] Sun YG, Xia YN. Shape-controlled synthesis of gold and silver nanoparticles. Science. 2002;**298**(5601):2176-2179. DOI: 10.1126/science.1077229

[23] Davis SC, Sheppard VC, Begum G, Cai Y, Fang YN, Berrigan JD, et al. Rapid flow-through biocatalysis with high surface area, enzyme-loaded carbon and gold-bearing diatom frustule replicas. Advanced Functional Materials. 2013;**23**(36):4611-4620. DOI: 10.1002/adfm.201203758

[24] Sun YG, Mayers BT, Xia YN. Template-engaged replacement reaction: A one-step approach to the large-scale synthesis of metal nanostructures with hollow interiors. Nano Letters. 2002;**2**(5):481-485. DOI: 10.1021/nl025531v

[25] Ghosh MK, Mittal KL. Polyimides: Fundamentals and Applications. New York, USA: Marcel Dekker; 1996

[26] Fang YN, Chen VW, Cai Y, Berrigan JD, Marder SR, Perry JW, et al. Biologically enabled syntheses of freestanding metallic structures possessing subwavelength pore arrays for extraordinary (surface

Plasmon-mediated) infrared transmission. Advanced Functional Materials. 2012;**22**(12):2550-2559. DOI: 10.1002/adfm.201102715

[27] Nozaki H, Aikawa N. Sarin poisoning in Tokyo subway. Lancet. 1995;**345**(8962):1446-1447

[28] Dolgin E. Syrian gas attack reinforces need for better anti-sarin drugs. Nature Medicine. 2013;**19**(10):1194-1195. DOI: 10.1038/nm1013-1194

[29] Ganesan K, Raza SK, Vijayaraghavan R. Chemical warfare agents. Journal of Pharmacy & Bioallied Sciences. 2010;**2**(3):166-178. DOI: 10.4103/0975-7406.68498

[30] Fang YN, Akbari M, Sydanheimo L, Ukkonen L, Tentzeris MM. Sensitivity enhancement of flexible gas sensors via conversion of inkjet-printed silver electrodes into porous gold counterparts. Scientific Reports. 2017;**7**:8988. DOI: 10.1038/s41598-017-09174-5

[31] Wang AQ, Liu JH, Lin SD, Lin TS, Mou CY. A novel efficient Au-Ag alloy catalyst system: Preparation, activity, and characterization. Journal of Catalysis. 2005;**233**(1):186-197. DOI: 10.1016/j.jcat.2005.04.028

[32] Gheorghe DE, Cui LL, Karmonik C, Brazdeikis A, Penaloza JM, Young JK, et al. Gold-silver alloy nanoshells: A new candidate for nanotherapeutics and diagnostics. Nanoscale Research Letters. 2011;**6**:554. DOI: 10.1186/1556-276x-6-554

[33] Lantto V, Rantala TS. Equilibrium and non-equilibrium conductance response of sintered SnO2 samples to CO. Sensors and Actuators B: Chemical. 1991;**5**(1-4):103-107. DOI: 10.1016/0925-4005(91)80228-c

[34] Gonchar AG, Rud BM, Siman NI, Tel'nikov EY, Rogozinskaya AA, Fiyalka LI, et al. Effect of electrode material on the electrical properties of tin dioxide thick films. Powder Metallurgy and Metal Ceramics. 2015;**54**(3-4):204-209. DOI: 10.1007/s11106-015-9700-0

[35] Ylinampa A, Lantto V, Leppavuori S. Some differences between Au and Pt electrodes in SnO2 thick-film gas sensors. Sensors and Actuators B: Chemical. 1993;**14**(1-3):602-604. DOI: 10.1016/0925-4005(93)85110-v

[36] Bondavalli P, Legagneux P, Pribat D. Sub ppm gas sensing using a CNTFET-based sensor Array fabricated using different metals as electrodes. Journal of the Korean Physical Society. 2009;**54**(1):510-513

[37] Capone S, Siciliano P, Quaranta F, Rella R, Epifani M, Vasanelli L. Moisture influence and geometry effect of Au and Pt electrodes on CO sensing response of SnO2 microsensors based on sol-gel thin film. Sensors and Actuators B: Chemical. 2001;**77**(1-2):503-511. DOI: 10.1016/s0925-4005(01)00754-7

[38] Mishra VN, Agarwal RP. Effect of electrode material on sensor response. Sensors and Actuators B: Chemical. 1994;**22**(2):121-125. DOI: 10.1016/0925-4005(94)87010-1

[39] Zhou XH, Xu YL, Cao QX, Niu SY. Metal-semiconductor ohmic contact of SnO2-based ceramic gas sensors. Sensors and Actuators B: Chemical. 1997;**41**(1-3):163-167. DOI: 10.1016/s0925-4005(97)80290-0

[40] Fukui K, Nakane M. Effects of tin oxide semiconductor electrode interface on gas-sensitivity characteristics. Sensors and Actuators

B: Chemical. 1993;**14**(1-3):589-590. DOI: 10.1016/0925-4005(93)85104-i

[41] Heinze S, Tersoff J, Martel R, Derycke V, Appenzeller J, Avouris P. Carbon nanotubes as Schottky barrier transistors. Physical Review Letters. 2002;**89**(10):1-4. DOI: 10.1103/ PhysRevLett.89.106801

[42] Wolf JC, Etter R, Schaer M, Siegenthaler P, Zenobi R. Direct and sensitive detection of CWA simulants by active capillary plasma ionization coupled to a handheld ion trap mass spectrometer. Journal of the American Society for Mass Spectrometry. 2016;**27**(7):1197-1202. DOI: 10.1007/ s13361-016-1374-4

[43] Francis GJ, Milligan DB, McEwan MJ. Detection and quantification of chemical warfare agent precursors and surrogates by selected ion flow tube mass spectrometry. Analytical Chemistry. 2009;**81**(21):8892-8899. DOI: 10.1021/ ac901486c

[44] Lee BJ, Jang SH, Sohn HL. Detection of toxic organophosphate nerve agents using DBR porous silicon chip. In: Ahn BT, Jeon H, Hur BY, Kim K, Park JW, editors. Advances in Nanomaterials and Processing, Pts 1 and 2. Solid State Phenomena. Vol. 124-126. Zürich: Trans Tech Publications Inc.; 2007. pp. 491-494

Perspective Chapter: Gold Nanoparticles Market – A Global Overview and New Challenges in the Post-Pandemic Economy

Jerome Verny, Ouail Oulmakki and Andrey Hernandez Meza

Abstract

Colloidal gold (AuNP) is a molecule obtained from pure gold (Au), and has several uses in the health, industrial, and chemical sectors. There are several processes to generate it and these methods are perfected over time. However, colloidal gold manufacturers and their customers are dependent on the pure gold market, its disruptions, and fluctuations. This paper first shows that the gold market is currently unstable due to the existing pandemic and geopolitical conflicts. The main gold producers, China, Russia, and Australia, together account for more than a quarter of the world's gold production, and only a few European countries produce gold in small quantities. Europe is therefore forced to import gold, including colloidal gold. Several innovations related to gold nanoparticles are emerging, notably in the miniaturization of industrial components or in the health sector during the pandemic. The objective of this chapter is therefore to understand the patterns into which these countries must fit to produce these particles and the economic, political, and scientific stakeholders involved in capturing these flows. Through the prism of the gold market, the electronics industry, and the health field, this chapter looks at these issues while putting into perspective the salient facts that could impact this market in the years to come.

Keywords: colloidal gold, gold market, innovation, industry, health crisis, geopolitical conflict

1. Introduction

Colloidal gold (AuNP) is a precipitate obtained from pure gold (Au), requiring products, such as gold powder or raw gold. The gold precipitate is called colloidal gold. It is classified as an inorganic nanomaterial. It is notably obtained from a chloride solution (sodium chloride, tin dichloride, etc.). There are three main manufacturing methods: Turkevich [1], Brust [2], and Perrault & Chan [3]. The color of colloidal gold varies between red and purple. It depends on the size and shape of the powder produced, whose particle diameter generally varies between 1 nm and 100 nm [4].

Turkevich's fabrication method, reviewed by Frens in the 1970s, consists of a first step of positioning on a hot plate a gold chloride, that is, gold in ionic form in an aqueous solution. This solution is colorless currently. By adding a small amount of sodium citrate, the gold is reduced and metallic gold nanoparticles of 15 nm in diameter appear suspended in the water. The precipitate then takes on a ruby-red color, attesting to the presence of the gold nanoparticles [5].

Brust's method, developed in 1994, makes it possible to prepare colloidal solutions of gold in organic solvents immiscible with water. The average diameter of the nanoparticles obtained is between 1 nm and 5 nm [2]. The objective of this synthesis is to react chloroauric acid with sodium tetrahydruroborate, which acts as a reducing agent, in the presence of tetraoctylammonium bromide, which acts as a stabilizing agent and phase transfer catalyst. It is then necessary to wait about 2 weeks for the nanoparticles to aggregate and precipitate [2].

In 2009, Perrault and Chan proposed a method for making colloidal gold in the 50–200 nm diameter range using hydroquinone as a reductant of chloroauric acid in an aqueous solution containing smaller gold nanoparticles. The use of citrate is then used to control the growth of the nanoparticles [3].

The use of colloidal gold is ancient. In ancient times, it was used as a dye, especially for porcelain. Today, it has three main uses: health, electronics, and chemistry field [6]. There are also some secondary uses in cosmetics (because colloidal gold has antiaging properties), photometry, etc. In the field of health, gold, as a trace element, is a universal natural antibacterial [7] and has anti-inflammatory properties. In the field of electronics, colloidal gold is used for its conductivity [8]. It is used in the manufacture of electronic components. In chemistry, as a catalyst, colloidal gold is used as a marker in immunoassays, imaging, and resonance sensors [9].

The purpose of this chapter is to provide an overview of the use of colloidal gold through the prism of its raw material, pure gold. First, the aim is to describe the gold market situation contextually, and to analyze its production and its use on a global scale. Then, we will detail the typologies and behaviors of the gold market in all its forms before focusing on the use of gold nanoparticle manufacturing. We will then analyze the market trends of products containing these molecules before demonstrating the interest in colloidal gold against the COVID-19 pandemic. Finally, we will conclude this chapter with a prospective conclusion focusing on the challenges that could affect this market in the coming years.

2. Context

As the methods of manufacturing colloidal gold are multiple and well known, the main difficulty is not to generate this molecule, but to obtain pure gold. It is therefore appropriate to focus on the trade of this rare material. There are 45 territories with active gold mines, with production led by China, Russia, and Australia, expected to reach more than 3500 tons in 2021 (**Figure 1**) [10].

Indeed, gold mining is a global industry, present on all continents except Antarctica [10]. It is extracted from mines of widely varying sizes and types around the world. Gold mines and mining operations are becoming increasingly geographically diverse, a far cry from the concentrated supply of some 50 years ago when most of the world's gold came from South Africa [11]. Overall mine production levels have increased significantly since 2008, although significant discoveries are increasingly rare.

Figure 1.
Major gold-producing countries in the world from 2010 to 2021 [10].
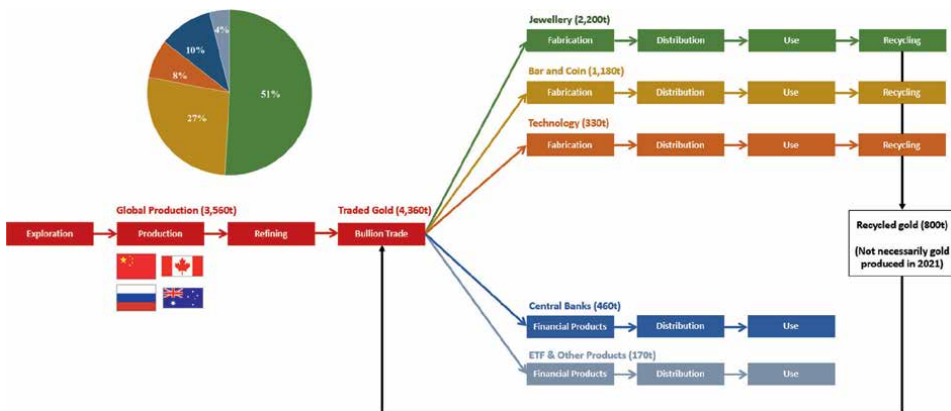
Figure 2.
Gold production and use cycles in 2021 (MOBIS based on several World Gold Council data 2022 [12–16]).

Gold is beyond its image as a shiny precious metal. It is a rare material with a variety of uses (see **Figure 2**). In total 52% of the gold produced on average between 2008 and 2017 was transformed into jewelry or 2.23 tons per year. In total 27% of the quantity mined was transformed into ingots and coins, 9% is used in the technology industry, 8% is used as a reserve for central banks, and 3% is invested in the stock market via ETFs [10]. Gold is also used in the medical sector. Some drugs contain it as well as some treatments against specific diseases, such as rheumatoid arthritis, Crohn's disease, psoriatic arthritis or cancer (**Figures 3** and **4**) [17].

In terms of gold nanoparticles, it should first be noted that the annual demand amounted to 1600 tons in 2020. The gold nanoparticle market can be segmented as follows [18]:

Figure 3.
Evolution of gold production in the world between 2010 and 2021.

Figure 4.
Segmentation of the gold nanoparticle market in 2021 [18].

- Electronics;

- Health Care;

- Chemicals;

- Other.

We observe that the growing application of nanotechnology in medical diagnostics, increasing R&D in gold nanoparticle technology, and growing demand in the electronics and development sector for specific applications are the major drivers of this market. However, stringent regulations and standards for nanomaterials may hamper the market growth [18].

Finally, the key players in the global gold nanoparticle market, after analyzing their capacity, market share, and latest developments, such as capacity expansions, plant closures, and mergers & acquisitions, are identified as follows [18]:

- Cytodiagnostics Inc. (Canada);

- Goldsol Inc. (Netherlands);

- BBI Solutions OEM Limited (United Kingdom);

- NanoHybrids, Inc. (USA);

- Nanopartz Inc. (USA);

- Nanosphere Inc. (USA);

3. The pure gold market: a pillar for the manufacture of colloidal gold

The Observatory of Economic Complexity (O.E.C.) data visualization informs about the gold trade market. We observe that since the price of gold fluctuates, its variation has a strong impact on the value of trade. It would be more interesting to visualize the
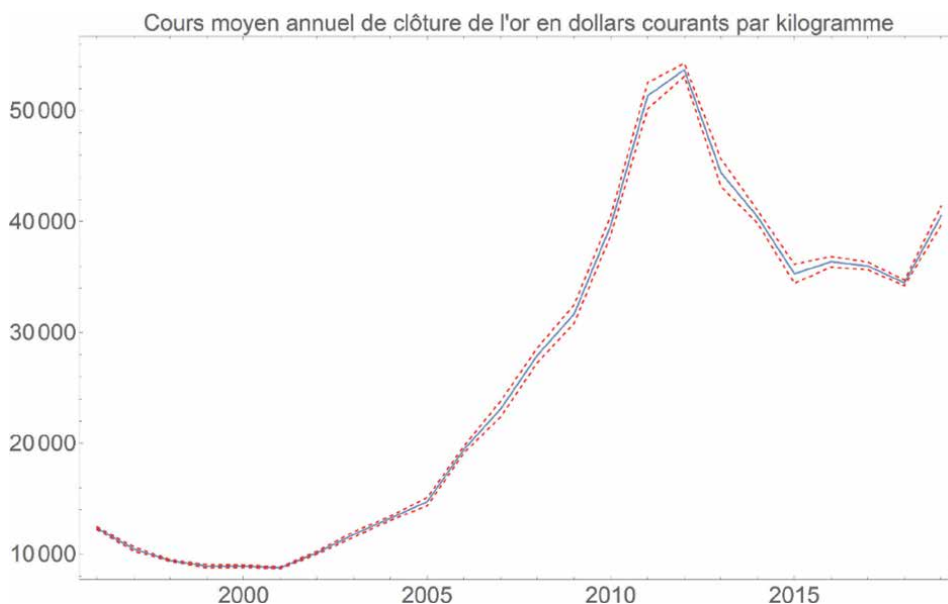
Figure 5.
Evolution of the average annual closing price of gold in current dollars per kilogram between 1996 and 2019.

variations in tons, and not in dollars. To achieve this, it is possible to use the variation in the price of gold between 1996 and 2019 (**Figure 5**). The value used is the average of all monthly closing prices. The years 1995 and 2020 are excluded for lack of value.

In fact, by cross-referencing O.E.C. data with average gold prices, it is possible to estimate the annual tonnage of gold sales between 1996 and 2019 (**Figures 6** and **7**). We observe that gold powder traded is decreasing between 1996 and 2019, while that of gold blocks has reached a kind of ceiling. Moreover, price fluctuation is not a relevant indicator for studying the movement of gold (**Figures 8** and **9**).
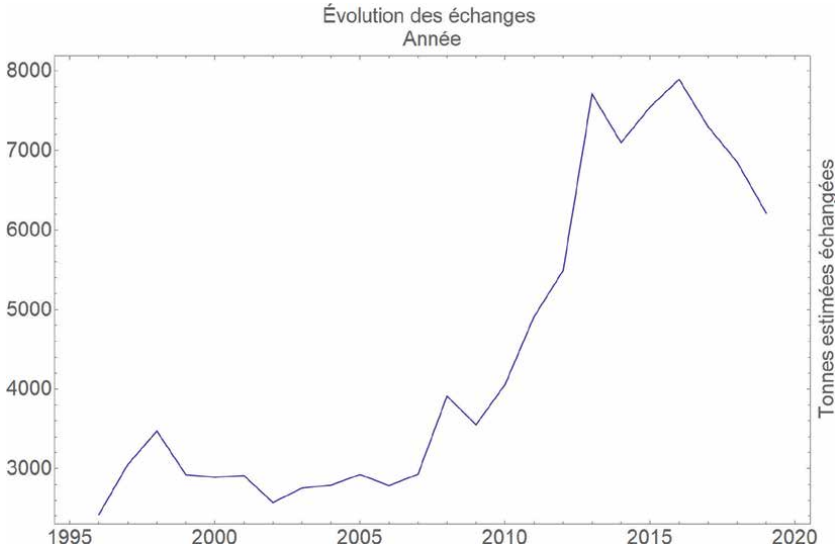
Figure 6.
Evolution of estimated tons of gold traded for gold blocks (710812) between 1996 and 2019.
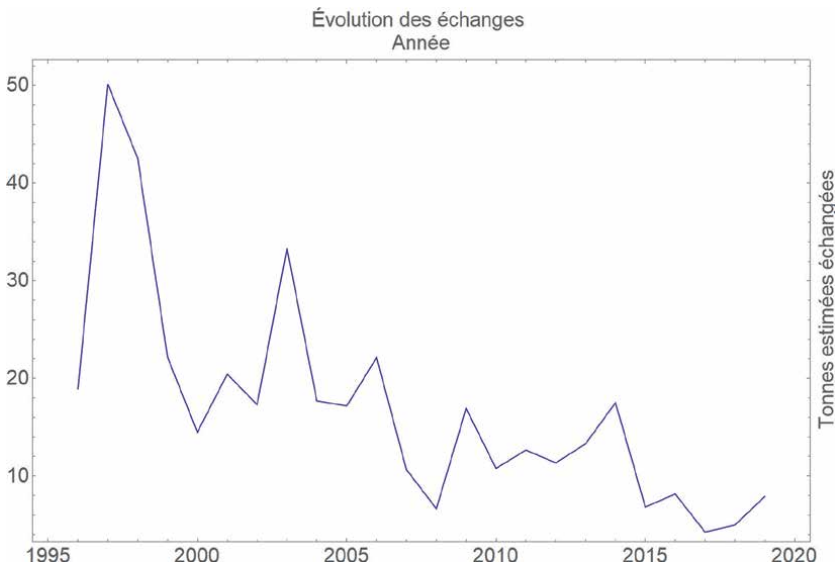
Figure 7.
Evolution of estimated tons of gold traded for gold powder (710811) between 1996 and 2019.
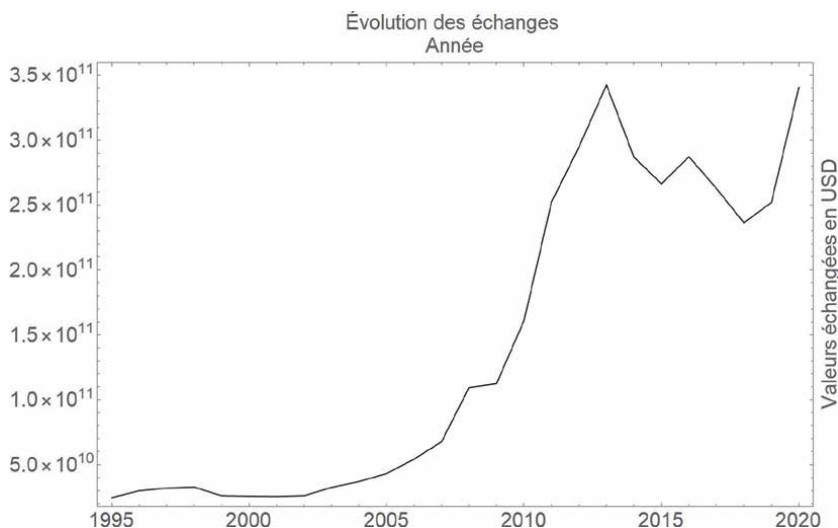
Figure 8.
Evolution of traded values for gold blocks (710812) in current dollars between 1995 and 2019.
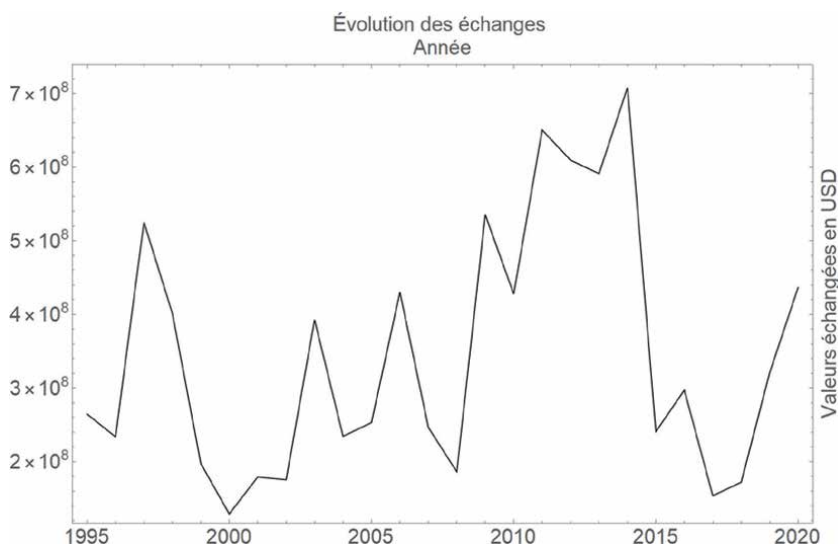
Figure 9.
Change in traded values for gold powder (710811) in current dollars between 1996 and 2019.

A closer analysis of the O.E.C. data tells us that the gold trade is not limited to the products of mining, but also the gold stock in circulation. Regarding the fact that gold stocks are mainly held by central banks, in reality, there is little gold in circulation, apart from the gold produced, but it is difficult to estimate. Moreover, this gold is impure, therefore, it requires treatment to be transformed into colloidal gold. The list of territories trading gold (in powder or blocks) is abundant (191 territories). Thus, it is more interesting to observe the exchanges between the producers and the rest of the world. Producers export little gold powder compared to gold blocks. Few producers import gold: only South Africa, Australia, Canada,

China, the United States, and Turkey. Gold is likely to be a backup resource for producers, as there are still few exports. It is therefore safe to assume that the majority of gold remains in the country.

It is important to note that the price of gold is very fluctuating and volatile due to several factors. The price of gold is estimated twice a day by the LBMA, whose administrator is the ICE Benchmark Administration Ltd. (IBA), which serves as the main global reference since 2015 [19]. Each price definition is based on a comparison of supply and demand. Thus, high demand and a low supply will logically push the LBMA to revise the price of gold upwards, while the opposite case leads to a decrease in the cost of this commodity.

Over the past 25 years, two distinct periods have emerged in terms of gold prices (**Figure 5**). Between 1995 and 2001, gold prices were relatively stable at around $300 to $400 per ounce. In the early 2000s, the U.S. economy was challenged by the bursting of the "dot-com bubble," which led to some huge financial difficulties among powerful companies, and the World Trade Center attacks. That event contributes to the rise in the value of gold, which is highly prized in times of crisis because, it is a safe haven par excellence [20]. Gold is the main asset that every investor, every saver, and every central bank seeks when the economy and finance falter or prediction some economic shocks. All this parameter takes is one or two detonators in an explosive context to trigger a gold rush. This is what happened in the early 2000s, the rise of the gold price was inevitable. Thus, between 2000 and 2006, the price of an ounce of gold doubled.

While prices rose sharply in the early 2000s, the end of the decade marked an economic turnaround that sent the value of gold soaring. With the subprime crisis affecting markets around the world since 2008, investors massively bet on the gold market as a safe haven. The price of the yellow metal was fueled by this, surpassing the $1000 per ounce mark for the first time in history in September 2009. The rise continued until July 2011 when the ounce of gold exceeded $1800. This rise after 2009 is explained by the beginning of the economic recovery: growth and employment are moving forward again, but with their inflationary corollary (loss of value of the dollar). This increase in the price of gold has several origins: the decline of the dollar, the currency in which gold is denominated, very strong demand for gold from countries with growing middle classes, and insufficient supply as stocks are depleted.

From 2012 onwards, the rise in the gold price reversed and begins to decline. There are no longer any major geopolitical conflicts, the dollar has not collapsed, the United States has not defaulted on its debt, the eurozone has not exploded and the stock markets have recovered. From 2012 to 2019, however, prices remain very high, with the value of an ounce fluctuating between about $1000 and $1300. In 2019, the trade war between the U.S. and China and the approaching agreement between the UK and the EU on Brexit are reigniting uncertainty in the markets and pushing prices back up.

The COVID-19 pandemic crisis has accentuated this trend with an ounce passing the sympathetic $2000 mark in July 2020. Since the outbreak of the SARS-CoV-2 virus, the ounce of gold has never fallen below $1700, and the Ukrainian-Russian conflict that began in February 2022 looks set to create a significant political instability in the coming years, leading to a supply crisis in raw materials helping to stabilize a high gold price for years to come.

The main demand for foreign gold purchases by countries around the world comes from central banks. Indeed, by 2021, with over 35,000 tons of gold held in their vaults [21], central banks, and international financial organizations are major players in the gold market. The amount of gold held by central banks corresponds to almost

one-fifth of the gold ever produced. Central banks buy gold bullion and with prices, the data fluctuates according to global economic conditions (**Figures 6** and **8**).

During the 1990s, central banks were net sellers of gold, a behavior that became more pronounced in the late 1990s. From 1999 to 2008, central banks "sold 3884 tons, that is, an annual sales volume of nearly 400 tons, which represents a tonnage greater than the annual production of South Africa, the world's leading producer at the time. Until 2009, central banks were the second-largest source of gold supply after mining. The main declines in central bank gold stocks during this period were observed in France (- 390 tons), Switzerland (- 250 tons), Spain (- 176 tons), and the Netherlands (- 82 tons)" [22].

Central banks changed their tune in 2008 with the financial crisis. Since then, their holdings of yellow metal have increased by nearly 5800 tons, or an average of 415 tons per year. This means that about 11% of the world's mining production ends up in the coffers of these institutions since this time [23]. This buying behavior can be observed particularly among certain central banks in emerging markets, whose demand for gold has increased considerably, favoring a gradual shift in the gold market toward Asia.

Furthermore, gold is strongly correlated to real interest rate levels, that is, the level of interest rates minus the rate of inflation (or more precisely inflation expectations). The correlation is so strong that it is graphically obvious (**Figure 10**). The lower the policy rates, the greater the demand for gold by central banks and the higher the price of gold. This is why we observe graphically a correlation between the volume of gold traded and the value of gold traded in dollars between 1995 and 2019 (**Figures 6** and **8**).

Gold powder has a different use than bullion. Gold powder refers to fine particles of gold, natural or artificially produced. Like the gold leaf, gold in powder form is used for decoration: gilding of jewelry or glassware, paint, makeup, but also food or skin care. The gold powder was also used as currency, particularly in West Africa during the pre-colonial West African empires [24].

The main importers of gold powder are the United Arab Emirates (16 tons), Belgium (10 tons), and Niger (3 tons). The three largest exporters are the Philippines (17 tons), Nigeria (16 tons), and the United States (2 tons) [25]. Since gold powder
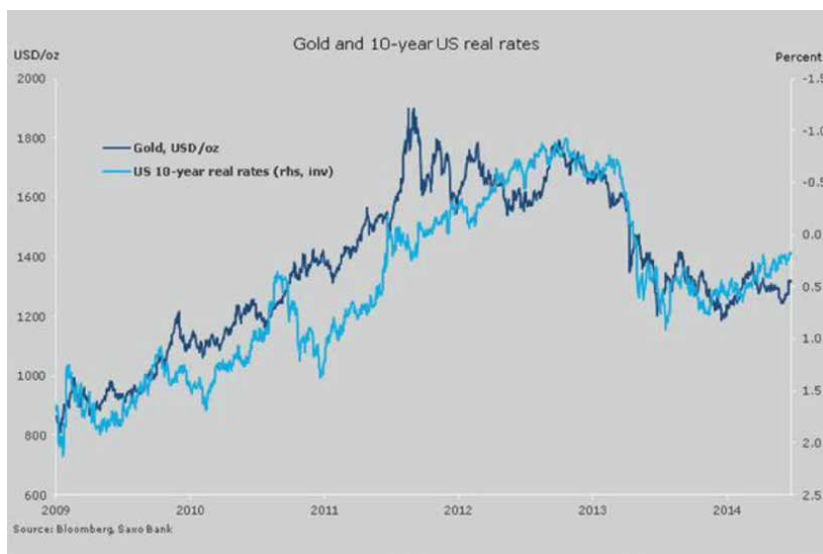

Figure 10.
Evolution of the price of an ounce of gold and the interest rates of the American central bank between 2009 and 2015.

requires a lot of work upstream of production and is used in smaller proportions, exchanges of this type are rarer than for raw gold or bars. Indeed, the share of gold powder trade in global trade is negligible (40 tons in 2021 out of the 4500 traded) [25]. Furthermore, there is no direct correlation between the demand for gold bullion and gold powder. The comparison of the curves in **Figures 6** and **8** with **Figures 7** and **9** confirms this trend. However, data series are available that allow for economic trend analysis of the gold powder economy.

In terms of quantity traded, unlike gold bars, gold powder had significantly higher volumes in the 1990s than in 2000 and 2010 (see **Figure 7**). This is due to the rise of gold-producing countries, such as China, which have taken advantage of their mined resources to produce gold-based manufactured goods, such as jewelry, and then export them. Today, there is a correlation between the position of the gold-producing countries and the gold jewelry exporting countries, which induces that most of the big jewelry producers are not need to import gold for their production. Most gold importing countries buy unmanufactured gold to process it themselves according to the products to be manufactured. However, some gold jewelry-producing countries remain dependent on gold powder imports, including Australia, India, the United Arab Emirates, and Italy (**Figure 11**) [26].

It should be added that the COVID-19 crisis has driven up trade in terms of gold powder. In fact, in 2019, the annual value of gold powder traded was about 10 tons compared to 40 tons in 2021 [25]. This is due to the use of gold powder processed into colloidal gold in antigenic tests for the disease (Part 7).

After having discussed the evolution of the price of gold, the exchange of gold blocks, and gold powder, we will now look at the exchange of gold of all forms according to the countries. **Figures 12–15** are intended to better focus on the major importing and exporting countries of gold in all its forms in the world since 1995.

In 2021, the top five importers of gold are Switzerland (2208 tons), India (1068 tons), the United Kingdom (927 tons), China (821 tons), and Hong Kong (523 tons) [25]. If the fact of seeing four countries producing little or no gold at the top of this ranking is not surprising, the case of China may raise questions. First of all, it should be noted that China is only sixth in the world in terms of gold reserves, with nearly 2000 tons, four times less than the United States. The reason why the Chinese are amassing as much gold as possible is that the Chinese government hopes that its yuan currency can become an international reference currency [27]. This trend has been confirmed since the early 2010s with an explosion in Chinese gold imports (**Figure 15**).

Other gold-producing countries also import large quantities of gold to regulate their economies, such as Australia, the USA, and Canada (see **Figure 15**). Countries

Figure 11.
Share of gold powder imports by country in total world imports by 2020 [26].
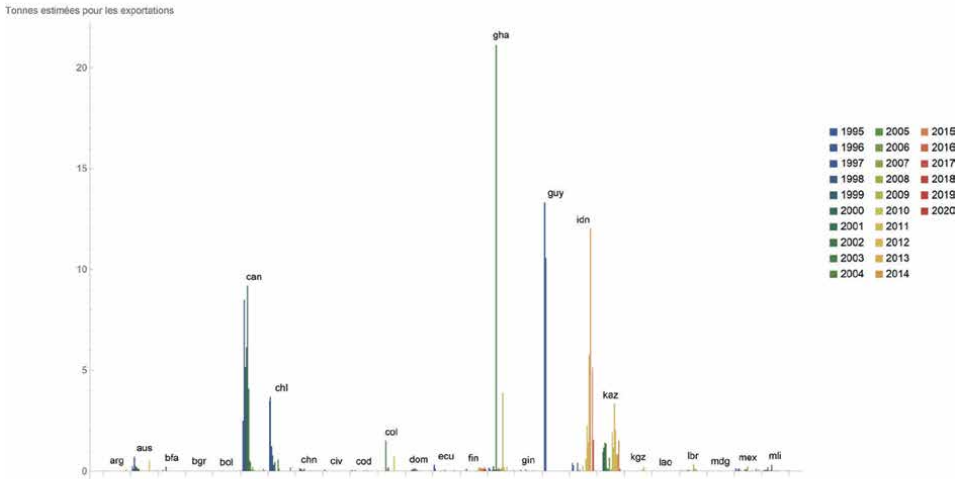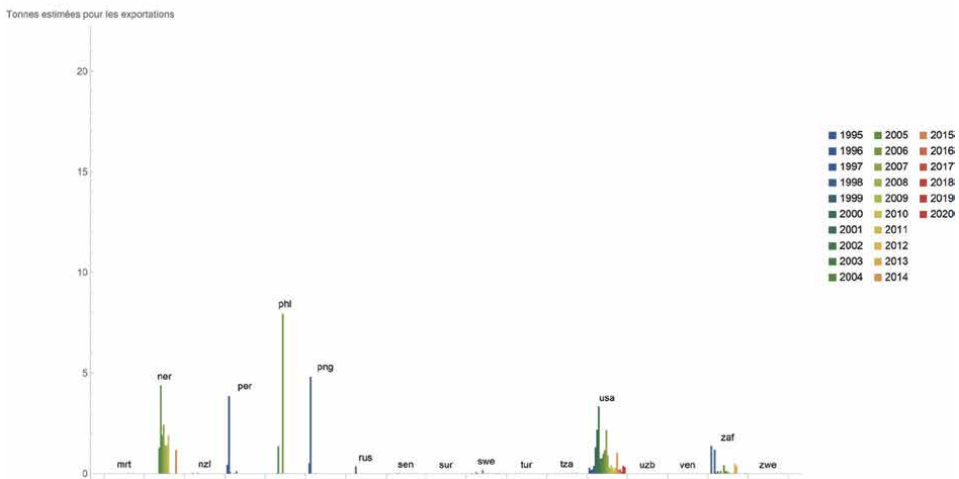
Figure 12.
Evolution of gold powder exports between 1996 and 2019 (tons).

without gold production but with strong economies import gold in large quantities to regulate their economies, manufacture gold-based products, or for gold refining. This is the case of Switzerland, the eighth country in the world in terms of gold reserves, producer of gold jewelry, and first world importer and exporter, with four out of five of the world's largest gold refineries located on its territory.

In 2021, the top five exporters of gold are Switzerland (1500 tons), the United Kingdom (716 tons), Hong Kong (538 tons), United Arab Emirates (487 tons), and the USA (481 tons) [25]. As we have said, Switzerland occupies this position because it is the hub of global gold refining. Expect the USA, all these countries are not among the main gold producers.

Figure 13.
Changes in gold powder imports between 1996 and 2019 (tons).

It may also seem surprising that of these five countries, only one is a major gold-producing country. The observation we can make from the figures is that the major gold-producing countries keep most of their products in their stocks. The need to hold on to one's gold can be seen immediately during periods of crisis, particularly between 2008 and 2012, when all producing countries exported less gold than in previous and subsequent years to limit risk aversion (**Figure 14**).

Smaller countries, on the other hand, will export a larger share of their production to benefit in the short term. This is the case, for example, of Peru or African countries that make significant profits each year by selling their stocks of gold produced rather

Figure 14.
Changes in gold block exports between 1996 and 2019 (tons).

than keeping it in the central bank or by exporting manufactured goods (see **Figure 14**). These resources are vital for these countries. For example, almost 10% of Peru's GDP and 60% of exports emanated from mining in 2018 (Estado [28]).

All these data are fundamental to understanding the colloidal gold market. According to (Inkwood [29]) 13 territories are producing colloidal gold: the United States, Canada, Germany, the United Kingdom, France, Italy, Spain, Russia, China, India, Japan, South Korea, and Australia. It is therefore manufactured in the main industrial countries. However, in this list, only the United States, Canada, Russia, China, and Australia have gold mines. The rest of the territories on the list are totally
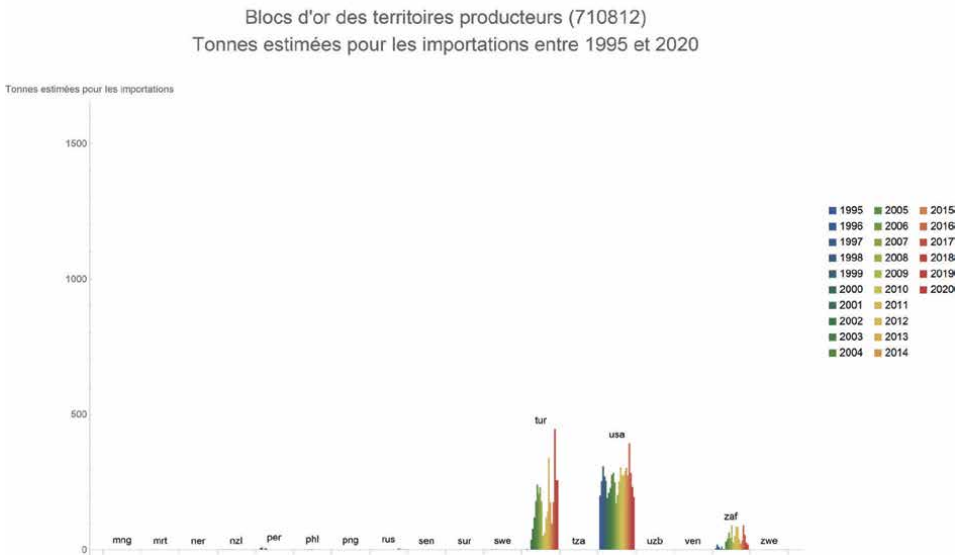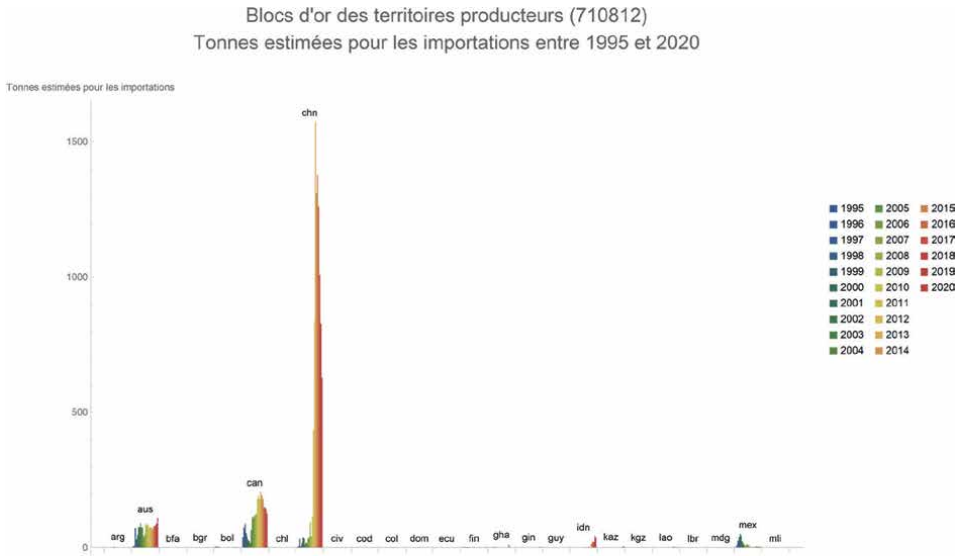
Figure 15.
Changes in gold block imports between 1996 and 2019 (tons).

dependent on their pure gold stocks, on the one hand, and their pure gold imports on the other.

Among the biggest dependents is Europe, where only Bulgaria and Finland produce gold. The main shortcoming of colloidal gold production is the scarcity of raw material on the planet. The production of the precipitate requires only a little pure gold, but it must be available. The value of gold prices remains very high, but there are few exporters among the producing territories.

4. Pandemic and gold demand market in the world

Before discussing the various uses of gold nanoparticles and the inherent markets in more detail, it is first necessary to analyze the behavior of the pure gold market during this period to assess possible correlations with colloidal gold. From the beginning of the pandemic in March 2020 until mid-2021, gold demand reached levels as low as in 2008 during the financial crisis [30]. Between 2019 and 2020, global gold demand declined 14% year-over-year, according to the World Gold Council. The organization says demand for gold jewelry fell 34% from the previous year, reaching a historic low [31]. At the industry level, between 2019 and 2020, the decline in gold demand has been estimated at around 7%.

At the end of 2021, a rebound in global gold demand was noted (+10%) compared to 2020 [10]. Demand for gold jewelry jumped by 67% over the period and represents more than half of the global demand for gold. At the industry level, over this period, an increase in gold demand is measured at around 9%. If a rebound in demand is noted, it remains 8% lower than the pre-pandemic level (**Figure 16**) [10].

At the beginning of the pandemic, the price of gold rose sharply. By the end of the first half of 2020, the price of an ounce of gold surpassed the $2000 mark [32] a peak not seen since the beginning of the century. This price increase is explained by a strong rebound in demand at the end of the various confinements imposed by most countries in the world. The explosion in demand has led to a logical rise in prices, especially as a sharp increase in the cost of maritime freight has been observed. This increase in the price of transport was therefore logically reflected in the routing of raw materials [33].

Moreover, as gold is considered a haven, the number of investments has increased significantly (+40% compared to 2019) during this period of economic crisis and the price of this metal on the stock market has soared [31]. This trend is confirmed by the

Figure 16.
Evolution of the world's gold demand between 2010 and 2021.

figures for the year 2021, where the World Gold Council announces that the demand from central banks has increased by 82% compared to 2020, reaching the number of 35,600 tons of gold stored by them, the highest quantity in over 30 years [10].

5. Gold nanoparticles in manufactured products
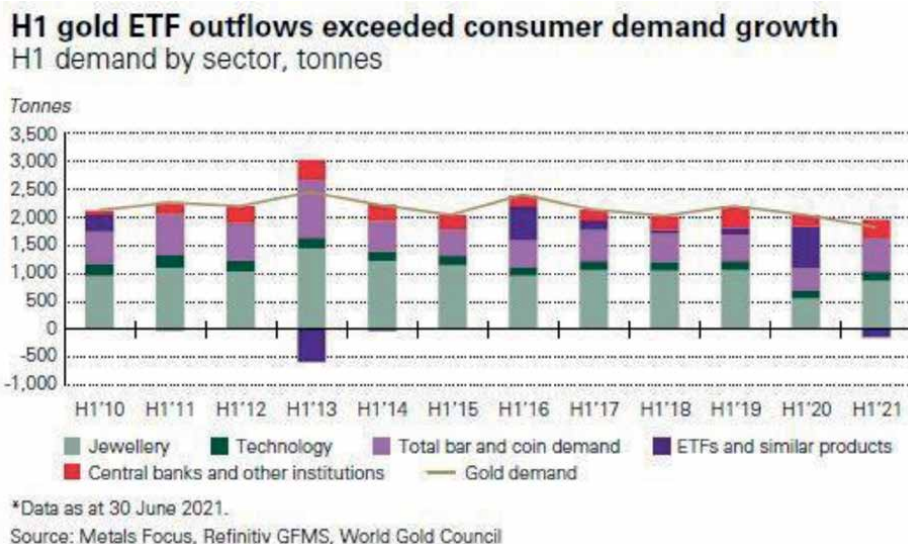
Gold and gold-based alloys are materials used extensively in industry, particularly in electronics and semiconductors. Between 200 and 300 tons of gold are put to use each year within these industries [34]. This important use is linked to its high resistance to corrosion, its good electrical and thermal conductivity, its simple use, its ability to create alloys, and its aptitude for soldering. Gold is mainly used to make contacts, connectors, films for electronic components, and even inks [35].

A small amount of gold is present in almost every electronic device we use daily. These include smartphones, computers, touchscreen tablets, televisions, GPS devices, and the like. While the amount of gold used per device is minute when you consider that nearly a billion smartphones are produced each year, and most of them include gold, the large amount of metal needed by the electronics industry is justified. With the profusion of such devices on the market, this amount is expected to increase in the coming years.

Gold nanoparticles have a more specific use: the miniaturization of components. Manufacturers are beginning to take advantage of the minute size of gold nanoparticles to serve as electronic connectors, particularly via metallic "nanotubes" [35], which are smaller, lighter, and more flexible than conventional metal tubes. The assembly of gold nanoparticles is therefore a technology of the future; as electronic components are constantly being reduced. The technique is already used by major manufacturers, such as Sony, Huawei, and Samsung [36].

This ultra-miniaturization of components using nanotechnology has a name: molecular electronics [37]. This has developed rapidly in recent years with the development of techniques needed to measure the electronic properties of molecules, whether single entities or small ensembles, in a variety of two- and three-electrode test platforms [38]. These testbed junctions have revealed the critical roles played not only by the chemical structure of the molecular component backbone but also by the nature of the contact between the electrode and the molecule [38].

Based on the success of molecular electronics feature measurements in test platforms, the next major challenge to be addressed before molecular electronics can be considered a truly viable and scalable technology is the construction of robust and reliable metal-molecule contacts [38]. A wide variety of molecular functional groups have been tested as contact groups for various substrates (primarily gold), including thiols, amines, carboxylic acids, dithiocarboxylic acids, esters, pyridyl, cyano, isocyano, isothiocyanato, nitro, methylselenide, methylthiol, dimethylphosphine, trimethylsilane, fullerenes, etc. [38].

The second major challenge in molecular electronics is the fabrication of the top contact electrode in metal-organic monolayer-metal devices based on a two-terminal vice. Metallization of organic monolayers has been studied for more than 30 years and, like metal-molecule contact, is still not a well-solved problem. A wide variety of techniques for depositing the top metal electrode have been described in the literature, including direct and indirect evaporation, the use of liquid metals, flip-chip lamination, electrodeposition, and surface diffusion-mediated deposition [38].

6. Trends in gold-containing electronics markets during the pandemic

The COVID-19 pandemic has led to a slowdown in the production chains of industries in countries around the world. Indeed, within OECD countries, production decreased by about 7% between 2019 and 2020. By the end of 2021, production levels had returned to pre-pandemic levels [39]. These difficult months have also had a strong impact on household consumption, with a 6.7% fall in volume in France in 2020 and a 5.2% rebound in 2021 [40].

In the electronics industry, the COVID-19 pandemic has led to unprecedented shortages. This crisis primarily concerns semiconductors, electronic chips necessary for the transmission of information, as well as their processing and storage. Indeed, since the beginning of the year 2020, semiconductor manufacturers are unable to meet the demand [41]. These components are essential in the manufacture of modern everyday goods, such as cars, electronic devices, bank cards, and video games.

Gold is a material used in the manufacture of certain semiconductors [42]. Semiconductor suppliers rely on gold and platinum to make robust electronic components through the alloying of several materials. These precious metals are chosen because they offer the high electrical conductivity and corrosion resistance necessary for superior performance. They also facilitate ohmic contact with the compound semiconductors [43].

With gold concentrations reaching 300–350 g/t for cell phones and 200–250 g/t for printed circuit boards [44] we can say that the amount of gold used per device is extremely low (25 milligrams on average per device). However, with 1.5 billion smartphones sold in 2021 and nearly 6 billion connected devices in operation worldwide, the number of precious metals and gold consumed is high. Indeed, according to these figures, if each electronic device contains 25 mg of gold on average, the total mass of gold present in these objects amounts to 1500 tons. For the simple smartphones sold in 2021, about 340 tons of gold are present (average established according to our estimation).

During the pandemic period, some gold-containing electronics markets slowed down sharply. Between 2019 and 2020, the smartphone market fell by 10.5%, and the new car market by 17%. However, this trend must be qualified. Despite declining production, the demand for electronic products has increased overall. The TV market grew by 1.1% (while projections called for an 8.7% decline in early 2020), the touch tablet market jumped by 13.6%, and the video game market by over 10%.

This discrepancy between a global increase in demand, boosted by the explosion of online trade, and a sharp slowdown in production has therefore led to this crisis in the electronics sector. As far as gold is concerned, it is therefore logical to come to this conclusion: industrialists' need for gold has decreased as a result of the slowdown in production, but in the various markets, demand has increased. Less gold was used in industrial production, but more gold was consumed in the electronics markets. The year 2021 and the beginning of 2022 have confirmed this trend, with demand still strong in the markets and difficulties still present from a production perspective. Semiconductor production demand is expected to increase significantly in the coming years as chips are increasingly integrated into the critical technologies of today and tomorrow.

Consumers are therefore turning more and more to the refurbished electronics market. In France, in 2021, the refurbished smartphone sector has seen a 15% increase, with most customers justifying this choice by the attractive prices charged, the shortages encountered as well as the ecological dimension linked to the reuse of resources, including gold.

7. Use of colloidal gold during the COVID-19 pandemic

As mentioned, the gold and gold nanoparticles sector is not only about electronics but also about health. One of the major challenges of the COVID-19 pandemic was the detection and traceability of people carrying the virus, which was possible through the use of screening tests. Several types of tests were mainly used: antigenic, PCR, and self-tests. The objective of RT-PCR tests is to make a reagent react with the genetic code of the virus (RNA). The antigenic test focuses on the structural proteins of the virus, the spike protein (S), and the nucleocapsid protein (N) [45].

Several types of molecules can be used to detect SARS-CoV-2. The antigenic test procedure consists of depositing a nasopharyngeal swab dipped in a reactive fluid onto a nitrocellulose membrane [46]. The sample is added to a starting zone containing a conjugate detection reagent, which consists of a specific antibody to one of the epitopes of the antigen to be detected and a detection reagent [47]. In principle, any colored particle can be used as a detection reagent, but latex (blue color) or gold nanoparticles (red color) are the most commonly used [48]. This principle is called immunochromatography.

Of the 227 tests approved by the EU (as of July 22, 2022), 44 work with colloidal gold, that is, nearly 20% [49]. During the year 2021, France recorded 168,215,000 tests performed, of which 48.8% were antigenic (82 million tests). Although there are no official statistics on the type of tests performed during the pandemic period, given the large number of samples taken, colloidal gold played a major role in detecting positive cases.

In addition, several studies have shown that gold nanoparticles can have an antiviral function and thus act on SARS-CoV-2 [50]. The scientists relied on other experiments carried out in the past, notably in the context of the treatment of the AIDS virus (HIV) and influenza (flu). Indeed, gold nanoparticles can inhibit the cell fusion of HIV-1 [51]. As for influenza, experiments have shown that gold nanoparticles have an attenuating impact on the infectivity of Influenza-A [52].

Unlike some of the molecules tested during the pandemic, gold nanoparticles have several advantages: they do not induce drug-resistant viral strains and have excellent virucidal properties [53]. However, treatments against SARS-CoV-2 are rarely approved by the authorities. Indeed, only eight treatments have been approved by the European Medicines Agency, and none of them contain gold nanoparticles. In the United States, auranofin, a treatment already on the market and approved by the FDA to relieve rheumatoid arthritis, is one avenue of research scientists are pursuing that could lead to a treatment for SARS-CoV-2 [54].

Colloidal gold and its gold nanoparticles are primarily used for virus detection due to their role in the operation of immunochromatography. While interesting research is being conducted on the antiviral potential of gold on the COVID-19 virus, it is not yet on the market as a treatment or vaccine.

8. Conclusion

To conclude this chapter, we have seen that the gold market is crucial to the global economy. With its multiple applications and its high value due to its scarcity, gold is a material whose production and trade directly impact the currency, stock market, jewelry, and industrial sectors.

The COVID-19 crisis has not spared the gold market, which has seen a significant increase in prices and an overall decrease in demand. While prices have declined in 2021 as most jurisdictions approach a return to normalcy, the gold market is still

feeling the impact in 2022. Prices are rising again and reaching very high levels due to the strong demand for gold-based exchange trade funds (ETFs) and the Russian-Ukrainian conflict. In fact, at the beginning of the war, players in the gold market, which is used as a haven in unstable times, saw demand increase by 34%.

At the end of the COVID-19 crisis and at the beginning of a geopolitical conflict in Europe in February 2022, the gold market is still unstable. The recent increase in interest rates by central banks to fight inflation is pushing players to invest in long-term assets, such as bonds, which is beginning to reduce demand for gold and thus its price. However, the instability of the market is likely to last because of the war in Ukraine, as the conflict has completely disrupted the production channels for raw materials. Prices are therefore nervous and unusually reactive as far as gold is concerned.

In the industry, the semiconductor shortage is here to stay. According to the largest manufacturers, mainly located in Asia, production levels should return to equilibrium at least by the beginning of 2024. In gold, industrial demand in the first quarter of 2022 remained stable. The technology sector has had a promising start to the year: demand is the highest recorded for the first quarter since 2018, thanks to a modest increase in the gold used in electronics.

The issue that is now agitating gold market players and authorities is Russian gold. As we have seen, Russia is one of the world's three largest producers, and the economic sanctions applied call for an outright ban on Russian gold imports, the country's second-largest source of profit after energy. The effect of this measure is to raise gold prices and deprive those who apply it of a preferred gold supplier. The prospect for gold importing countries is to readjust their supply strategies and find gold at a competitive price.

Finally, colloidal gold, which requires little gold and has disruptive functionalities to be exploited in the years to come, particularly in industry and health, should see its market continue to expand despite the current economic shocks. The need for gold nanoparticles during the COVID-19 crisis demonstrated the interest and potential of this technology for scientists and health authorities. As research continues to evolve, more profits could be made from the use of colloidal gold in the years to come, increasing the size of its market and the number of players driving its supply and demand.

Acknowledgements

Author details

Jerome Verny[1*], Ouail Oulmakki[1] and Andrey Hernandez Meza[2]

1 NEOMA Business School, France

2 HighFi Research Lab, Sorbonne-Nouvelle University, France

*Address all correspondence to: jerome.verny@neoma-bs.fr

IntechOpen

References

[1] Turkevich J, Bonner F, Schissler D, Irsa P. Stable and unstable isotopes in catalytic research. Discussions of the Faraday Society. 1950;**8**:352-356

[2] Brust M et al. Synthesis of thiol-derivatised gold nanoparticles in a two-phase Liquid–Liquid system. Journal of the Chemical Society, Chemical Communications. 1994;7:801-802

[3] Perrault SD, Chan WCW. Synthesis and surface modification of highly monodispersed, spherical gold nanoparticles of 50-200 nm. Journal of the Chemical Society, Chemical Communications. 2009;**131**(47):17042-17043

[4] Holkar CR et al. Chapter 14 - Scale-up technologies for advanced nanomaterials for green energy: Feasibilities and challenges. [book auth.] Bharat A. Bhanvase, et al. Nanomaterials for Green Energy. 2018:433-455

[5] Institut des NanoSciences de Paris. 2011. Processus de synthèse de nanoparticules d'or par la méthode de Turkevich. www.images.cnrs.fr. [Online] 2011. Available from: https://images.cnrs.fr/photo/20110001_0895

[6] Yeh Y-C, Creran B, Rotello VM. Gold nanoparticles: Preparation, properties, and applications in bionanotechnology. Nanoscale. 21. 2012;**4**(6):1871-1880

[7] Gu X et al. Preparation and antibacterial properties of gold nanoparticles: A review. Environmental Chemistry Letters. 2020;**19**(24):167-187

[8] Huang D et al. Plastic-compatible low resistance printable gold nanoparticle conductors for flexible electronics. Journal of The Electrochemical Society. 2003;**150**(7):G412-G417

[9] Gilbride B et al. Catalytic ferromagnetic gold nanoparticle immunoassay for the detection and differentiation of Mycobacterium tuberculosis and Mycobacterium bovis. Analytica Chimica Acta. 2021;**1184**

[10] World Gold Council. 2022. Global mine production. gold.org. [Online] 2022. Available from: https://www.gold.org/goldhub/data/gold-production-by-country

[11] Thomsen M. Peak Oil and Peak Gold - The Pundits Got Peak Oil Wrong But Peak Gold May Be Here by Michael Thomsen. 2016. p. 2016

[12] World Gold Council. 2022. Gold Demand Trends Full Year 2021. www.gold.org. Available from: https://www.gold.org/goldhub/research/gold-demand-trends/gold-demand-trends-full-year-2021

[13] World Gold Council. 2022. Gold Market Structure and Flows. www.gold.org. Available from: https://www.gold.org/about-gold/market-structure-and-flows

[14] World Gold Council. 2022. Gold mining. www.gold.org. Available from: https://www.gold.org/gold-supply/gold-mining

[15] World Gold Council. 2022. World gold council members. www.gold.org. Available from: https://www.gold.org/about-us/our-members

[16] World Gold Council. Gold Demand Trends Full Year 2021. www.gold.org. 2022. Available from: https://www.gold.org/goldhub/research/gold-demand-trends/gold-demand-trends-full-year-2021

[17] Lim Z-ZJ et al. Gold nanoparticles in cancer therapy. Acta Pharmacologica Sinica. 2011;**32**:983-990

[18] Expert Market Research. 2022. Global gold nanoparticles market outlook. www.expertmarketresearch.com. [Online] 2022. Available from: https://www.expertmarketresearch.com/reports/gold-nanoparticles-market

[19] ICE Benchmark Administration. 2022. ICE Benchmark Administration and the LBMA Gold Price. www.theice.com. [Online] 2022. Available from: https://www.theice.com/article/iba-lbma-gold-price

[20] Baur DG, McDermott, Thomas KJ. Why is gold a safe haven? Journal of Behavioral and Experimental Finance. 2016;**10**

[21] Reuters. 2022. Why central banks buy gold. www.reuters.com. [Online] 2022. Available from: https://www.reuters.com/article/sponsored/why-central-banks-buy-gold

[22] Aufauvre N. Le marché de l'or et les réserves des banques centrales. Annales des Mines - Réalités industrielles. 2018;**4**:60-65

[23] Chen J. 2020. Global official gold reserves represent 17% of world's stock. www.mining.com. [Online] 2020. Available from: https://www.mining.com/global-official-gold-reserves-represent-17-of-worlds-stock/

[24] National Museum of American History. 2022. Akan gold weight. www.americanhistory.si.edu. [Online] 2022. Available from: https://americanhistory.si.edu/collections/search/object/nmah_1068461

[25] International Trade Centre. 2022. Liste des importateurs pour le produit sélectionné Produit : 7108 Or, y.c. l'or platiné, sous formes brutes ou mi-ouvrées, ou en poudre. www.trademap.org. [Online] 2022. Available from: https://www.trademap.org/Country_SelProduct_TS.aspx?nvpm=2%7c%7c%7c%7c%7c7108%7c%7c%7c4%7c1%7c1%7c1%7c2%7c1%7c2%7c2%7c1%7c1

[26] Observatory of Economic Complexity. 2021. Gold powder non-monetary. www.oec.world. [Online] 2021. Available from: https://oec.world/en/profile/hs/gold-powder-non-monetary?yearSelector2=tradeYear24&growthSelector=value2

[27] Tréguier, Eric. 2013. Si la Chine accumule les lingots d'or, c'est pour mieux imposer sa monnaie, le yuan. www.challenges.fr. [Online] 2013. Available from: https://www.challenges.fr/finance-et-marche/si-la-chine-accumule-les-lingots-d-or-c-est-pour-mieux-imposer-sa-monnaie-le-yuan_1836

[28] Estado Peruano. 2019. Minem: Casi el 10% del PBI y el 61% de las exportaciones del 2018 fueron producto de la minería. www.gob.pe. [Online] 2019. Available from: https://www.gob.pe/institucion/minem/noticias/29754-minem-casi-el-10-del-pbi-y-el-61-de-las-exportaciones-del-2018-fueron-producto-de-la-mineria

[29] Research I. Global gold nanoparticles market forecast. 2019;**2019-2027**:2019

[30] Reuters. 2021. Gold demand has yet to recover fully from COVID-19, says WGC. www.reuters.com. [Online] 2021. Available from: https://www.reuters.com/article/us-gold-demand-wgc-idUSKBN2EZ0B4

[31] World Gold Council. Gold Demand Trends Full year and Q4 2020. www.gold.org. 2021. Available from: https://www.gold.org/goldhub/

research/gold-demand-trends/
gold-demand-trends-full-year-2020

[32] CNBC. 2020. Gold triumphs
record $2,000 per ounce peak on U.S.
stimulus bets. www.cnbc.com. [Online]
2020. Available from: https://www.
cnbc.com/2020/08/04/gold-markets-
coronavirus-dollar-in-focus.html

[33] CNUCED. 2021. Transport maritime:
Pourquoi la covid-19 fait exploser les
taux de fret par porte-conteneurs. www.
unctad.org. [Online] 2021. Available
from: https://unctad.org/fr/news/
transport-maritime-pourquoi-la-covid-
19-fait-exploser-les-taux-de-fret-par-
porte-conteneurs

[34] Comptoir National de l'Or. 2018.
Or et nanotechnologies : de nouveaux
débouchés prometteurs. www.gold.
fr. [Online] 2018. Available from:
https://www.gold.fr/news/2018/06/20/
or-et-nanotechnologies-de-nouveaux-
debouches-prometteurs/

[35] CNRS. Les propriétés uniques de l'or
dans les nanotechnologies : un nouveau
filon pour les scientifiques

[36] Parker PM. The 2022 Report on
Carbon Nanotubes (CNT) Transparent
Conductors: World Market Segmentation
by City. 2021. p. 2021

[37] Ratner MA. Introducing molecular
electronics. Materials Today.
2002;**5**(2):20-27

[38] Osorio HM et al. Preparation of
nascent molecular electronic devices
from gold nanoparticles and terminal
alkyne functionalised monolayer films.
Journal of Materials Chemistry C.
2014;**2**:7348-7355

[39] OCDE. 2022. Production and
sales (MEI). www.stats.oecd.
org. [Online] 2022. Available

from: https://stats.oecd.org/Index.
aspx?DataSetCode=MEI_REAL

[40] INSEE. 2022. En 2021, la
consommation des ménages rebondit
mais reste en deçà de sa tendance d'avant-
crise. www.insee.fr. [Online] 2022.
Available from: https://www.insee.fr/fr/
statistiques/6467002

[41] Marinova G, Bitri A. Challenges and
opportunities for semiconductor and
electronic design automation industry
in post-Covid-19 years. IOP Conference
Series Materials Science and Engineering.
2021;**1208**:1

[42] Ellis Timothy W. The future of
gold in electronics. Gold Bulletin.
2004;**37**(1):66-71

[43] Ivey DG. Platinum metals in ohmic
contacts to III-V semiconductors.
Platinum Metals Review. 1999;**43**(1):2-12

[44] Hagelüken C, Corti CW. Recycling
of gold from electronics: Cost-effective
use through 'Design for Recycling'. Gold
Bulletin. 2010;**43**(3):209-220

[45] Jagtap S et al. Evaluation of spike
protein antigens for SARS-CoV-2
serology. Journal of Virological Methods.
2021;**296**:271-280

[46] Wang X et al. Electrospun
nitrocellulose membrane for
immunochromatographic test strip with
high sensitivity. Microchimica Acta.
2020;**187**:12

[47] Yamaoka Y et al. Highly specific
monoclonal antibodies and epitope
identification against SARS-CoV-2
nucleocapsid protein for antigen
detection tests. Cell Reports Medicine.
2021;**2**:6

[48] Azuma T et al. Thermometric lateral
flow immunoassay with colored latex

beads as reporters for COVID-19 testing. Scientific Reports. 2022, 2022;**12**

[49] European Commission. 2022. EU Common list of COVID-19 antigen tests. pp. 11-45

[50] Sarkar J et al. Antiviral potential of nanoparticles for the treatment of Coronavirus infections. Journal of Trace Elements in Medicine and Biology. 2022;**72**

[51] Kumar V, Ganesan S. Gold nanoparticles as an HIV entry inhibitor. Current HIV Research. 2012;**10**:8

[52] Kim J et al. Porous gold nanoparticles for attenuating infectivity of influenza A virus. Journal of Nanobiotechnology. 2020;**18**:54

[53] Gurunathan S et al. Antiviral potential of nanoparticles-can nanoparticles fight against coronaviruses? Nanomaterials (Basel). 2020;**10**:9

[54] Rothan HA et al. The FDA-approved gold drug auranofin inhibits novel coronavirus (SARS-COV-2) replication and attenuates inflammation in human cells. Virology. 2020;**547**:7-11

Chapter 4

Perspective Chapter: Effect of Gold Seed Layer Annealing on the Surface Roughness and Nanostructure Growth

Younas Iqbal and Mohd Kamarulzaki Bin Mustafa

Abstract

ZnO has gain a great attention in many applications due to its wide band gap. Orientation and alignment of ZnO nanorods are the key objectives of fundamental applied research. They may be produced by both physical and chemical methods, however the chemical method has the advantages of low temperature and pressure conditions. The electronic properties of ZnO nanorods are more superior then the thin films. Most of the applications of ZnO nanorods depends on the morphology, orientation and interspacing among them. Seed layer on the substrate has a key role in the morphology of ZnO nanorods. In this chapter the, orientation, alignment and a clear mechanism of ZnO nanorods production in hydrothermal method is presented. The experimental results deduced that the ZnO nanorods are produced in the precursor solution and move down to the substrate through 001 face stab between the successive grains generated through annealing of gold seed layer, and as a result an oriented and aligned array of the nanorods are formed on the substrate.

Keywords: ZnO, nanorods, orientation

1. Introduction

ZnO is a distinctive material and has been extensively studied by researchers for its potential in variety of applications such as piezoelectric, pyroelectric, dielectric, plate panel display sensor devices, field effect transistor and ultraviolet light emitting devices [1]. In nanostructure form, ZnO is extensively explored over the past decades exhibit unique properties as compared to its bulk form. Nanostructured ZnO consists of structures with in a range of 100 nm in diameter [2]. Zinc oxide is a compound semiconductor which consists of Zn^{+2} and O^{-2}. Zinc belongs to group II of transition metals and oxygen to group VI element, therefore it is called a metal oxide semiconductor. The nanostructured materials have been broadly studied due to their potential uses in fabricated micro and nanoscale devices. The research on ZnO peaked around the end of 1970s and the start of 1980s. The field is incited by theoretical predictions and feasibly experimental conformations of ferromagnetism at room temperature

for potential spintronics applications. Then the interest was ended, partly because it was not possible to dope ZnO both n- and p-type, which is a crucial requirement for applications of ZnO in optoelectronics, and the interested moved to structures of reduced dimensionality. Scientists have created numerous nanostructures, but it is unknown which type nanostructure is ideal for electronic and optoelectronic device applications. The ZnO thin film has a vital role in sensors, catalyst and transducer since 1960. **Figure 1** indicates that the literature survey about ZnO nanomaterials increasing significantly for the chemical and gas sensors [3, 4].

The special properties of 1D ZnO nanostructures are their chemical stability, and electrochemical selectivity that provide an adjustable platform essential for the sensors. Therefore, the ZnO nanostructures NRs/SWs are extensively investigated for gas sensor, humidity sensor, biosensor, biomarker, pressure/force/load sensors, pH sensors and UV sensors. During the last decades nanotechnology has focused its attention to one dimensional (1-D) materials. By reducing the size to nanoscale, novel electrical, optical, mechanical, and chemical properties are introduced, which are mostly believed to be the increase surface area and quantum confinement effect. For instance, it has been experimentally proved that single crystalline ZnO nanorods can have an electron field mobility 10 times greater than ZnO thin film transistor.

This chapter presents the importance of oriented zinc oxide (ZnO) nanorods in various applications and devices. ZnO is a semiconducting material at room temperature, has a wide direct band gap (3.37 eV) and a large exciton binding energy (60 meV) [5]. The high exciton binding energy (60 meV) of ZnO at room temperature is responsible for stable electron–hole pair recombination and excellent luminescence properties. The wide band gap materials are more effective in high temperature and high power applications for their ability to withstand high power due to their substantially higher breakdown voltage.

The performance of nanoscale optoelectronic devices and biosensing are significantly influenced by orientation and alignment of ZnO nanorods, however despite
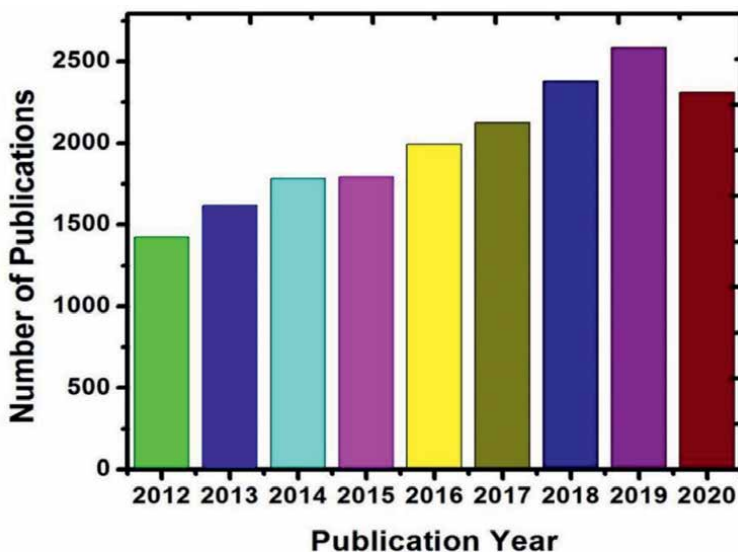

Figure 1.
Web of knowledge database lists on the number of publications of ZnO nanostructures for chemical and gas sensors.

of prodigious research there is no clear mechanism for the formation and orientation of ZnO nanorods has been identified. In this study the oriented ZnO nanorods were fabricated through hydrothermal technique from the lowest precursor concentration. The concentrations of precursors were varied from 1 to 9 mM at same deposition temperature (90°C) and time (6 hours) on annealed and un annealed gold coated substrate. The root mean square roughness of the seed layer increased from 6.11 to 8.839 nm through annealing at 500°C.

Recently, the well-aligned ZnO nanorods have obtained a lot of curiosity due to their potential demand in nanodevices for electronics, optoelectronics, photonics, and electrochemical nanodevices [6]. A lot of effort has gone into getting the aligned and controlled morphology of the ZnO nanostructures. The use of well aligned ZnO nanorods has motivated the researchers to control the alignment of ZnO nanorods for the performance of nanoscaled-based optoelectronics devices [7], nanolaser [8], chemical and gas sensor [9], solar cell [10] and Schottky diodes [11]. The need and advantage of ZnO nanorods to be aligned in biosensing applications is to make way to attachment of antibodies on a maximum number of sites on the nanorods in a way to improve the sensitivity of the device. The nanorod overlapping could prevent antibodies from adhering to the spot if the nanorods are not well aligned. The orientation and uniform spacing of ZnO nanorods can also improve the light ensnaring and charge separation in polymer solar cell, and a result the efficiency and field emission characteristics are significantly enhanced [12]. The vertically aligned ZnO nanorods creates more surface defects and oxygen vacancies, have a better photocatalytic efficiency due to their increased specific surface area, which makes the nanorod an effective photocatalyst in photocatalytic applications [13]. By growing vertically oriented ZnO nanorods there is a probability to increase the electron transport rate [14]. Lattice matching of the substrate with ZnO is a key factor for the synthesizing of vertical aligned nanorods. Wenjie Mai et al. [15] used several substrates (GaN, SiC, Si, and sapphire), and concluded that the vertical aligned wurtzite ZnO (a = 0.3249 nm, c = 0.5207 nm) nanorods can be produced on wurtzite SiC (a = 0.3076 nm, c = 0.3046 nm) and GaN (0.3189 nm, 0.5185 nm) Fan et al. [16] used GaN and sapphire, to produce the vertical aligned ZnO nanowires and concluded that GaN is more suitable for the growth of aligned nanorods due the similar crystal structure and lattice matching. There are some recent researches reported on the growth of oriented ZnO nanorods on Transparent conducting oxide (TCO) glass substrates 1.e FTO (F-doped SnO), ITO (Sn doped In_2O_3) and IZO:Ga without using. The results indicated that the orientation and alignment of ZnO nanorods on IZO:Ga is more better than the other two with a sequence i.e. ITO < FTO < IZO:Ga.

2. Preference of 1-D ZnO on other nanostructures

The research on the nanostructures is increased after the discovery of carbon nanotubes in 1991. ZnO was investigated in 1912 for the first time, however its practical applications were focused after discovering its piezoelectric properties in 1960 [17], this resulted in the first electronic use of zinc oxide as a thin layer for surface acoustic wave devices. After significant research phases in the 1950s and 1970s, zinc oxide as a semiconducting material is currently experiencing a revival. The electrical and optical properties ZnO with pencil like crystal with hexagonal shape were reported in 1960. After that a variety of nanostructures (Plates, columns, pyramids, spheres, stellar-shaped crystals, dendrites and whiskers) were obtained by Yamada

and Tobisawa under extreme nonequilibrium conditions of a converging shock-wave using an explosive charge [18]. The size of nanostructure is in between the range of 1–100 nm (100,000 times smaller than the human hair diameter). ZnO is one of the mostly research metal oxide. It is an inorganic semiconducting material that is rarely seen in nature and appears as a white crystalline powder. ZnO is usually referred to as zinc white because it appears as a "white powder." Due to the presence of manganese and/or other impurities, it can seem yellow to reddish. Zinc, like magnesium and iron, is a naturally occurring metallic element and is found in the body's and skin and is essential for maintaining health and balance. Since the discovery of quantum confinement effect that enhanced the properties of bulk material, this material the attention due to its large number of nanostructures (Nanoparticle, nanostrips, nanorods, nanowires, nanorings, nanocombs, nanocages nanosprings) [19].

With the discovery of semiconducting metal oxide nanobelts in 2001, the one dimensional nanostructures has attracted the attention due to their unique applications in optoelectronics, optics, catalysis and piezoelectricity [19]. Nanostructures have a large surface area, and surface processes have a big influence on electronic processes. The uniform and ordered growth of ZnO nanostructures is highly desirable and is potentially applicable in many devices, however the complex, morphologies of ZnO nanostructures complicate their functionality, i.e. limit their practical applications [20]. The 1-D ZnO nanostructures can provide a favorable combination of chemical selectivity, electrochemically and chemically tunable platform for the sensor response. This leads the 1-D ZnO nanostructures an active candidate for potential applications in gas sensor, biosensor, biomarkers, humidity sensor, pH sensor, chemical sensors and UV sensors due to their high surface area and low cost of fabrication. In the last few decades nanotechnology has focused its attention to one dimensional (1-D) materials. By reducing the size to nanoscale, novel optical, mechanical, chemical and electrical properties are introduced, which are mostly believed to be the increase surface area and quantum confinement effect. For instance, it has proved that the electron field mobility of single crystalline ZnO nanorod can be 10 times higher than that of ZnO thin film transistors [21]. 1-D ZnO is one of the most intensively studied nanorods (NRs) material. Peulon, was the first who developed ZnO nanorods in 1996 using an electrodeposition method. Direct carrier conduction path and large surface to volume ratio of 1-D ZnO nanostructures are the key factors in getting an edge over other types of nanostructures. ZnO nanorods are flexible metal oxide nanomaterials which have been successfully used in different fields such as chemical and biological sensing, optoelectronics, energy harvesting and ultraviolet (UV) photodetection [22]. ZnO nanorods are potential material for optoelectronic applications due to have less defects then thin-film structures.

3. Effect of annealing on gold seed layer and orientation of ZnO

3.1 Chromium (Cr) and Gold Seed layer annealing

The ZnO nanorods were produced on two substrates with different roughness through same synthesis method and using same parameters. A Cr/Au (20/50 nm) coated glass substrates were selected for the growth of ZnO nanorods. Some of the Cr/Au (20/50 nm) coated glass substrates were subjected to a preheated oven, annealed at 500°C for 30 minutes. The seed layer is annealed for three reasons: increased adhesion strength, improved crystallinity, density of peaks and valleys [23, 24] and
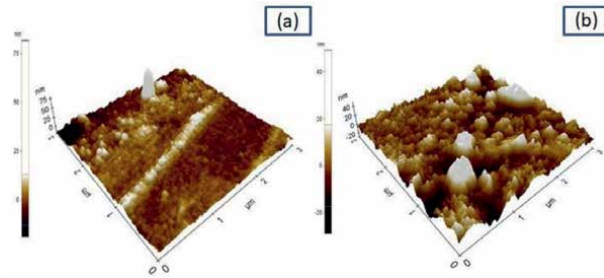
Figure 2.
AFM images of Au seed layer roughness (a) Un annealed and (b) Annealed.

roughness. The 3D, AFM images of annealed and un annealed Cr/Au coated glass substrate is shown in **Figure 2**, where different colors on the seed layer image corresponds to different height structures. The Au seed layer for nonannealed sample is non continues with large void spaces and less heights entity (maximum height 20 nm). The Au seed layer is substantially rebuilt, its surface morphology changes, and islands of various sizes are created after 30 minutes of annealing at 500°C. The annealed seed layer, which is crystalline and has several grains, offers sites where ZnO nanorods can be oriented. The increase in the diffusion of gold particles at high temperatures and their agglomeration into massive structures may be the cause of this alteration after annealing.

In **Table 1** various roughness parameters, Rpv, Rq, Ra, and RZ represent peak to valley value (difference between minimum and maximum), root mean square roughness, roughness average, and 10 points average, which is the arithmetic of 5 highest peaks and 5 lowest valleys in line, respectively, the Min and Max values represent the deepest valley and highest peaks in the scanned area. **Table 1** represents that the root mean square roughness (Rq) and roughness average are increase from 6.771 to 8.839 nm and 4.074 to6.506 nm respectively.

3.2 ZnO nanorods growth

ZnO nanorods produced on both annealed and un annealed Cr/Au seed layer present a completely different morphology as discussed by Mustafa et al. [25] and Younas et al. [26]. The nanorods produced on annealed Cr/Au seed layer has better orientation then the nanorods produced on un annealed seed layer with same precursors concentration as shown in **Figures 3** and **4**. **Figure 3** shows FESEM images of nanorods produced on un annealed seed layer from 8 mM precursors concentration zinc nitrate hexahydrate $(Zn(NO_3)_26H_2O)$ and hexamethylenetetramine $(C_6H_{12}N_4)$, at same deposition time and temperature at various magnifications. The $(Zn(NO_3)_26H_2O)$ provide the Zn^{2+} ion essential for the production of ZnO nanorods,

Surface parameters	R_{pv}(nm)	R_a(nm)	R_Z(nm)	R_q(nm)	Max(nm)	Min(nm)	Mid(nm)
Annealed	78.008	6.506	76.503	8.839	49.184	−28.824	10.180
Un Annealed	100.734	4.074	98.954	6.711	81.694	−19.040	31.327

Table 1.
The various roughness parameters of annealed and un-annealed seed layer.
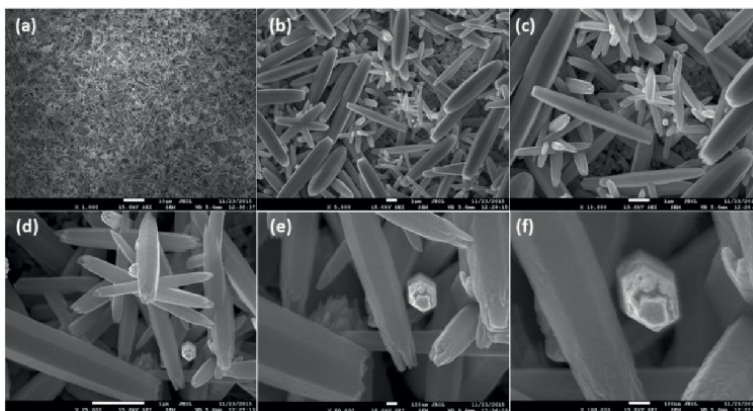
Figure 3.
Surface morphology of ZnO nanorods for 8 mM produced on un annealed seed layer at (a) 1000× (b) 5000× (c) 10,000 (d) 25,000 (e) 50,000 (f) 100,000 magnifications.
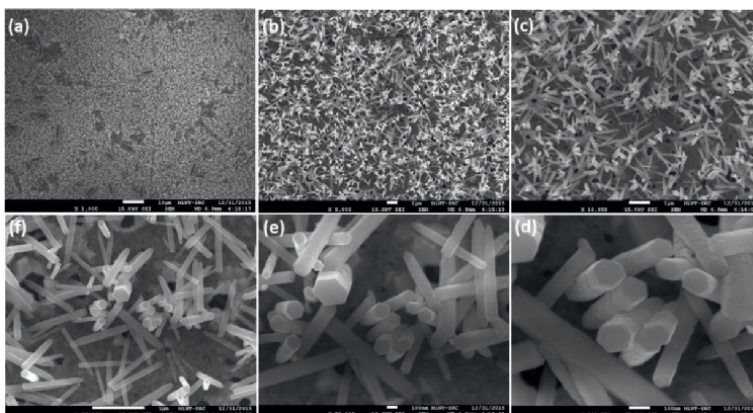
Figure 4.
Surface morphology of ZnO nanorods for 8 mM produced on annealed seed layer at (a) 1000× (b) 5000× (c) 10,000 (d) 25,000 (e) 50,000 (f) 100,000 magnification.

whereas the hexamethylenetetramine is used for capping the non-polar facets and providing the hydroxide source.

As can be seen in **Figure 4**, with the same concentrations, deposition times, and temperatures as the un annealed gold seed layer, the nanorods formed at the annealed seed layer have better alignment. The lower magnification image of **Figures 3(a)** and **4(a)** indicates that whole substrates are filled with dense nanorods.

The improvement in orientation and alignment of nanorods confirm that the ZnO nanorods synthesized in hydrothermal method does not grow on the substrate, but these nanorods are formed in the solution, and when these nanorods become denser they come down in solution through (002) face collected on the substrate. It means that along with heterogeneous growth of ZnO nanorods on the substrate there is a homogeneous nucleation of ZnO nanorods inside the solution along the polar axis. The homogeneous nucleation starts inside the solution and terminate the growth on a substrate by heterogeneous nucleation. In **Figure 4** some nanorods penetrates into other which confirm that the ZnO nanorods formed in growth solution are not
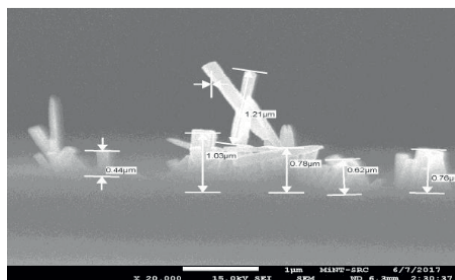
Figure 5.
Cross section representation ZnO nanorods at 8 mM precursor solution.

in completely solid form, but are in soft crustal which become harder and rigid with growth time and cooling.

The main reason for the growth in (001) polar faces is that the wurtzite ZnO is electrostatically unstable and as a result redistributes its surface charge and lowers its surface energy. **Figure 5** shows the presence of a few additional nanorods fall upon the initially formed nanorods film from the growth solution, reveals that the formation nanorods are started in the growth solution.

4. Internal mechanism of ZnO nanorods growth and orientation

The main reasons for the researchers trying to produce the vertically aligned ZnO nanorods are their best performance in nanoscaled-based laser [27] Optoelectronic devices [7] solar cells [28] and Schottky diodes [29]. In literature, various techniques with their benefits and drawbacks have been employed for the deposition of vertically aligned nanorods, however they required a very sophisticated equipment and manufacturing process. In order to produce well aligned and oriented ZnO nanorods of a substrate, a seed layer is sprayed before the nanorods growth. The seed layer surfaces are either positive or negative charged, therefore will attract ions of opposite charges (Zn^{+2} or OH-1). These ions will successively attract ion with opposite charge to cover the surface and will react to form ZnO. Thus the nanorods grow layer by layer promoting good alignment. ZnO has polar (001, 00-1) and nonpolar surfaces {01-1, 2-1-1}. At the beginning there are both lateral and axial growth through the nonpolar and polar surfaces respectively, however when the nanorods growth reached certain limit then the axial growth is more significant than lateral growth. The preferred direction is along the (001) direction because the dipole moment is along this direction.

The high atomic organization order, which provides sites for heterogeneous ZnO nanorods nucleation on the substrates, is responsible for this behavior. The initial growth of the nanorods is started on the grains produced on the annealed substrate, and further growth is proceeded by the heterogeneous nucleation in the solution. It's also possible that some of the nanorods growth took place in the fluid through homogenous nucleation, and then fall down on the seed layered substrate [26]. The increase of the nucleation sites on the annealed seed layer improves the alignment and orientation of the nanorods. As a result of the energetically advantageous nucleation sites for heterogeneous nucleation, oriented nanorods are generated on annealed gold seed multilayer substrates, as shown in **Figure 6**. The exposed basal planes of ZnO nanorods are polar, attracts more ion species due to high surface energy and as a result
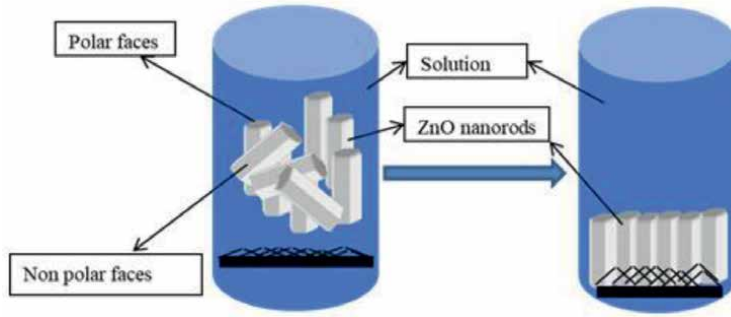
Figure 6.
Proposed growth mechanism of ZnO nanorods in hydrothermal method.

faster growth occurs in this direction through homogeneous nucleation in the growth solution and there is probability of vertically aligned ZnO nanorods to be produced. The developed nanorods become denser with the passage of time and as a result come down in the solution towards the substrate and penetrate between the grains produced due to the annealing, and as a result an oriented and aligned nanorods array is produced on the substrate.

5. Conclusion

The 1D nanostructure of ZnO (nanorods) has been used for a variety of applications due to their high surface to volume ratio, novel electrical properties and electronic conduction. The shape and configuration of ZnO nanorods plays a vital role in its performance and device application. The ZnO nanorods produced on annealed and un annealed gold seed layer reveals that nanorods produced on annealed seed layer has a better alignment and orientation as compared to the nanorods produced on un annealed seed layer. In this chapter the role and importance of the seed layer roughness on the orientation and alignment is presented. A proposed mechanism for the production of ZnO nanorods through hydrothermal method is presented.

Author details

Younas Iqbal[1,2,3]* and Mohd Kamarulzaki Bin Mustafa[2,3]

1 Microelectronics and Nanotechnology, Shamsuddin Research Centre, University Tun Hussein Onn, Malaysia

2 Institute for Computational Materials Science, School of Physics and Electronics, Henan University, Kaifeng, China

3 Engineering Research Center for Nanomaterials, Henan University, Kaifeng, China

*Address all correspondence to: younasiqbal48@yahoo.com

IntechOpen

References

[1] Kim DY et al. The properties of plasma-enhanced atomic layer deposition (ALD) ZnO thin films and comparison with thermal ALD. Applied Surface Science. 2011;**257**:3776-3779

[2] Pei LZ et al. Single crystalline ZnO nanorods grown by a simple hydrothermal process. Materials Characterization. 2009;**60**(9):1063-1067

[3] Sberveglieri V. ZnO quasi-1D nanostructures: Synthesis, modeling, and properties for applications in conductometric chemical sensors. Chemosensors. 2016;**4**

[4] Drmosh QA et al. Zinc oxide-based acetone gas sensors for breath analysis: A review. Chemistry, an Asian Journal. 2021;**16**(12):1519-1538

[5] Stachowicz M et al. Nonpolar short-period ZnO/MgO superlattices: Radiative excitons analysis. Journal of Luminescence. 2021;**238**:118288

[6] Zhang Y et al. Synthesis, characterization, and applications of ZnO nanowires. Journal of Nanomaterials. 2012;**2012**:624520

[7] Khun K et al. Fabrication of well-aligned ZNO nanorods using a composite seed layer of zno nanoparticles and chitosan polymer. Materials (Basel). 2013;**6**(10):4361-4374

[8] Zhang Y, Russo RE, Mao SS. Quantum efficiency of ZNO nanowire nanolasers. Applied Physics Letters. 2005;**87**(LBNL-58315; Journal ID: ISSN 0003-6951; APPLAB; R&D Project: 00000; TRN: US200815%%792):Medium: X

[9] Caicedo N et al. Detection mechanism in highly sensitive ZnO nanowires network gas sensors. Sensors and Actuators B: Chemical. 2019;**297**:126602

[10] Sufyan M et al. Hydrothermally synthesize zinc oxide (ZnO) nanorods as an effective photoanode material for third-generation Dye-sensitized solar cells (DSSCs). Materials Letters. 2021;**297**:130017

[11] Khan A et al. Analysis of junction properties of gold–zinc oxide nanorods-based Schottky diode by means of frequency dependent electrical characterization on textile. Journal of Materials Science. 2014;**49**(9):3434-3441

[12] Cao Y-T et al. The photoluminescence, field emission and femtosecond nonlinear absorption properties of Al-doped ZnO nanowires, nanobelts, and nanoplane-cone morphologies. RSC Advances. 2019;**9**(59):34547-34558

[13] Ji B et al. Vertically aligned ZnO@ZnS nanorod chip with improved photocatalytic activity for antibiotics degradation. ACS Applied Nano Materials. 2018;**1**(2):793-799

[14] Winantyo R, Murakami K. ZnO nanorods formation for dye-sensitized solar cells applications. International Journal of Technology. 2017;**8**(8): 1462-1469

[15] Mai W et al. Vertically aligned ZnO nanowire arrays on GaN and SiC substrates. Chemical Physics Letters. 2008;**460**:253-256

[16] Fan H et al. Patterned growth of aligned ZnO nanowire arrays on sapphire and GaN layers. Superlattices and Microstructures. 2004;**36**(1):95-105

[17] Ellmer K, Klein A. ZnO and its applications, in transparent conductive

zinc oxide: Basics and applications in thin film solar cells. In: Ellmer K, Klein A, Rech B, editors. Springer. Berlin Heidelberg: Berlin, Heidelberg; 2008. pp. 1-33

[18] Yamada K, Tobisawa S. Fine crystals of zinc oxide formed by a conically converging shock-wave technique. Journal of Applied Physics. 1989;**66**(11):5309-5314

[19] Wang ZL. Nanostructures of zinc oxide. Materials Today. 2004;**7**(6):26-33

[20] Khranovskyy V, Yakimova R. Morphology engineering of ZnO nanostructures. Physica B: Condensed Matter. 2012;**407**(10):1533-1537

[21] Borysiewicz M. ZnO as a functional material, a review. Crystals. 2019;**9**:505

[22] Sha R et al. ZnO nano-structured based devices for chemical and optical sensing applications. Sensors and Actuators Reports. 2022;**4**:100098

[23] Weintraub BA. One-dimensional zinc oxide nanomaterials synthesis and photovoltaic applications. Georgia Institute of Technology; 2010

[24] Lu L et al. Effects of annealing conditions on the photoelectrochemical properties of dye-sensitized solar cells made with ZnO nanoparticles. Solar Energy. 2010;**84**(5):844-853

[25] Mustafa M et al. Effect of precursor's concentration on structure and morphology of ZnO nanorods synthesized through hydrothermal method on gold surface. AIP Conference Proceedings. 2017. AIP Publishing LLC

[26] Iqbal Y et al. Orientation and actual growth mechanism of ZnO nanorods through hydrothermal method on gold seed layer. AIP Advances. 2021;**11**(12):125006

[27] Chou Y-H et al. Ultrastrong mode confinement in ZNO surface plasmon nanolasers. ACS Nano. 2015;**9**(4):3978-3983

[28] Lin MY et al. Well-aligned vertically oriented ZnO nanorod arrays and their application in inverted small molecule solar cells. Journal of Visualized Experiments. 2018;**134**

[29] Yuan Z. Low-temperature growth of well-aligned ZnO nanorod arrays by chemical bath deposition for Schottky diode application. Journal of Electronic Materials. 2015;**44**(4):1187-1191

Chapter 5

Microbial Fuel Cell Formulation from Nano-Composites

Fozia Anjum, Nadia Akram, Samreen Gul Khan,
Naheed Akhter, Muhammad Shahid and Fatma Hussain

Abstract

Petroleum and oil industry is a rich source of nonrenewable energy that ultimately results in threatening of ecosystem due to emission of greenhouse gases into the environment. In the current panorama of the energy demand, industries focus on alternate and renewable energy resources to meet energy gaps. Thus, an expedient fuel cell based on microbes can be valued as an economical and eco-friendly substitute of energy generator. These microbial fuel cells have commercialized platinum electrodes to generate cost-effective energy after oxidation of organic wastes catalyzed by biocatalyst. Nowadays, conventional carbon electrode as an anode is taking popularity in microbial fuel cell but displays poor performance. So, to improve the chemistry of electrodes, nano-composites fabricated from polar polymeric material as well as cost-effective oxides of metals are the raw material. In this chapter, green synthesis of nano-composites from conducting polymers and oxides of transition metals has been discussed. Anode modification by composite to treat wastewater as well as its role to generate electricity has been discussed briefly.

Keywords: microbes, fuel cell, organic wastes, biocatalyst, transition metal oxides

1. Introduction

At present, the world is facing the crisis of energy as a result of overpopulation in the world. With the passage of time, enormous numbers of industries are increasing that result in the dire need of energy. In the past, scientists introduced number of alternative energy dynamics such as energy generation or conversion by using gravitational force, water, water waves, heat, wind, and solar rays, but these resources could not fulfill the energy requirements [1]. So it is the time to stimulate the research objectives to generate or explore the green, eco-friendly, and renewable energy alternatives that not only meet the energy demands but also encourage the environmental factors such as organic waste utilization that ultimately reduce the burden on the land. These environmental concerns have invigorated the scientists to look into sustainable, ecofriendly, and renewable energy or power-generating categories such as microbial fuel cells [2–4].

2. Microbial fuel cells

Microbial fuel cells are tools that play with microbial activities as biocatalyst for the inter-conversion of electrical and chemical energy involving electron transfer between two electrodes in the presence of proton exchange membrane under optimized conditions comparable with natural environment [2–4]. Microbial fuel cells are catalyzed by microbes for conversion of energy into power generation more efficiently. These microbes such as bacteria, fungi, and algae can utilize any organic matter as substrate and oxidize them to generate energy without involving any intermediate step for domestic, industrial power generation and wastewater treatment [5]. By utilizing microbial redox reaction of substrate in conjunction with chemical and electrical energy, microbial fuel cells, a promising innovation, can be revolutionized to recycle heat energy of natural as well as man-made resources into electrical energy without emission of any greenhouse gases [6, 7].

2.1 Microorganisms used for MFCs

A number of microbes such as members of Proteobacteria, Cytophagales, Firmicutes, Acidobacteria, strains of yeast strains such as *Saccharomyces cerevisiae* [8], *Candida melibiosica* [9, 10], *Hansenula* anomala [11], *Pseudopalaina polymorpha* [12]), and Blastobotrys adeninivorans [13] have potential to transfer electrons produced from metabolism to generate electricity [14]. These microbes can be isolated, purified, and identified from naval sedimentation, loam, running water sediments, wastewater, and activated sludge [15–17]. These microbes, particularly some strains of bacteria, show efficient behavior toward electron transfer through cytochromic pathways and proteins [18]. Some microbes transfer electrons without making any contact physically with the surface of electrode, whereas other microbes require synthetic or naturally produced mediators for electron transfer [19]. Microbes can work solely or in consortia colonies. In consortia, microbes show synergistic effects for bio-decomposition of complex organic matter [20]. **Table 1** displays the data of microorganisms that were exploited by a number of scientists for energy generation in microbial fuel.

2.2 Microbes-electrode material interaction

Microbes form active sites on the surface of anode and are responsible for the oxidation of organic matter provided in the fuel cell. Oxidation reaction of organic matter results in the generation of electrons as well as protons as a result of microbial attachment and colonization [43, 44]. In microbial fuel cell, material of anode plays a key role to accelerate not only the flow of electron following conduction but also biofilm formation. In microbial fuel cell, anodes in the form of plates, rods, or brushes are made conventionally from different materials such as graphite, paper, cloth, or felts of carbon [45]. Generally, carbon is a suitable material for electrode formation as it is resistant to oxidation.

2.3 Shortcoming for microbial fuel cell

In spite of all these merits of microbial fuel cells, some drawbacks make it unfit for power generation at industrial scale. Microbial fuel cells face the challenges of low-voltage production due to weak biofilm formation, low-efficiency electrodes, and proton exchange membrane. As microbial oxidation of substrate generates electrons

Microbes	Organic matter as substrate	References
Streptococcus lactis	$C_6H_{12}O_6$	[21]
Erwinia dissolvens	$C_6H_{12}O_6$	[21]
Lactobacillus plantarum	$C_6H_{12}O_6$	[21]
Aeromonas hydrophila	CH_3COOH	[22]
Proteus mirabilis	$C_6H_{12}O_6$	[23]
Geobacter metallireducens	CH_3COOH	[24]
Pseudomonas aeruginosa	$C_6H_{12}O_6$	[19]
Klebsiella pneumoniae	$C_6H_{12}O_6$	[25]
Blastobotrys adeninivorans	$C_6H_{12}O_6$	[26]
Candida melibiosica	$C_6H_{12}O_6$	[27]
Saccharomyces cerevisiae	$C_6H_{12}O_6$	[28]
Desulfovibrio desulfuricans	$C_{12}H_{22}O_{11}$	[29]
P. anomala	$C_6H_{12}O_6$	[30]
Clostridium beijerinckii	$C_6H_{10}O_5$, $C_6H_{12}O_6$	[31]
Candida sp.	$C_6H_{12}O_6$	[32]
S. cerevisiae	$C_3H_6O_3$	[33]
Shewanella oneidensis	$C_3H_6O_3$	[34]
C. melibiosica	$C_6H_{12}O_6$	[35]
Methylomusa anaerophila	CH_3OH	[36]
Escherichia coli	$C_6H_{12}O_6$, $C_{12}H_{22}O_{11}$	[37]
Gluconobacter oxydans	$C_6H_{12}O_6$, C_2H_5OH	[38, 39]
Shewanella putrefaciens	$C_3H_6O_3$	[40]
S. cerevisiae	$C_6H_{12}O_6$	[41]
Geobacter sulfurreducens	CH_3COOH	[42]

Table 1.
Microbes used in microbial fuel cell.

that are not fully attracted toward the cathode surface and ultimately resulted in the less output energy and short-term stability limit its utility. This attraction of electrons toward the electrode can be enhanced by increasing the exposed surface area of electrode by using nanoparticles or any nano-composite material to increase bio-catalytic activity of microbes [45]. A number of scientists reported the microbial fuel cell in which anode was impregnated with chemical catalyst [46–48]. This anode impregnation increased the active sites of anode to value power density, but bacterial cells entrapped into these pores to clog them thus, ultimately the cell death resulted in decline in the electrochemical reaction on the cell surface.

3. Nano-structured microbial fuel cells

Nano-composite materials are used for coating surface of electrodes to enhance their efficiency. These composite materials are multiphase and each phase having
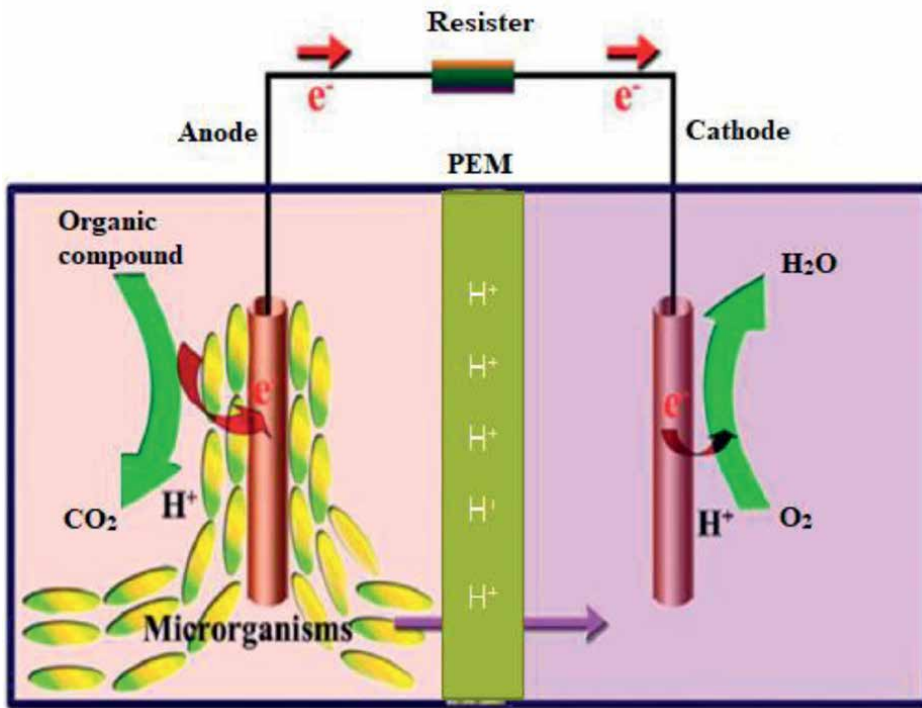
Figure 1.
Microbial Fuel cell [51].

multiple dimensions of nano-meters. These nano-materials are of different types such as carbon nano-tubes coated with poly pyrrole, carbon nano-tube composites coated with poly aniline, and nano-fibers of activated carbon [48–50]. During the process of energy generation by microbial fuel cells, oxidation of substrate takes place at the anode with the emission of electrons leaving behind the protons. These electrons are attracted toward the nano-material-coated electrodes ultimately for energy generation, whereas protons react with oxygen to produce water after passing through proton exchange membrane, and carbon dioxide is the side product in this process (**Figure 1**). Reactivity of oxygen can be catalyzed by using nano-carbons or metals [52].

Nanotechnology has played an impact on the performance of microbial fuel cells and its constituents. Best of the knowledge about microbial fuel cell presentation, its constituents, and applications are presented in **Table 2** as reported in a literature survey comprehensively by Mashkour et al. [53]. They reported not only microbes-nano-composite interaction but also potential exploitation of nano-materials for electron transfer to generate electricity as well as green water reclamation.

3.1 Microbes, cell compartments, and mechanism

In microbial fuel cell, microbes such as bacteria, fungi, or algae that reside on anode/bio-anode are called exoelectrogens, which donate electrons, and microbes that reside on cathode/bio cathodes are called electrotrophs, which attract electrons coming from the anode (**Figure 2a**) [67, 68]. At anode surface, microbes form biofilm

Nanostructured microbial fuel cell constituents			Applied fields of nanostructured microbial fuel cell				
Microbial culture–nanocomposite interaction	Anode/PEM/Cathode	Power generation	Microbs catalyzed Redox reaction	Microbial Hydrogen Emission	Clean water reclamation	Nano bio detector	References
Yes	Yes/Yes/Yes	Yes	Yes	Yes	Yes	Yes	[53]
No	No/No/Yes	Yes	No	No	No	No	[54]
Yes	No/No/No	No	No	No	No	No	[55]
	Yes/No/Yes	Yes	No	No	No	No	[56]
	No/No/No	Yes	Yes	No	No	No	[57]
No	Yes/No/Yes	No	Yes	No	No	No	[58]
No	Yes/No//No	Yes	No	No	No	No	[59]
Yes	Yes/Yes/Yes	Yes	No	No	No	No	[60]
No	No/Yes/No	Yes	No	No	Yes	No	[61]
Yes	Yes/No/Yes	No	No	No	No	No	[62]
Yes	No/No/No	No	No	No	No	No	[63]
No	Yes/No/No	Yes	No	No	No	No	[64]
No	No/No/Yes	Yes	No	No	No	No	[65]
No	Yes/No/Yes	Yes	No	No	No	No	[66]

Table 2.
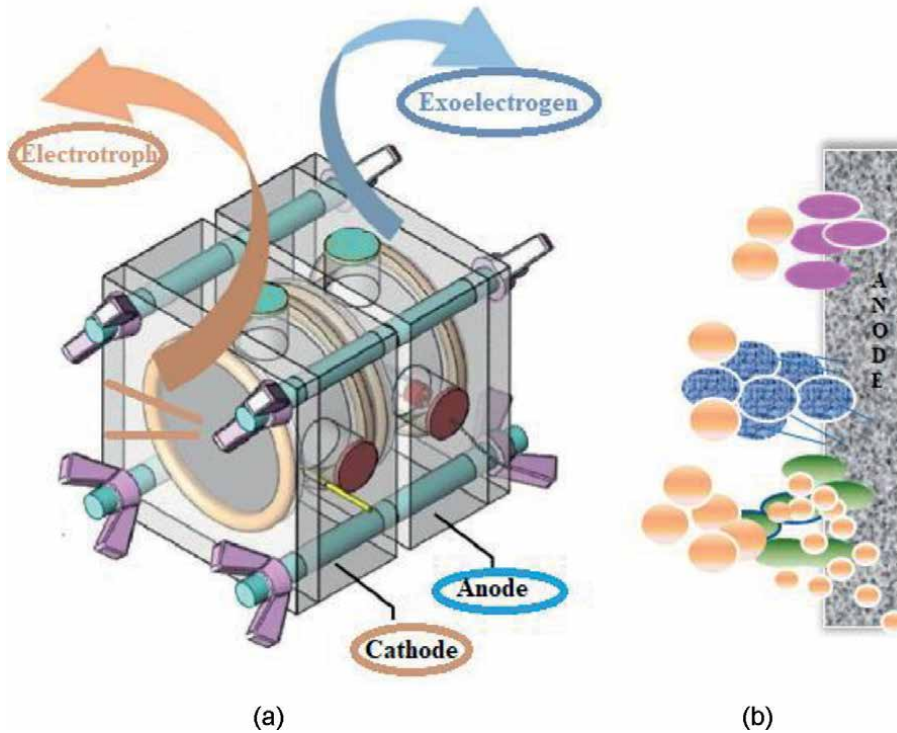*Nano structured microbial fuel cell and its exploitation.*

Figure 2.
Anode and cathode inhabiting microbes in microbial fuel cell (a), electron transmission from exoelectrogens electrode surface: direct contact (voilet), nanowire (textured blue), and mediators (green and orange) (b).

and decompose organic matter to generate electrons and protons. These electrons through nano-composite intermediates, bio-mediators, or direct contact are accepted by cathode having carbon dioxide as electron acceptor, thus, responsible for power generation (**Figure 2b**) [15]. At cathode surface, electrotrophic microbes reside, which require energy for their activities from electrons reached through electron transport mechanism generated as a result of organic matter decomposition. These microbes play a key part in the instrumentation to electro-synthesize the product.

3.2 Bacterial fuel cells

Bacterial fuel cells are novel innovation applicable in multidisciplinary fields of physical and biological and applied sciences. Bacterial fuel cell enclosed the components such as bacteria, proton exchange membrane, anode, and cathode [69]. These fuel cells are prepared by using electrode modified by nano-composite material made from metal oxides loaded with bacterial biomass. These cells exhibit better performance for electricity generation, treatment of polluted water, and as a biosensor for the detection of pullutants [1, 70].

3.3 Fungal fuel cell

In microbial fuel cell compartment, fugal mycelia can be interacted with nano-material-modified electrodes and taken as anodic or cathodic biocatalyst to transfer

electrons sometime using mediators such as methylene blue (MB) and neutral red (NR). These fungal fuel cells can be manipulated to treat polluted water in addition to generating electricity. This fungal-mediated anode works in an anaerobic environment in a sterilized system requiring no input energy or any chemical [71]. Potential exploitation of fungal fuel cell is an economical, eco-friendly, and green alternative technology that plays with living microbes to oxidize organic matter leaving behind minimum side products, thus resulting in the electricity generation. As microbial fuel cell factories, fungal microbes can work at optimal temperature using wide range of organic matter as substrates with minimum requirement of energy [72, 73]. These fungal fuel cells can be a future candidate for the treatment of wastewater, bioremediation of organic wastes, thus valued the organic wastes for energy generation, biofuel and chemical production on commercial scale. In fungal fuel cell, redox reaction takes place via series of electrochemical and fungal metabolic pathways. At the anode, microbial oxidation of substrate takes place that results in the generation of electrons and protons. Electrons are attracted toward the cathode where these electrons are captured to be reduced [74].

3.4 Microbial fuel cell components

Microbial fuel cell is composed of two distinct anodic and cathodic chambers separated by separator such as proton exchange membrane. Electrochemical system of fuel cell is mediated by microbes due to their potential to catalyze electron transfer from anode to cathode called exoelectrogens. These exoelectrogens play a significant role in the oxidation of organic matter and subsequent release of electrons, which then migrate from anode to cathode through external circuit for power generation, whereas protons are delivered through proton exchange membrane to cathode and react with oxygen to form water (**Figure 3**). Microbial fuel cell alignment, optimal
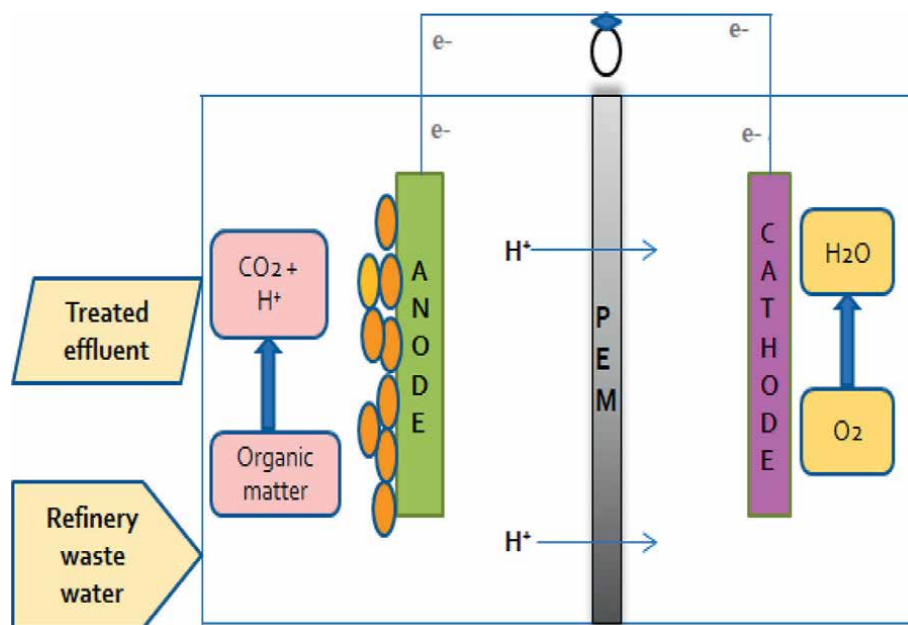

Figure 3.
Fungal fuel cell.

Microbial fuel cell constituents	Potential attributes of constituents
Microorganisms: Bacteria, fungi	microbial growth rate, microbial attachment, extracellular electron transfer, the activity of biofilm in a redox reaction, biofilm resistance
Anode: Poly aniline/ TIO$_2$ Polypyrrole/ carbon nano tube, Ni/ Carbon nano fibers, Polyaniline/ 3D graphene	Conductivity, Increased exposed surface area, porous network, enhanced charge transfer, More compatible to microbes,
Cathode	Conductive, More exposed surface area, porous network to enhance charge transfer, reducing environment at cathode, reduce oxygen,
Proton exchange membrane	conductive, exchange of ions, oxygen transfer, water formation, separation, to make charge balance

Table 3.
Potential effects of nanotechnology on enhancing the attributes of different constituents of MFC.

substrate, fungal culture load, texture of anode and cathode, and other environmental factors are the key factors that affect the working of fuel cell. These components involving nanotechnology are enhancing the different attributes of microbial fuel cells (**Table 3**).

3.4.1 Microbial fuel cell anode modified with nano-composite

Microbial growth and other activities such as electron movement are greatly influenced by the anodic performance, and anodic performance is directly dependent on the anodic texture. Anode under optimal conditions of microbial environment has good potential for electrical conduction [42, 75]. Anode in the form of carbon material such as paper or fabric has been in practice might be due to their biocompatibility as well as economical but reduction in exposed surface area for microbial attachment [9, 10, 53], thus, limiting their use for microbial colonies formation and energy generation [11, 76].

Exposed surface area of anode can be increased by using economical and cheap nano-composite material that not only increases the microbial growth but also improves the microbial attachment to the surface of anode. This enhancement in microbial attachment or rich colonization of microbes or exoelectrogens accelerates the rate of oxidation of organic matter that ultimately results in the release of electrons and protons, thus, increasing the rate of electron transfer in microbial fuel cell [75, 76]. **Table 4** gives an overview of the extraordinary performance of anode modified with various nano-composite materials filmed with different microbial culture and subsequent progression in the power generation of microbial fuel cell under investigation. For anode alteration, multiphase nano-tubes made from carbon sheets expose maximum active sites for microbial attachment followed by the maximum oxidation of organic matter to release electrons and protons. Electrons are attracted toward the cathode made from carbon sheet coated with platinum as reported by Nambiar et al. [77]. Power generated in this work optimally up to 256%. Out-performance of microbial fuel cells constructed by modified anode is reported by a number of scientists (**Table 4**). They reported best synergistic catalytic effects of microbial cells and nano-composite in microbial fuel cell formulation. In this cell, anode was made from nano-composite of oxide of titanium and poly aniline using culture of *Escherichia Coli.* In this microbial fuel

Exoelectrogen	Modified anode	Cathode	Power density (Milli Watt/ m2	Reference
Escherichia Coli	Sheet of TiO2 modified with Polyanilin	Graphitic paper	Out perform	[1]
Escherichia Coli	Carbon nano tubes filmed with polypyrrole	—	228	[48]
Enterobacter cloacae	Carbon paper modified with nano tubes of carbon	Sheet of carbon	256% improvement	[77]
Escherichia Coli	Three dimensional graphene hybridized with polyaniline	—	Out perform	[49]
Escherichia Coli	Micro-nano fibers of carbon with dispersed web of nickel nano particles	—		[50]
Geobacter sulfurreducens	Sheet of carbon modified with carbon nano tubes	Graphitic plate	200% improvement	[78]
Shewanella loihica	Sheet of TiO2 modified with Polyanilin	Carbon cloth coated with platinum	63% improvement	[79]
Shewanella putrefaciens	Felts of carbon modified with graphene oxide	Sheet of platinum	240	[80]
Escherichia coli	Poly ethylene dioxy thiophene/ graphene/nickel-nanoparticles	Graphitic sheet	3200	[81]
Saccharomyces cerevisiae	Felts of carbon modified with nanoparticles of gold	Graphitic sheet	2271	[82]
Shewanella xiamenensis	Sheet of TiO2 modified with Polyanilin	Graphitic sheet	179	[83]
S. loihica	Carbon felts modified with iron oxide	Paper of carbon with coating of platinum	797	[70]

Table 4.
Performance of electrode modified with nano-composite/exoelectrogen in microbial fuel system.

cell, current and voltage measurements were made by using digital multimeter, and external resistance was set at 1.95 kΩ. During microbial fuel cell working, electrons and protons are released as a result of anaerobic oxidation of substrate. Through external circuit, these electrons move from anode to cathode where reaction takes place in the presence of oxygen and protons [84–86]. Another economical and cost-effective microbial fuel cell with 0.18 voltages was reported by Zoua et al. [48], who formulated fuel cell using anode made from composite of carbon nanotubes filmed around with polypyrrole using culture *Escherichia coli*. It was found that fuel cell voltage was dependent on composite material loaded. Similarly, Yong et al. [49] assembled the microbial fuel cell using three-dimensional graphene hybridized with poly aniline that was filmed with culture of microbes on three dimensions to facilitate electron transfer through super-conductive passage. Another research finding reported the microbial fuel cell involving porous network

of micro- and nano-fibers of carbon with dispersed nickel by using biofilm of *E. coli* [50]. This prepared cell exhibited wonderful catalytic reduction of oxygen and facilitated excellent electron conduction to anode. Nambiar et al. [77] constructed microbial fuel cell using sheet of carbon as cathode, whereas anode was made from carbon paper modified with multidimensional carbon nanotubes loaded with *Enterobacter cloacae* culture. They found 256% improvement in cell working.

3.4.2 Microbial fuel cell cathode modified with nanocomposite

To improve the performance of electrotrophs, in microbial fuel cell cathode or electrotroph can be modified by using nano-composite to increase the exposed surface are for the adsorption of gas molecules. This modification of cathode by photocatalytic nano-composite may lead to enhanced chemical reactions on the surface of cathode. **Table 5** displays the research findings of microbial fuel cell with different electrotrophs in which cathode was modified with nano-materials to produce acetate. Bian et al. [89] have increased the exposed surface area of cathode using nano-rods of carbon along with porous nickel fibers loaded with *Sporomusa ovate*. These microbes captured CO_2 from the surface of cathode due to porous nickel fibers. On cathode surface, carbon nanotubes have increased the adsorption capacity for CO_2 that resulted in the significant increase in current density of cathode up to 332 mA/m^2 due to enhanced charge transfer. Similarly, under the same conditions, Aryal et al. [88] used sheet of grapheme oxide for microbial culturing of electrotrophs, and increased acetate production was detected 7–8 times comparable with electrode made from carbon paper. Consistently, Han et al. [90] reported the optimal acetate production and increased cathodic current density in comparison with cloth of carbon by using three-dimensional cathode biofilm of *Clostridium ljungdahlii* modified with incorporation of carbon nanotubes and graphene. Recently, modified cathode advanced the CO_2 fixation by Methano bacterium to enhance the acetate production [59]. For generation of acetate from HCO_3, cathode was modified with nanoparticles of oxides of molybdenum and tungsten, whereas *Serratia marcescens* was used as an electrotroph for microbial electro-synthesis system assisted by light. Generally, nano-materials having excellent biocompatibility with microbes can play a crucial role for increasing the exposed surface area of cathode to absorb more CO_2 in microbial electro-synthesis system using electrotrophs for chemical production. This chemical production in fuel cell is catalyzed by Pt as catalyst that is more expensive and toxic toward the microbes, so economic nano-materials with more exposed surface area can be an excellent substitute of Pt catalyst to accelerate the cathode reaction such as reaction of oxygen reduction [93, 94]. The performance of cathode modified with nano-materials in microbial fuel cell has been investigated by a number of scientists as reported in **Table 5**.

3.5 Microbial fuel cell electrode modified with metallic nanoparticles

Nanoparticles made from transition and noble metals such as copper, zinc, nickel, cobalt, silver gold, platinum, and palladium have been exploited for electrode formation in energy generation owing to their excellent electrochemical, opto-magnetic, and mechanical properties [87, 91]. These nanoparticles have distinctive characters of displaying enlarged exposed surface area and dynamic shape. Metallic nanoparticles in the form of electrodes are being used in analytical equipment, optoelectronics, catalysis, biosensor fabrication, devices to monitor diseases such as cancerous cells,

Electrotrophs	Modified cathode	Anode	Power density (Milli Watt/ m2 (Modified/ control)	Reference
Sporomusa ovate with alcohol tolererance	Carbon cloth modified with oxides of graphene, tetraethylenepentamine	Graphite rods	2358/420	[87]
S. ovata	paper of reduced graphene oxide	Graphite rod	Up to 700%	[88]
S. ovata	Hollow rods of nickel modified with carbon nano tubes	Fabric of carbon	232/214	[89]
Clostridium ljungdahlii	Carbon cloth modified with carbon nanotubes and graphene	Graphite rod	595/135	[90]
S. ovata	Porous Copper modified with graphene oxide	Graphite rod	Up to 300%	[91]
Autotrophs	Carbon felts modified with oxides of manganese	Felts of carbon	Up to 200%	[92]
Serratia marcescens	Carbon felts modified with nano composite of oxides of tungsten and molybdenum	Carbon rod	2500/1500	[57]
Methanobacterium	Graphene oxide-PEDOT modified carbon fabric	Fabric of carbon	2540/840	[59]
Mixed culture	Carbon nano tubes modified with cobalt dopped with nitrogen	Felts of carbon	2479/714	[45]

Table 5.
Performance of electrode modified with nano-composite/electrotroph in microbial fuel system.

drug discovery, toxic metal detector for environmental monitoring as well as therapeutics [45, 92, 95, 96].

3.5.1 Microbial fuel cell electrode modified with gold nanoparticles

Metallic gold is an inert substance, which is the best representative of the catalyst as well as an electrode in the form of nanoparticles [35, 97] that have potential utilities in lab equipment, optoelectronics, and biomedicines. Gold nanoparticles having different dimensions are produced by using microbes as reducing agent. In microbial fuel cell, electrode surface can be modified with more stable and biocompatible nanoparticles of gold in the form of colloids called electron detector [81, 82, 98–101]. Literature supported the exploitation of modified electrode with gold nanoparticles for immobilization of redox enzymes and proteins, carbon paper modified with Au nanoparticles generated high-intensity current as well as healthy microbial biofilm formation as reported by Sun et al. [96]. Electrode modified with Au nanoparticles can be prepared by different methods such as sputtering and layer-by-layer methods. Sputtering method involves the deposition of Au vapors on the surface of electrode to make a uniform film, whereas layer-by-layer method involves the assembly of different layers of gold on the surface of electrode under the influence of electrostatic force

to make multilayered thin film with uniform thickness. Guo et al. [101] assembled the Au nanoparticles and polyethylene imine under the electrostatic force of attraction to form multilayers of gold on the surface of electrode made of carbon paper. Gold nanoparticles-modified carbon paper electrode exhibited enhanced capabilities of electron transfer and power generation. Kalathil et al. [102] prepared gold nanoparticles in situ that facilitated not only the electricity generation but also hydrogen emission under controlled conditions of discrete capacitors loading in a microbial fuel cell. Similarly, Kasem et al. [102] reported the significant increase in adhesion of microbes on the surface of anode modified by using nanoparticles of gold or cobalt that ultimately boost the performance of fuel cell as a result of electron transfer. Han et al. [97] generated electricity by degrading methylene blue by using microbial fuel cell having gold nanoparticles on the cathode surface. They concluded that microbial fuel cell did well for power generation just because of modified cathode with gold nanoparticles. Cheng et al. [103] modified the anode surface by following the method of layer-by-layer binding of nano-composites of reduced graphene oxide and gold in microbial fuel cell for power generation up to 33.7 Wm^{-3} as well as wastewater management. Intensity of current approached 69.4 Am^{-3}, which might be due to more exposed active points of gold nanoparticles to attract electron on the surface of electrode. Similarly, a number of potential scientists reported the power generation by microbial fuel cells using electrode modified with nanoparticles of gold (**Table 6**).

3.6 Applications of nano-composite-based microbial fuel cell

3.6.1 Electricity generation

Microbial fuel cell is an excellent alternative for electricity generation due to flow of electron and proton between nano-material-modified exoelectrogen and electrotrophs. This cell is more eco-friendly and economic to use as microbes require energy for their growth activities, so organic wastes are the good source of substrate, which is decomposed by microbes as a result of oxidation that results in the generation of electron as well as proton. From anode in the medium source, electron transfer to cathode through external source of electromotive force [84, 111, 112].

3.6.2 Wastewater treatment

Microbial fuel cells are used to bio-remediate the industrial and domestic wastewater leaving behind less waste comparable with other treatment technologies. During this bio-remediation, a number of elements of potential importance in different fields, chemicals, and dyes stuffs are removed from this wastewater using exoelectrogen [113], whereas nitrogen and phosphorous-containing compounds can be eliminated from wastewater by using electrotrophs.

3.6.3 Nano biodetector

Microbial fuel cell can be used as self-motivated and highly sensitive biosensor to evaluate the qualities of wastewater by sensing the value of dissolved oxygen, toxic compounds, volatile organic compounds, biological oxygen demand, and microbial load [3, 114–116]. Some of their features such as low detection limit, poor durability, and less reproducibility make it unfit for applicability on commercial scale [115, 116]. However, modification of anode and cathode by using nano-composite material can

Exoelectrogen	Modified anode with gold nano particles	Technique	Power density (Milli Watt/m^2)	Reference
bacteria	gold nanoparticles (Au NPs) modified carbon paper	Layer-by-layer assembly	346 mWm^{-2}	[101]
Shewanella oneidensis	gold nanoparticles (Au NPs) modified carbon paper	Sputtering	47% higher than C electrode	[96]
Yeast *Saccharomyces cerevisia*	surfactant-mediated gold nanoparticles on carbon felt anode	In situ deposition	2771 ± 569 mW·m^{-2}	[82]
Geobacter sulfurreducens	Gold mediated graphite anode	Stripping pattern	688 ± 159	[104]
E. coli	carbon nanotube-gold-titania nanocomposite	Nano suspension coating	2.4 mW m^{-2}	[95]
Bacteria	gold nanoparticles (Au NPs) modified carbon paper	In situ deposition	—	[102]
G. sulfurreducens	Gold modified polystyrene	Sputtering	—	[105]
S. platensis	Gold modified carbon felt	Sputtering	1.64 mW/m,	[106]
S. platensis	Gold modified carbon paper	Sputtering	10 mW/m^2	[107]
S. oneidensis	gold line microarray electrode PMMA	Sputtering	1400 mA m^{-2}	[108]
S. oneidensis	carbon nanotubes blended with BioAu	sputtering	178.34 ± 4.79 mW/m^2	[40]
bacteria	titanium and gold deposited plain silicium (one side)	sputtering	2.5 mW/m^2	[109]
bacteria	titanium and gold deposited plain silicium	sputtering	86.0 mW/m^2	[109]
bacteria	Gold modified carbon paper (one side)	sputtering	346.9 mW/m^2	[109]
Saccharomyces cerevisiae	Gold modified carbon fiber	sputtering	12.9 mW/m^2	[110]

Table 6.
Exploitation of electrode modified with gold nanoparticles in microbial fuel cell.

enhance the working of fuel cell as a nano-biosensor. For the detection of contaminants in the wastewater, anode can be modified as exoelectrogen to sense the waste bin in the water. In the same way, cathode can be modified as an electrotroph to detect pollutant, and system detection power can be enhanced by increasing the voltage current.

4. Upcoming prospects for research

Microbial fuel cells modified by nano-materials are used for the detection and bio-remediation of wastewater as well as biosensor for contaminants. A number of enormous materials are available for improving the reproducibility and vast applicability of fuel cells. However, more utilization of fuel cells modified with nano-materials may lead to emission of some toxic nano-metals into air, water, or soil, thus being environmental concerns. In future prospects, fuel cells modified with nano-materials should be formulated in such ways that minimize the risk factor to living organisms especially humans and ecosystem.

Author details

Fozia Anjum[1]*, Nadia Akram[1], Samreen Gul Khan[1], Naheed Akhter[2], Muhammad Shahid[3] and Fatma Hussain[3]

1 Department of Chemistry, Government College University, Faisalabad, Pakistan

2 Department of Biochemistry, Government College University, Faisalabad, Pakistan

3 Department of Biochemistry, University of Agriculture, Faisalabad, Pakistan

*Address all correspondence to: drfoziaanjum@gcuf.edu.pk

IntechOpen

References

[1] Qiao Y, Bao SJ, Li CM, Cui XQ, Lu ZS, Guo J. Nanostructured polyaniline/ titanium dioxide composite anode for microbial fuel cells. ACS Nano. 2007;**2**(1):113-119

[2] Izadi P, Rahimnejad M, Ghoreyshi A. Power production and wastewater treatment simultaneously by dual-chamber microbial fuel cell technique. Biotechnology and Applied Biochemistry. 2015;**62**(4):483-488

[3] Ivars-Barcelo F, Zuliani A, Fallah M, Mashkour M, Rahimnejad M, Luque R. Novel applications of microbial fuel cells in sensors and biosensors. Applied Sciences. 2018;**8**(7):1184

[4] Masoudi M, Rahimnejad M, Mashkour M. Fabrication of anode electrode by a novel acrylic based graphite paint on stainless steel mesh and investigating biofilm effect on electrochemical behavior of anode in a single chamber microbial fuel cell. Electrochimica Acta. 2020;**344**:136168

[5] Kiran V, Gaur B. Microbial fuel cell: Technology for harvesting energy from biomass. Reviews in Chemical Engineering. 2013;**29**(4):189-203

[6] Xu L, Zhao Y, Doherty L, Hu Y, Hao X. The integrated processes for wastewater treatment based on the principle of microbial fuel cells: A review. Critical Reviews in Environmental Science and Technology. 2016;**46**(1):60-91

[7] Berchmans S. Microbial fuel cell as alternate power tool: Potential and challenges. In: Microbial Fuel Cell. Springer; 2018. pp. 403-419

[8] Gunawardena A, Fernando S, To F. Performance of a yeast-mediated

biological fuel cell. International Journal of Molecular Sciences. 2008;**9**:1893-1907. DOI: 10.3390/ijms9101893

[9] Babanova S, Hubenova Y, Mitov M. Influence of artificial mediators on yeastbased fuel cell performance. Journal of Bioscience and Bioengineering. 2011;**112**:379-387. DOI: 10.1016/j. jbiosc.2011.06.008

[10] Hubenova Y, Mitov M. Extracellular electron transfer in yeast-based biofuel cells: A review. Bioelectrochemistry Spec. Issue "Biological fuel cells". 2015;**106**:177-185

[11] Prasad D, Arun S, Murugesan M, Padmanaban S, Satyanarayanan RS, Berchmans S. Direct electron transfer with yeast cells and construction of a mediatorless microbial fuel cell. Biosensors and Bioelectronics. et al., 2007;**22**:2604-2610

[12] Shkil H, Schulte A, Guschin DA, Schuhmann W. Electron transfer between genetically modified hansenula polymorpha yeast cells and electrode surfaces via os complex modified redox polymers. ChemPhysChem. 2011;**12**:806- 813. DOI: 10.1002/cphc.201000889

[13] Haslett ND, Rawson FJ, Barriëre F, Kunze G, Pasco N, Gooneratne R, et al. Characterisation of yeast microbial fuel cell with the yeast Arxulaadeninivorans as the biocatalyst. Biosensors & Bioelectronics. 2011;**26**:3742-3747

[14] Franks AE, Nevin KP. Microbial fuel cells, a current review. Energies. 2010;**3**:899-919. DOI: 10.3390/en3050899

[15] Pisciotta JM, Zaybak Z, Call DF, Nam JY, Logan BE. Enrichment of microbial electrolysis cell biocathodes

from sediment microbial fuel cell bioanodes. Applied and Environmental Microbiology. 2012;**78**(15):5212-5219

[16] Caccavo F, Lonergan DJ, Lovley DR, Davis M, Stolz JF, McInerney MJ. *Geobacter sulfurreducens* sp. nov., a hydrogen- and acetate-oxidizing dissimilatory metal-reducing microorganism. Applied and Environmental Microbiology. 1994;**60**:3752-3759

[17] Zhuwei D, Haoran L, Tingyue G. A state of the art review on microbial fuel cells: A promising technology for wastewater treatment and bioenergy. Biotechnology Advances. 2007;**25**(5):464-482

[18] Lovley DR. Long-range electron transport to Fe(III) oxide via pili with metallic-like conductivity. Biochemical Society Transactions. 2012;**40**(6):1186-1190

[19] Rabaey K, Boon N, Höfte M, Verstraete W. Microbial phenazine production enhances electron transfer in biofuel cells. Environmental Science and Technology. 2005;**39**(9):3401-3408

[20] Ishii S, Suzuki S, Tenney A, Norden-Krichmar TM, Nealson KH, Bretschger O. Microbial metabolic networks in a complex electrogenic biofilm recovered from a stimulus-induced metatranscriptomics approach. Scientific Reports. 2015;**5**(1):1-14. DOI: 10.1038/srep14840

[21] Vega CA, Fernández I. Mediating effect of ferric chelate compounds in microbial fuel cells with Lactobacillus plantarum, Streptococcus lactis, and Erwinia dissolvens. Bioelectrochemistry and Bioenergetics. 1987;**17**(2):217-222

[22] Pham CA, Jung SJ, Phung NT, Lee J, Chang IS, Kim BH, et al. A novel electrochemically active

and Fe(III)-reducing bacterium phylogenetically related to Aeromonas hydrophila, isolated from a microbial fuel cell. FEMS Microbiology Letters. 2003;**223**(1):129-134

[23] Choi Y, Jung E, Kim S, Jung S. Membrane fluidity sensing microbial fuel cell. Bioelectrochemistry. 2003;**59**(1-2):121-127

[24] Min B, Cheng S, Logan BE. Electricity generation using membrane and salt bridge microbial fuel cells. Water Research. 2005;**39**(9):1675-1686

[25] Rhoads A, Beyenal H, Lewandowski Z. Microbial fuel cell using anaerobic respiration as an anodic reaction and biomineralized manganese as a cathodic reactant. Environmental Science and Technology. 2005;**39**(12):4666-4671

[26] Haslett ND, Rawson FJ, Barriëre F, Kunze G, Pasco N, Gooneratne R, et al. Characterization of yeast microbial fuel cell with the yeast *Arxula adeninivorans* as the biocatalyst. Biosensors & Bioelectronics. 2011;**26**:3742-3747

[27] Babanova S, Hubenova Y, Mitov M. Influence of artificial mediators on yeast-based fuel cell performance. Journal of Bioscience and Bioengineering. 2011;**112**:379-387

[28] Kasem E, Tsujiguchi T, Nakagawa N. Effect of metal modification to carbon paper anodes on the performance of yeast-based microbial fuel cells part I: In the case without exogenous mediator. Key Engineering Materials. 2013;**534**:76-81

[29] Ieropoulos IA, Greenman J, Melhuish C, Hart J. Comparative study of three types of microbial fuel cell. Enzyme and Microbial Technology. 2005;**37**(2):238-245

[30] Kaneshiro H, Takano K, Takada Y, Wakisaka T, Tachibana T, Azuma M. A milliliter-scale yeast-based fuel cell with high performance. Biochemical Engineering Journal. 2014;**83**:90-96

[31] Liu Q, Liu B, Li W, Zhao X, Zuo W, Xing D. Impact of ferrous iron on microbial community of the biofilm in microbial fuel cells. Frontiers in Microbiology. 2017;**8**:1-9. DOI: 10.3389/fmicb.2017.00920

[32] Lee Y-Y, Kim TG, Cho K-S. Isolation and characterization of a novel electricity-producing yeast, Candida sp. IR11. Bioresource Technology. 2015;**192**:556-563

[33] Gal I, Schlesinger O, Amir L, Alfonta L. Yeast surface display of dehydrogenases in microbial fuel-cells. Bioelectrochemistry. 2016;**112**:53-60

[34] Lamberg P, Bren KL. Extracellular electron transfer on sticky paper electrodes: Carbon paste paper anode for microbial fuel cells. ACS Energy Letters. 2016;**1**(5):895-898

[35] Sekrecka-Belniak A, Toczyłowska-Maminska R. Fungi-based microbial fuel cells. Energies. 2018;**11**(10):2827

[36] Amano N, Yamamuro A, Miyahara M, Kouzuma A, Abe T, Watanabe K. Methylomusa anaerophila gen. Nov., sp. nov., an anaerobic methanol-utilizing bacterium isolated from a microbial fuel cell. International Journal of Systematic and Evolutionary Microbiology. 2018;**68**(4):1118-1122

[37] Feng C, Tsai CC, Ma CY, Yu CP, Hou CH. Integrating cost-effective microbial fuel cells and energy-efficient capacitive deionization for advanced domestic wastewater treatment. Chemical Engineering Journal. 2017;**330**:1-10

[38] Lee SA, Choi Y, Jung S, Kim S. Effect of initial carbon sources on the electrochemical detection of glucose by *Gluconobacter oxydans*. Bioelectrochemistry. 2002;**57**(2):173-178

[39] Plekhanova Y, Tarasov S, Kolesov V, Kuznetsova I, Signore M, Quaranta F, et al. Effects of polymer matrices and carbon nanotubes on the generation of electric energy in a microbial fuel cell. Membranes. 2018;**8**(4):99

[40] Wu X, Qiao Y, Shi Z, Li CM. Enhancement of interfacial bioelectrocatalysis in Shewanella microbial fuel cells by a hierarchical porous carbon–silica composite derived from distiller's grains. Sustainable Energy & Fuels. 2018;**2**(3):655-662

[41] Badea SL, Enache S, Tamaian R, Niculescu VC, Varlam M, Pirvu CV. Enhanced open-circuit voltage and power for two types of microbial fuel cells in batch experiments using *Saccharomyces cerevisiae* as biocatalyst. Journal of Applied Electrochemistry. 2019;**49**(1):17-26

[42] Krige A, Sjöblom M, Ramser K, Christakopoulos P, Rova U. On-Line Raman Spectroscopic Study of Cytochromes Redox State of Biofilms in Microbial Fuel Cells. Molecules. 2019;**24**(3):646

[43] Palanisamy G, Jung HY, Sadhasivam T, Kurkuri MD, Kim SC, Roh S-H. A comprehensive review on microbial fuel cell technologies: Processes, utilization, and advanced developments in electrodes and membranes. Journal of Cleaner Production. 2019;**221**:598-621

[44] Lv C, Liang B, Zhong M, Li K, Qi Y. Activated carbon- supported multi-doped graphene as high-efficient catalyst to modify air cathode in microbial fuel cells. Electrochimica Acta. 2019;**304**:360-369

[45] Ghasemi M, Daud WRW, Hassan SH, Oh SE, Ismail M, Rahimnejad M, et al. Nano-structured carbon as electrode material in microbial fuel cells: A comprehensive review. Journal of Alloys and Compounds. 2013;**580**:245-255

[46] Rosenbaum MA, Franks AE. Microbial catalysis in bioelectrochemical technologies: Status quo, challenges and perspectives. Applied Microbiology and Biotechnology. 2014;**98**:509-518

[47] Park DH, Zeikus JG. Improved fuel cell and electrode designs for producing electricity from microbial degradation. Biotechnology and Bioengineering. 2002;**81**:348-355

[48] Zoua Y, Xianga C, Yanga L, Suna LX, Xua F, Caoc Z. A mediatorless microbial fuel cell using polypyrrole coated carbon nanotubes composite as anode material. International Journal of Hydrogen Energy. 2008;**33**:4856-4862

[49] Yong YC, Dong XC, Chan-Park MB, Song H, Chen P. Macroporous and monolithic anode based on polyaniline hybridized three-dimensional graphene for high-performance microbial fuel cells. ACS Nano. 2012;**6**(3):2394-2400

[50] Singh S, Verma N. Fabrication of Ni nanoparticles dispersed carbon micro nanofibers as the electrodes of a microbial fuel cell for bio-energy production. International Journal of Hydrogen Energy. 2014;**11**:073

[51] Zhao C-e, Gai P, Song R, Chen Y, Zhang J, Zhu J-J. Nanostructured material-based biofuel cells: Recent advances and future prospects. Chemical Society Reviews. 2017;**46**:1545-1564. DOI: 10.1039/c6cs00044d

[52] Santoro C, Arbizzani C, Erable B, Ieropoulos I. Microbial fuel cells: From fundamentals to applications. A

review. Journal of Power Sources. 2017;**356**:225-244

[53] Mashkour M, Rahimnejad M, Raouf F, Navidjouy N. A review on the application of nanomaterials in improving microbial fuel cells. Biofuel Research Journal. 2021;**30**:1400-1416

[54] Peer J, Baek G, Shi L, Rossi R, Logan BE. The effect of high applied voltages on bioanodes of microbial electrolysi cells in the presence of chlorides. Chemical Engineering Journal. 2021;**405**(1):126742

[55] Wang R, Li H, Sun J, Zhang L, Jiao J, Wang Q, et al. Nanomaterials facilitating microbial extracellular electron transfer at interfaces. Advanced Materials. 2021;**33**(6):2004051

[56] Narayanasamy S, Jayaprakash J. Application of carbon- polymer based composite electrodes for microbial fuel cells. Reviews in Environmental Science and Biotechnology. 2020;**19**:595-620

[57] Cai Z, Huang L, Quan X, Zhao Z, Shi Y, Puma GL. Acetate production from inorganic carbon (HCO^-) in photo-assisted biocathode microbial electrosynthesis systems using WO3/MoO3/g-C3N4 heterojunctions and *Serratia marcescens* species. Applied Catalysis. 2020b;**B. 267**:118611

[58] Kaur R, Marwaha A, Chhabra VA, Kim KH, Tripathi S. Recent developments on functional nanomaterial-based electrodes for microbial fuel cells. Renewable and Sustainable Energy Reviews. 2020;**119**:109551

[59] Li Q, Fu Q, Kobayashi H, He Y, Li Z, Li J, et al. GO/PEDOT modified biocathode promoting CO2 reduction to CH4 in microbial electrosynthesis. Sustainable Energy & Fuels. 2020;**4**(6):2987-2997

[60] Olabi A, Wilberforce T, Sayed ET, Elsaid K, Rezk H, Abdelkareem MA. Recent progress of graphene based nanomaterials in bioelectrochemical systems. Science of The Total Environment. 2020;**749**:141225

[61] Shabani M, Younesi H, Pontié M, Rahimpour A, Rahimnejad M, Zinatizadeh AA. A critical review on recent proton exchange membranes applied in microbial fuel cells for renewable energy recovery. Journal of Cleaner Production. 2020;**264**:121446

[62] Mouhib M, Antonucci A, Reggente M, Amirjani A, Gillen AJ, Boghossian AA. Enhancing bioelectricity generation in microbial fuel cells and biophotovoltaics using nanomaterials. Nano Research. 2019;12(9):2184-2199. DOI: 10.1007/s12274-019-2438-0

[63] Zhang Y, Jiang J, Zhao Q, Wang K, Yu H. Analysis of functional genomes from metagenomes: Revealing the accelerated electron transfer in microbial fuel cell with rhamnolipid addition. Bioelectrochemistry. 2018a;**119**:59-67

[64] Hindatu Y, Annuar M, Gumel A. Mini-review: A node modification for improved performance of microbial fuel cell. Renewable and Sustainable Energy Reviews. 2017;**73**:236-248

[65] Kannan M. Current status, key challenges and its solutions in the design and development of graphene based ORR catalysts for the microbial fuel cell applications. Biosensors & Bioelectronics. 2016;**77**:1208-1220

[66] Ci S, Cai P, Wen Z, Li J. Graphene-based electrode materials for microbial fuel cells. Science China Materials. 2015;**58**(6):496-509

[67] Logan BE, Regan JM. Electricity-producing bacterial communities in microbial fuel cells. Trends in Microbiology. 2006;14(12):512-518

[68] Logan BE. Exoelectrogenic bacteria that power microbial fuel cells. Nature Reviews. Microbiology. 2009;**7**:375-381

[69] Logan BE, Rossi R, Saikaly PE. Electroactive microorganisms in bioelectrochemical systems. Nature Reviews. Microbiology. 2019;**17**(5):307-319

[70] Yang Q, Yang S, Liu G, Zhou B, Yu X, Yin Y. Boosting the anode performance of microbial fuel cells with a bacteria-derived biological iron oxide/carbon nanocomposite catalyst. Chemosphere. 2021;**268**:128800

[71] Slate AJ, Whitehead KA, Brownson DAC, Banks CE. Microbial fuel cells: An overview of current technology. Renewable and Sustainable Energy Reviews. 2019;**101**:60-81. DOI: 10.1016/j.rser.2018.09.044

[72] Sayed ET, Tsujiguchi T, Nakagawa N. Catalytic activity of baker's yeast in a mediatorless microbial fuel cell. Bioelectrochemistry. 2012;**86**:97-101. DOI: 10.1016/j.bioelechem.2012.02.001

[73] Schaetzle O, Barrière F, Baronian K. Bacteria and yeasts as catalysts in microbial fuel cells: Electron transfer from micro-organisms to electrodes for green electricity. Energy & Environmental Science. 2008;**1**:607-620

[74] Hemen Sarma PN, Bhattacharyya DA, Jadhav PP, Thakare M, Pandit S, Mathuriya AS. Fungal-mediated electrochemical system: Prospects, applications and challenges. Current Research in Microbial Sciences. et al., 2021;**2**:100041

[75] Patel N, Rai D, Chauhan D, Shahane S, Mishra U, Bhunia B. Carbon

nanotube based anodes and cathodes for microbial fuel cells. In: Microbial Fuel Cells: Materials and Applications. Vol. 46. Materials Research Forum LLC; 2019. pp. 125-150

[76] Salar-García M, Ortiz-Martínez V. Nanotechnology for wastewater treatment and bioenergy generation in microbial fuel cells. In: Advanced Research in Nanosciences for Water Technology. Springer; 2019. pp. 341-362

[77] Nambiar S, Togo C, Limson J. Application of multi-walled carbon nanotubes to enhance anodic performance of an Enterobacter cloacae-based fuel cell. African Journal of Biotechnology. 2009;**8**(24):6927-6932. Available from: http://www.academicjournals.org/AJB ISSN 1684-5315

[78] Jiang Q, Xing D, Zhang L, Sun R, Zhang J, Zhong Y, et al. Interaction of bacteria and archaea in a microbial fuel cell with ITO anode. RSC Advances. 2018a;**8**:28487-28495. DOI: 10.1039/c8ra01207e

[79] Yin T, Zhang H, Yang G, Wang L. Polyaniline composite TiO2 nanosheets modified carbon paper electrode as a high performance bioanode for microbial fuel cells. Synthetic Metals. 2019;**252**:8-14

[80] Zhu W, Yao M, Gao H, Wen H, Zhao X, Zhang J, et al. Enhanced extracellular electron transfer between Shewanella putrefaciens and carbon felt electrode modified by bio-reduced graphene oxide. Science of The Total Environment. 2019;**691**:1089-1097

[81] Hernández LA, Riveros G, González DM, Gacitua M, del Valle MA. PEDOT/graphene/nickel-nanoparticles composites as electrodes for microbial fuel cells. Journal of Materials Science: Materials in Electronics. 2019;**30**(13):12001-12011

[82] Duarte KD, Frattini D, Kwon Y. High performance yeast- based microbial fuel cells by surfactant-mediated gold nanoparticles grown atop a carbon felt anode. Applied Energy. 2019;**256**:113912

[83] Truong DH, Dam MS, Bujna E, Rezessy-Szabo J, Farkas C, Vi VNH, et al. In situ fabrication of electrically conducting bacterial cellulose-polyaniline-titanium-dioxide composites with the immobilization of Shewanella xiamenensis and its application as bioanode in microbial fuel cell. Fuel. 2021;**285**:119259

[84] Zhang Q, Zhang L, Wang H, Jiang Q, Zhu X. Simultaneous efficient removal of oxyfluorfen with electricity generation in a microbial fuel cell and its microbial community analysis. Bioresource Technology. 2018b;**250**:658-665. DOI: 10.1016/j.biortech.2017.11.091

[85] Lu L, Xing D, Ren ZJ. Microbial community structure accompanied with electricity production in a constructed wetland plant microbial fuel cell. Bioresource Technology. 2015;**195**:115-121

[86] Masoudi M, Rahimnejad M, Mashkour M. Enhancing operating capacity of microbial fuel cells by using low-cost electrodes and multi anode-cathode connections in a membrane-less configuration. International Journal of Hydrogen Energy. 2021;**46**(11):8226-8238

[87] Yaqoob AA, Ibrahim MNM, Rafatullah M, Chua YS, Ahmad A, Umar K. Recent advances in anodes for microbial fuel cells: An overview. Materials. 2020;**13**:2078. DOI: 10.3390/ma1309207

[88] Aryal N, Halder A, Zhang M, Whelan PR, Tremblay PL, Chi Q, et al. Freestanding and flexible graphene papers as bioelectrochemical cathode for

selective and efficient CO2 conversion. Scientific Reports. 2017;**7**(1):1-8

[89] Bian B, Alqahtani MF, Katuri KP, Liu D, Bajracharya S, Lai Z, et al. Porous nickel hollow fiber cathodes coated with CNTs for efficient microbial electrosynthesis of acetate from CO2 using Sporomusa ovata. Journal of Materials Chemistry A. 2018;**6**(35):17201-17211

[90] Han S, Liu H, Zhou C, Ying HJ. Growth of carbon nanotubes on graphene as 3D biocathode for NAD+/NADH balance model and high-rate production in microbial electrochemical synthesis from CO2. Journal of Materials Chemistry A. 2019;**7**(3):1115-1123

[91] Choudhury P, Prasad Uday US, Bandyopadhyay TK, Ray RN, Bhunia B. Performance improvement of microbial fuel cell (MFC) using suitable electrode and Bioengineered organisms: A review. Bioengineered. 2017;**8**:471-487

[92] Kumar R, Singh L, Zularisam AW, Hai FI. Microbial fuel cell is emerging as a versatile technology: A review on its possible applications, challenges and strategies to improve the performances. International Journal of Energy Research. 2018;42(2):369-394

[93] Mashkour M, Rahimnejad M. Effect of various carbon-based cathode electrodes on the performance of microbial fuel cell. Biofuel Research Journal. 2015;**2**:296-300

[94] Xue W, Zhou Q, Li F. The feasibility of typical metal– organic framework derived Fe, Co, N co-doped carbon as a robust electrocatalyst for oxygen reduction reaction in microbial fuel cell. Electrochimica Acta. 2020;**355**:136775

[95] Wu Y, Zhang X, Li S, Lv X, Cheng Y, Wang X. Microbial biofuel cell operating 20 effectively through carbon nanotube blended with gold–titania nanocomposites 21 modified electrode. Electrochimica Acta. 2013;**109**:328-332

[96] Sun M, Zhang F, Tong Z-H, Sheng G-P, Chen Y-Z, Zhao Y, et al. A gold-sputtered carbon paper as an anode for improved electricity generation from a microbial fuel cell inoculated with *Shewanella oneidensis* MR-1. Biosensors & Bioelectronics. 2010;**26**:338-343

[97] Han HT, Khan MM, Kalathil S, Lee J, Cho MH. Simultaneous enhancement of methylene blue degradation and power generation in microbial fuel cell by gold nanoparticles, Industrial & Engineering Chemistry Research. Just Accepted Manuscript. 2013;52(24):8174-8181. DOI: 10.1021/ie4006244. Publication Date (Web): 27 May 2013 Downloaded from: http://pubs.acs.org on June 1, 2013

[98] Rong H, Zhang S, Muhammad S, Zhang J. Noble metal-based nanocomposites for fuel cells. Novel Nanomaterials. London, UK: IntechOpen; 2018. pp. 291-310. DOI: 10.5772/intechopen.71949

[99] Zhang H, Lu HY, Hu NF. Fabrication of electroactive layer-by-layer films of myoglobin with gold nanoparticles of different sizes. The Journal of Physical Chemistry B. 2006;**110**:2171-2179

[100] Dessie Y, Tadesse S. Advancements in bioelectricity generation through nanomaterial-modified anode electrodes in microbial fuel cells. Review published: 17 May 2022 doi: 10.3389/fnano.2022.876014, Frontiers in Nano Technology

[101] Guo W, Pi Y, Song H, Tang W, Sun J. Layer-by-layer assembled gold nanoparticles modified anode and its application in microbial fuel cells. Colloids and Surfaces A: Physicochemical and Engineering Aspects. 2012;415:105-111

[102] Kalathil S, Jintae Lee, and Moo Hwan Cho. 2013. Gold nanoparticles produced in situ mediate bioelectricity and hydrogen production in a microbial fuel cell by quantized capacitance charging ChemSusChem 2013, 6, 246 – 250 247, DOI: 10.1002/cssc.201200747

[103] Cheng Y, Mallavarapu M, Naidu R, Chen Z. In situ fabrication of green reduced graphene-based biocompatible anode for efficient energy recycle. Chemosphere. 2018;**193**:618-624

[104] Richter H, McCarthy K, Nevin KP, Johnson JP, Rotello VM, Lovley DR. Electricity generation by Geobacter sulfurreducens attached to gold electrodes. Langmuir. 2008;**24**:4376

[105] Amirdehi MA, Saem S, Zarabadi MP, Moran-Mirabal JM, Greener J. Microstructured anodes by surface wrinkling for studies of direct electron transfer biofilms in microbial fuel cells. Advanced Materials Interfaces. 2018:1800290

[106] Gu HY, Fu C-C, Su C-H, Hung T-C, Hsieh C-H, Suryani D, et al. Effects of biomass weight and light intensity on the performance of photosynthetic microbial fuel cells with Spirulina platensis. Bioresource Technology. 2009;**100**:4183-4186

[107] Lin H, Wu X, Nelson C, Miller, Zhu J. Electricity generation and nutrients 30 removal from high-strength liquid manure by air-cathode microbial fuel cells, Journal of Environmental Science and Health Part A, 2016;**51**(3):240-250

[108] Chen S, Chen X, Hou S, Xiong P, Xiong Y, Zhang F, et al. A gold microarray electrode on a poly(methylmethacrylate) substrate to improve the performance of microbial fuel cells by modifying

biofilm formation. RSC Advances. 2016;**6**:114937-114943. DOI: 10.1039/C6RA22152A

[109] Alatraktchi FA, Zhang Y, Noori JS, Angelidaki I. Surface area expansion of electrodes with grass-like nanostructures and gold nanoparticles to enhance electricity generation in microbial fuel cells. Bioresource Technology. 2012;**123**:177-183

[110] Kasem E, Tsujiguchi T, Nakagawa N. Effect of metal modification to carbon paper anodes on the performance of yeast-based microbial fuel cells part II: In the case with exogenous mediator, methylene blue. Key Engineering Materials. 2013;**534**:82-87

[111] Chandra R, Venkata Mohan S, Roberto P-S, Ritmann BE, Cornejo RAS. Biophotovoltaics: Conversion of Light Energy to Bioelectricity through Photosynthetic Microbial Fuel Cell Technology. Microbial Fuel Cell. 2017:373-387. DOI: 10.1007/978-3-319-66793-5_19

[112] Regmi R, Nitisoravut R, Charoenroongtavee S, Yimkhaophong W, Phanthurat O. Earthen pot-plant microbial fuel cell powered by vetiver for bioelectricity production and wastewater treatment. Clean. - Soil, Air, Water. 2018a;**46**:1700193. DOI: 10.1002/clen.201700193

[113] Feng J, Qian Y, Wang Z, Wang X, Xu S, Chen K, et al. Enhancing the performance of *Escherichia coli*-inoculated microbial fuel cells by introduction of the phenazine-1-carboxylic acid pathway. Journal of Biotechnology. 2018;**275**:1-6

[114] Cui Y, Lai B, Tang X. Microbial fuel cell-based biosensors. Biosensors. 2019;**9**(3):92

[115] Chen L, Tremblay PL, Mohanty S, Xu K, Zhang T. Electrosynthesis

of acetate from CO_2 by a highly structured biofilm assembled with reduced graphene oxide–tetraethylene pentamine. Journal of Materials Chemistry A. 2016;**4**(21):8395-8401

[116] Do MH, Ngo HH, Guo W, Chang SW, Nguyen DD, Liu Y, et al. Microbial fuel cell-based biosensor for online monitoring wastewater quality: A critical review. Science of the Total Environment. 2020;**712**:135612

Chapter 6

RCWA Simulation Study of Enhanced Infrared Absorption Spectroscopy by Au Nanoparticle Array Combined with Optical Cavity Effect

Daichi Mitobe and Yushi Suzuki

Abstract

Surface-enhanced infrared absorption is a phenomenon by which the infrared absorption intensity of molecules near metal nanoparticles (NPs) is increased considerably. In surface-enhanced infrared absorption spectroscopy, the absorption intensity depends on the strength of the field acting on the NPs layer. The optical cavity effect generates a strong electric field. If this strong electric field is applied to the NPs, then the IR absorption intensity will be enhanced further. This simulation study assessed the possibility of applying the enhanced electric field generated by the pseudo-optical cavity effect to the NP array. Results indicated that the IR absorption is markedly enhanced.

Keywords: au nanoparticle array, enhanced infrared absorption, optical cavity effect, rigorous coupled wave analysis

1. Introduction

An optical cavity is a method of confining light in a cavity (air layer or transparent dielectric layer) and of generating a larger field by the interference of the confined light [1, 2]. In this case, a standing wave is formed in the cavity. In a complete optical cavity system, a transparent layer with a high refractive index is surrounded by an atmosphere with a low refractive index. By setting the incident angle from the high refractive index layer to the low refractive index layer as equal to or larger than the critical angle, the reflectance at both interfaces of the high refractive index layer becomes unity. Therefore, the light incident on this layer is confined in the layer completely: a large field is formed. In this system, a high refractive index prism is used to inject light into the high refractive index layer, so that the simplest system is at least a four-layer system. We realized a simpler three-phase pseudo-optical cavity system using a high refractive index prism—air layer—bulk metal layer [3]. In this system,

an air layer with a low refractive index is in contact with a high refractive index prism. The other interface is air-metal, with reflectance that is almost unity in the infrared region. Experiments and calculations demonstrated that, even in this case, an enhanced electromagnetic field is obtained within the air film (air layer) as a result of reflection and interference, which indicates that the pseudo-optical cavity effect might occur, even if the reflectance at both interfaces of the layer is not unity, as long as the reflectance is higher than a certain value. For instance, the pseudo-cavity effect might be achieved even in a three-layer system composed of a low refractive index layer-medium refractive index layer-high refractive index layer. As one example, a three-layer system of air (or vacuum)-polymer (or fluoride)-silicon (or germanium) is proposed. If the pseudo-optical cavity is achieved in this system and if an anti-node of standing wave is formed at the air-polymer interface, then infrared absorption by molecules present near the air-polymer interface can be enhanced. By appropriately setting parameters such as the dielectric constant of the layer and the layer thickness, anti-nodes can be formed at the interface.

Surface enhanced infrared absorption (SEIRA) is a method of enhancing the infrared absorption intensity of molecules existing around the particles using nano-sized metal fine particles (NP) [4, 5]. The NPs used for this process, including research by which enhanced infrared absorption was discovered, have been used widely in evaporated films because they are easily prepared [6–9]. In recent years, many studies using nano-sized metals with special shapes such as nano-antennas and nano-resonators have been reported [10–20]. These structures are used to excite surface plasmons (polaritons) to create an enhanced field (called hotspots). These complex metal structures are manufactured using lithography technology and other techniques. These structures provide powerful hotspots, but their fabrication requires extensive apparatus, which is difficult to arrange at a laboratory level. If a metal structure that can be created more easily were to provide a sufficient enhanced field, then this limitation could be relaxed. Therefore, we aim at obtaining greater absorption enhancement using vapor-deposited films or metal films with similar structures. The enhanced infrared absorption can greatly improve the infrared spectroscopy detection limit, which might facilitate analysis in many fields. The infrared absorption intensity of molecules A has a relational expression of $A \propto N\alpha|E|^2$, wherein N represents the amount of the molecule, α is the absorption coefficient of the molecule, and E stands for is the electric field strength. In other words, the key factor for development of sensing technology such as infrared spectroscopy is obtaining a strong electric field. Enhanced infrared absorption is a method of obtaining large absorption by increasing the electric field strength around the NP [21, 22]. The enhanced field formed around the NP depends on the electric field strength acting on the NP. Put simply, by imposing a large electric field on the NP array, the electric field formed around it will be larger, resulting in greater absorption intensity of the molecules. If the large electric field generated by the optical cavity effect described above is applicable to the evaporated film, then large infrared absorption is obtainable, thereby further increasing the potential for infrared spectroscopy.

For this study, we examine the potential of enhanced infrared absorption coupled with optical cavity effects. For this purpose, we use rigorous coupled wave analysis (RCWA) [23] to simulate the enhanced mechanism numerically by combining the optical cavity with a square column array modeling the deposited metallic thin film.

2. Calculation

Rigorous coupled wave analysis (RCWA) was used for the simulation examined for this study. Actually, RCWA is a semi-analytical method in computational electromagnetics, typically used to solve diffraction of a field by a given periodic grating structure [24, 25]. Because it is difficult to evaluate the evaporated metal thin film directly as a result of its irregular shape, we adopt a square column array that models the evaporated film. It has been confirmed that the RCWA simulation using a Au square column array shows good agreement with measurement results obtained using the nanoarray prepared using an evaporated film or electron beam lithography [26, 27]. For this study, we conducted simulations under the following three conditions.

2.1 Simulation of infrared absorption spectra of model molecules by pseudo-optical cavity effect

A three-layer system consisting of the low refractive index layer—medium refractive index layer—high refractive index layer can act as a pseudo-optical cavity. A simulation to assess that hypothesis was performed in a four-layer system with an additional model molecule layer to achieve infrared absorption (vacuum layer—model molecular layer—buffer layer—Si substrate layer). The buffer layer thickness was changed from 50 to 4000 nm to simulate absorption spectra. The model molecular layer thickness was set as 12 nm. As the buffer layer, a material with a refractive index of 1.442 (the imaginary part is 0) was used. This value was used to reduce, to the greatest extent possible, effects of the presence of a model molecular layer on the reflectance and phase shift at a low refractive index layer—medium refractive index layer interface. In this system, the transmission spectra were simulated. The absorbance values were obtained from the results. To obtain a reference spectrum, simulation was also performed with a vacuum layer—model molecular layer—substrate layer, without a buffer layer. The same optical constant as a buffer layer was set on the substrate to eliminate the influence of a refractive index of the substrate on a reference spectrum. The enhancement factor is calculated by dividing the absorption intensity of a model molecule on the buffer layer by the absorption intensity of a model molecule without a buffer layer.

Furthermore, for the cavity effect, a refractive index of a buffer layer is considered to affect the interference inside a cavity. Therefore, simulations for which the refractive indexes of buffer layers are set respectively to 1.2 and 1.6 are also performed to obtain the absorbances.

2.2 Simulation of infrared absorption spectra of model molecule by combination pseudo-optical cavity effect with a square column array

To clarify the applicability of the enhanced field generated by the pseudo-optical cavity formed in the medium refractive index layer to the enhanced infrared absorption, simulations were conducted with a vacuum layer—model molecule and Au NP array layer—buffer layer—Si substrate layer (**Figure 1**). The Au NP size was 80 × 80 nm. The height was 12 nm. In addition, the distance of NP was 20 nm. These morphological parameters were chosen to approximate the scale of the evaporated film. The model molecules were placed in gaps of the Au NP array. Also, the height was set as equal to the height of NP (12 nm). As the buffer layer, a material with a
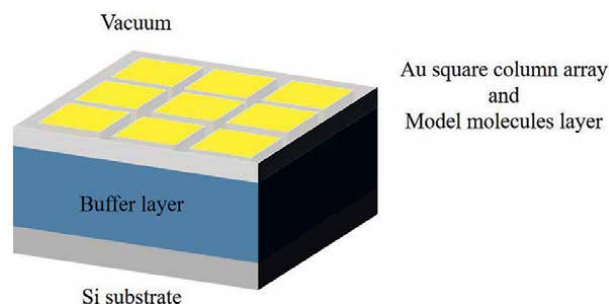
Figure 1.
Schematic diagram of the four-layer system used in the simulation, as seen from the side. The model molecules were placed in gaps of the Au NP array.

refractive index of 1.442 (the imaginary part is 0) was used. As in 2.1, the buffer layer thickness was varied from 50 to 4000 nm. The transmission spectra were simulated. Also, the absorbances were obtained from the results. In addition, the same optical constant as the buffer layer was used for the substrate. We performed simulation of the vacuum layer—model molecule and Au NP array layer—substrate layer, using the same parameters as those used above. The enhancement factors in the cavity effect by the buffer layer were evaluated from the ratio of absorbance with and without the buffer layer.

2.3 Simulation of infrared absorption spectra of model molecule by combination of pseudo-optical cavity effect with nanoarray and Au plane

In the system adopted for use in this study, the magnitude of the interference field generated by the pseudo-optical cavity is sensitive to the reflectance at both interfaces of the medium refractive index layer. As the amount of light confined in the cavity increases, the field generated by the interference strengthens; the cavity effect becomes greater. Therefore, to improve the reflectivity at the interface between the medium refractive index layer and the high refractive index layer (substrate), a metal plane layer is placed to act as a mirror (**Figure 2a**). The model molecule absorption intensity is simulated by this system. The Au layer thickness is 200 nm, which is sufficient to prevent infrared light transmission. The parameters of NP array and the buffer layer adopted the same values as in 2.2. Unlike 2.1 and 2.2, there is almost no transmitted light. Therefore, the reflection spectra were simulated. The values for absorbance were obtained from the results.

To investigate details of the electric field enhancement mechanism, we simulate the distribution of the electric field in the normal direction inside the buffer layer. If the existence of standing waves in the layer is confirmed, then it can be proved that the electric field enhancement results from the optical cavity effect. A model molecule layer with 10 nm thickness is placed in the buffer layer in the in-plane direction. By changing the position of this layer in the plane normal direction, the electric field intensity at each position in the buffer layer is evaluated from the absorption intensity of the model molecule (**Figure 2b**). In this case, no model molecules are placed in the NP array gaps.

The Lorentz oscillator model, formulated as described below, was adopted as the model molecule.
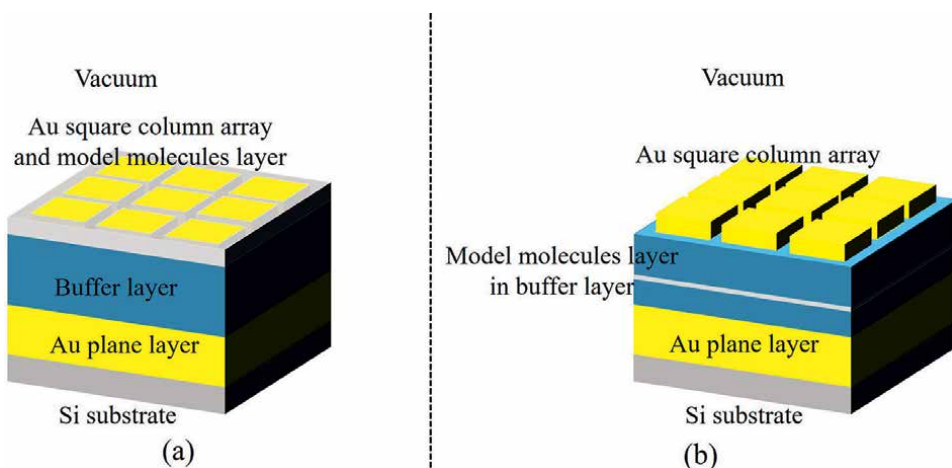
Figure 2.
Schematic diagram of (a) a five-layer system used in the simulation and (b) with a model molecular layer with a 10 nm thickness in the buffer layer.

$$\varepsilon(\omega) = \varepsilon_{int} + f \Big/ \left(\omega_0^2 - \omega^2 + i\gamma\omega \right) \tag{1}$$

herein, ε_{inf} = 2.08, f = 2.8 × 10^{27} s^{-2}, γ = 8.0 × 10^{12} s^{-1}, and ω_0 = 3.216 × 10^{14} s^{-1}.

The wavenumber range of calculation was 1900–1500 cm^{-1}. The spectral resolution was 4 cm^{-1}. The incident light of the TM mode was set at an incident angle of 0°. For calculations, S^4 free software was used [28]. The dielectric constants of the substrate (Si) and metal particles (Au) were referred from values reported in the literature [29, 30].

3. Results and discussion

3.1 Simulation results of infrared absorption spectra of model molecules by pseudo-optical cavity effect

The complete optical cavity system constitutes a four-layer system, forming an intense field within the cavity. A simpler three-layer pseudo-optical cavity system has been realized using a high index prism—air gap—bulk metal. Experiments and calculations have proved that an enhanced electromagnetic field is obtainable in the air gap, which indicates that the pseudo-optical cavity effect might occur even if the reflectance at both interfaces of the layer is not unity, as long as the reflectance is higher than a certain value. Therefore, we investigated that the three-layer system consisting of low refractive index layer (air)—medium refractive index layer—high refractive index layer (Si) can function as a pseudo-optical cavity.

Figure 3 shows the 3D infrared absorption spectra of model molecules simulated by RCWA in the four-layer, the vacuum layer—model molecular layer—buffer layer—Si substrate.

As depicted in **Figure 3**, the absorption intensity does not change monotonically with the buffer layer thickness. To assess the change in the maximum value of the absorption intensity clearly, **Figure 4** shows a plot of the change in the absorption intensity with respect to the buffer layer thickness.
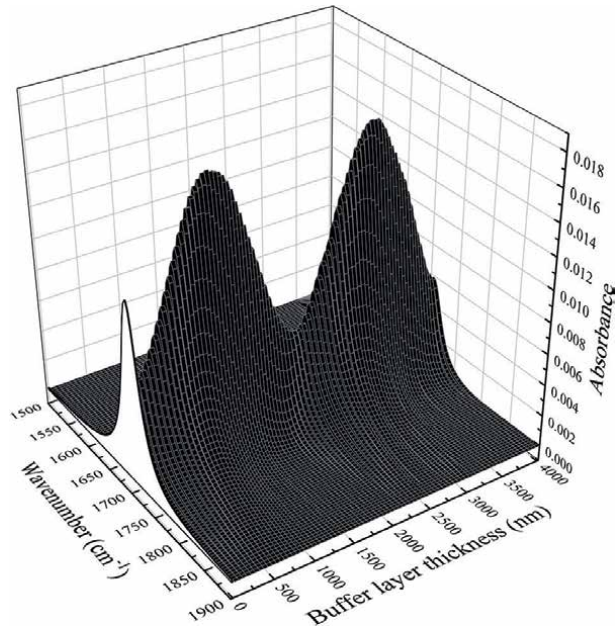
Figure 3.
3D infrared absorption spectra of the model molecule as a function of buffer layer thickness. The infrared absorption spectrum with buffer layer thickness of 0 is the spectrum of the model molecule on a bare substrate.
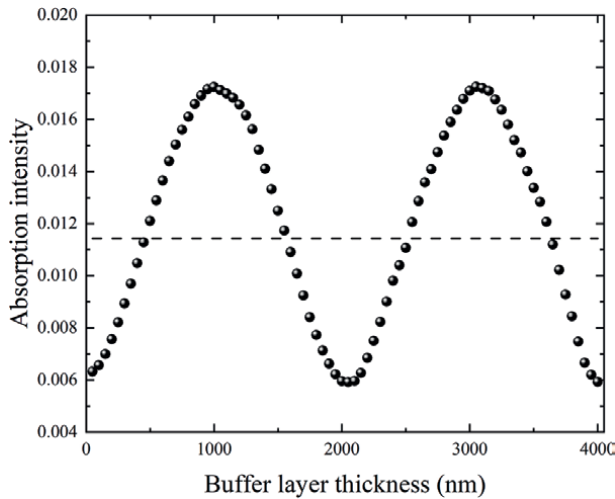

Figure 4.
Infrared absorption intensity of the model molecule as a function of buffer layer thickness. The dashed line represents the reference spectrum intensity.

As portrayed in **Figure 4**, the absorption intensity increases as the buffer layer thickness increases, reaches a maximum value (around 1000 nm), and then begins to decrease. After reaching the minimum value (2000 nm), it increases again. In short, as the buffer layer thickness increases, the absorption intensity increases and decreases periodically. As the buffer layer thickness increases, the light path length increases. The change in the light path length changes the interference conditions in

the buffer layer, leading to electric field strengthening or weakening. The change in the absorption intensity portrayed in **Figure 4** is explainable as a result of this interference effect. This behavior indicates that this system is acting as a pseudo-optical cavity. The maximum value of the periodically varying absorption intensity is about 0.017, which is larger than the absorption intensity of the reference spectrum: approximately 0.011. The enhancement attributable to the cavity effect is about 1.5 times.

The actual optical path length also depends on the refractive index of the buffer layer. **Figure 5** presents the calculation with the refractive index changed and the other conditions being roughly equal.

From this figure, it is apparent that the period of the absorption intensity changes. The maximum value of the intensity depends on the refractive index of the buffer layer. These reasons are explainable as follows. An increase in the refractive index is associated with an increase in the light path length. In other words, the optical thickness increases for the same physical film thickness. Therefore, the period of the absorption intensity change against the physical film thickness becomes shorter. The reflectance at the interface between the buffer layer and the substrate becomes smaller as the difference in refractive index between the buffer layer and the substrate becomes smaller. When the refractive index of the buffer layer is close to the refractive index of the Si substrate ($n_{Si} = 3.42$), the reflectance at the interface becomes lower, which reduces the light trapped in the buffer layer. Also, the standing wave formed in the buffer layer becomes weaker, thereby reducing the maximum peak intensity. These results support that the system acts as a pseudo-optical cavity and that it therefore affects the infrared absorption intensity of the model molecule.

3.2 Simulation results of spectra combining pseudo-optical cavity effect with enhanced infrared absorption in a square column array

The enhanced field formed around the NPs in enhanced infrared absorption depends on the electric field strength acting on the NP. The results of 3.1 showed that
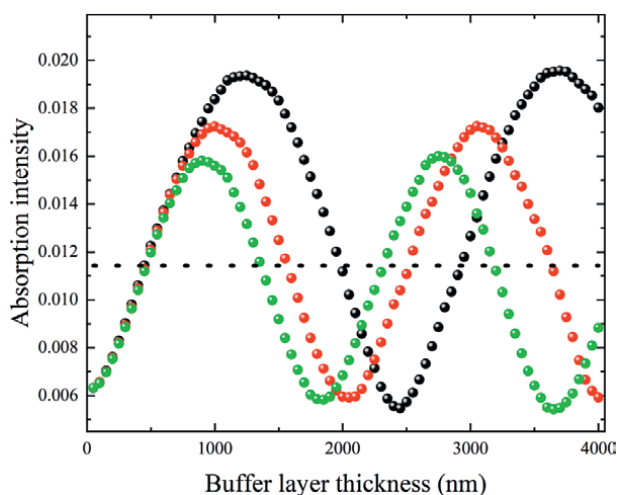

Figure 5.
The absorption intensity as a function of buffer layer thickness with the refractive index is varied. Each mark represents the index of refraction of the buffer layer: 1.2 for black, 1.442 for red, and 1.6 for green. The dashed line shows the absorption intensity of the model molecule on the bare substrate.

a three-layer system composed of the low refractive index layer—medium refractive index layer—high refractive index layer functions as a pseudo-optical cavity. Therefore, we investigate the infrared absorption spectra of the model molecule around the NP when the enhanced field generated by the pseudo-optical cavity acts on the NP placed at the vacuum layer—buffer layer interface.

Figure 6 shows RCWA simulation results of the 3D infrared absorption spectra of the model molecule of the model molecule placed in the gap of the Au NP array set at the vacuum layer—buffer layer interface and of the model molecule in the gap of the Au NP without the buffer layer.

The change in the spectrum with increasing buffer layer thickness is the same as that in 3.1.

The dependence of the absorption intensity on the buffer thickness is portrayed in **Figure 7** to clarify the change in the maximum absorption intensity with thickness.

As portrayed in **Figure 7,** as the buffer layer thickness increases, the absorption intensity of the model molecule changes periodically dependently of it, confirming the same behavior as that presented in 3.1.

The enhancement factor in enhanced infrared absorption because of NP array is about 18.5 times. Moreover, the enhancement factor of the cavity effect is about 1.5 times. If it is a combination of the effects explained above, it is expected to be about 27.75 times, which is the product of each enhancement factor. The enhancement factor obtained from the simulation results is about 28 times, which is almost identical. From these findings, it can be confirmed that the electric field enhanced by the pseudo-cavity effect in the buffer layer acted on the NP array. Thereby, greater enhancement was obtained.
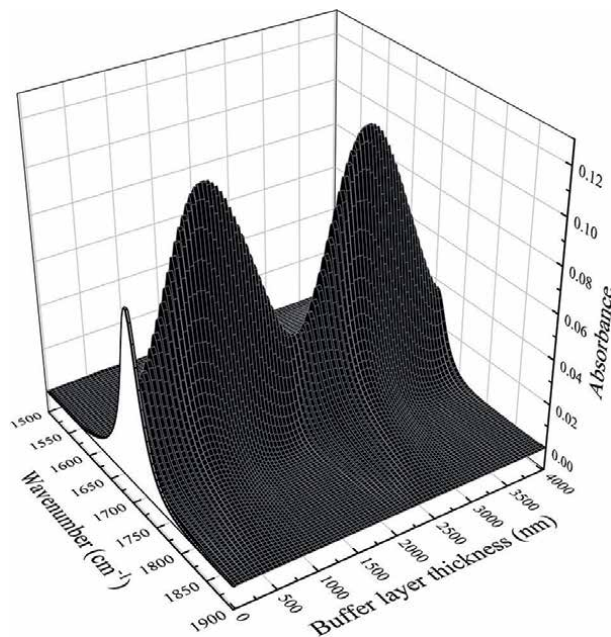

Figure 6.
3D enhanced infrared absorption spectrum of the model molecule as a function of the buffer layer thickness. The infrared absorption spectrum with buffer layer thickness of 0 is the spectrum in a Au NP array without the buffer layer.
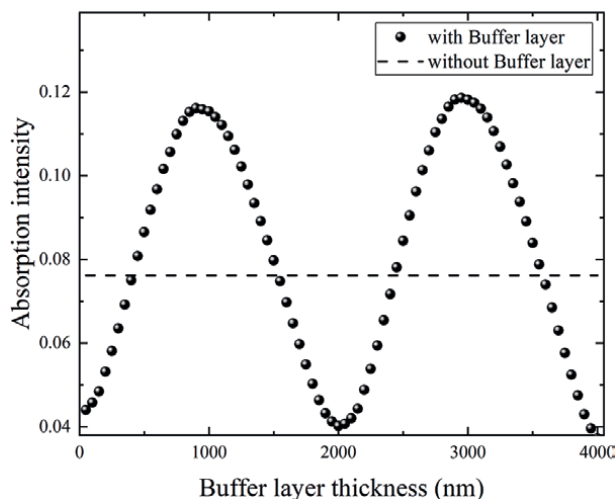
Figure 7.
Variation of absorption intensity as a function of buffer layer thickness. The dashed line represents the reference spectrum intensity.

3.3 Simulation results of spectra combining pseudo-optical cavity effect with enhanced infrared absorption in a square column array with Au plane

The enhanced electric field in the pseudo-optical cavity layer (buffer) is sensitive to reflectance at both interfaces of the layer. Therefore, a Au planar layer is placed between the buffer layer and the substrate to increase the reflectivity at this interface, thereby enhancing the optical cavity effect.

The infrared absorption spectra of model molecules placed in the gap of NP array in the system with a Au planar layer between the buffer layer and the substrate are presented in **Figure 8**.

In this system, as in 3.1 and 3.2, it can be confirmed that the absorption intensity depends on the buffer layer thickness. **Figure 9** presents variation of the absorption intensity with the buffer layer thickness.

Even for systems in which the Au layer is added, a periodic change in absorption intensity with respect to the buffer layer thickness is observed, indicating the presence of a cavity effect. We confirmed that greater enhancement is obtainable by placing a Au planar layer at the buffer layer-substrate interface to improve the reflectivity at this interface. Although using a complex metal structure, Debbrecht et al. [31] reported results of a similar study of enhancement caused by the optical cavity effect.

Comparing the IR absorption enhancement factor of the model molecules with and without the Au layer, it is about 28 for the case without the Au layer and about 95 for the case with the Au layer because the presence of the Au layer increased the reflectivity at the interface (**Figure 10**) and created a larger cavity field in the buffer layer, which acted on the NP array.

Next, the distribution of the electric field intensity formed in the buffer layer in the direction of the interface normal is simulated. The buffer layer thickness is 860 nm, which is the maximum absorption intensity, and 2000 nm, which is the minimum. The resulting electric field distribution in the buffer layer is presented in **Figure 11**.

The vertical axis represents the distance from the Au planar film interface on the substrate, the upper end of which is the NP layer interface. The behavior of the
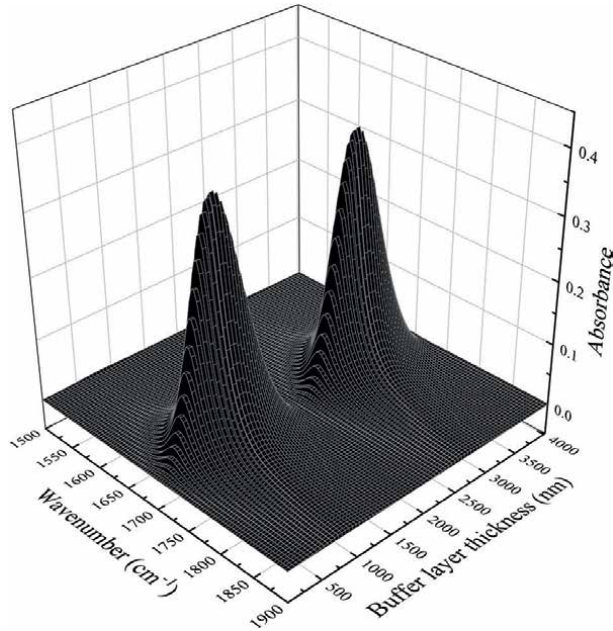
Figure 8.
3D infrared absorption spectra of the model molecule as a function of the buffer layer thickness when the Au plane layer is placed between the buffer layer and the substrate.
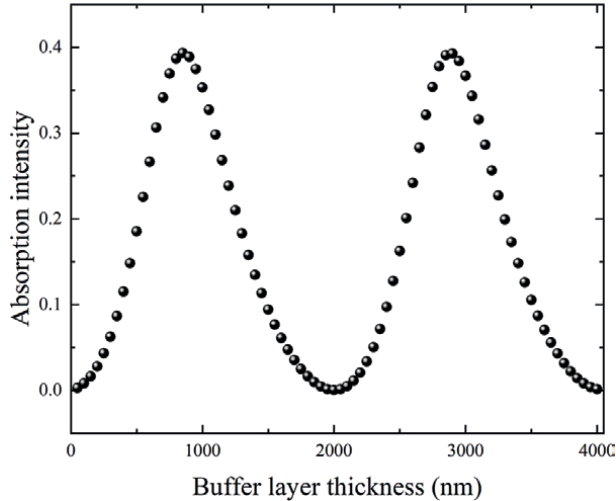

Figure 9.
Infrared absorption intensity with a Au plane layer as a function of buffer layer thickness.

change in absorption intensity in **Figure 11b** is one cycle of the sine function, which indicates that a standing wave is established in the buffer layer. This standing wave is the result of interference of light within the buffer layer, indicating that this system realizes a pseudo-optical cavity effect. In this case, standing wave nodes are formed at the NP layer interface. As a result, the electric field acting on the NP layer is weak. The absorption intensity attributable to the model molecules in the NP
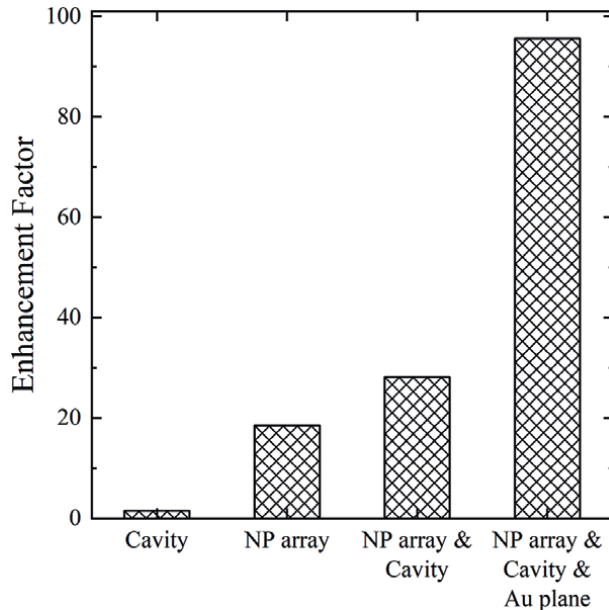
Figure 10.
Comparison of infrared absorption enhancement factors in each system configuration. Horizontal axis labels represent the configurations. Cavity: the system consisting of the vacuum layer-buffer layer-Si substrate layer (Section 3.1). NP array: the system consisting of the vacuum layer-Au square column array layer-Si substrate layer (Section 3.2). Cavity & NP array: the system consisting of the vacuum layer-Au square column array layer-buffer layer-Si substrate layer (Section 3.2). Cavity & NP array & Au plane: the system consisting of the vacuum layer-Au square column array layer-buffer layer-Au planar layer-Si substrate layer (Section 3.3).
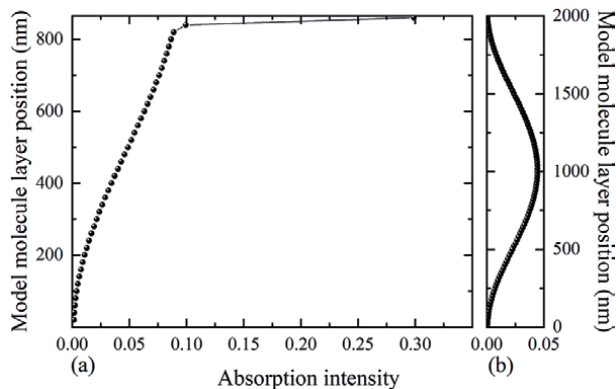

Figure 11.
Distributions of the electric field intensity in the buffer layer with thicknesses of (a) 860 nm, which gives the maximum intensity, and (b) 2000 nm, which gives the minimum intensity.

layer is low. By contrast, in **Figure 11a**, a half-period sine wave is formed. Its anti-node acts on the NP layer, resulting in large absorption. Although not shown, it was confirmed that the IR absorption intensity of the model molecules in the NP layer corresponds to the electric field intensity of the buffer layer acting on the NP layer, even for other buffer layer thicknesses. Results demonstrated that the absorption intensity of the model molecules in the NP layer changes depending on the strength of the electric field in the buffer layer acting on the NP layer. The sudden increase in

the electric field around 860 nm thickness in **Figure 11a** is explainable by effects of the enhanced field in the NP layer penetrating the buffer layer.

For this study, we used a simpler NP array and buffer layer. The following results were obtained by adjusting the system configuration and by making the buffer layer thickness variable.

From findings reported in 3.1, it was demonstrated that the infrared absorption of the model molecules existing at the vacuum layer-buffer layer interface by the pseudo-optical cavity in the vacuum layer-buffer layer-substrate layer three-layer system can be enhanced. Findings reported in 3.2 demonstrated that the infrared absorption of the model molecules around the NPs is enhanced when the field enhanced because of the pseudo-optical cavity is applied to the NP layer. From findings presented in 3.3, it was confirmed that the addition of a Au planar layer can increase the buffer layer interface reflectivity and can further enhance IR absorption. This system, a nanostructured metal layer-buffer layer-planar metal layer-substrate layer, resembles the system reported in references [32–35]. However, the references reported that the large enhancement is attributable to interaction between the long-range plasmons excited in the planar metal layer and the local plasmons excited in the array. An optimum distance can be derived for interaction between the plasmons of two types. The results presented herein confirm that the absorption intensity increases and decreases cyclically with increasing buffer layer thickness. This finding suggests that the infrared absorption enhancement in this paper cannot be explained by plasmon interaction. That is to say, when a metallic structure with a scale similar to that of the evaporated film is used, enhancement attributable to "plasmon interaction" with the planar metallic layer is not observed, but enhancement because of cavity effects, as shown in systems 3.1 and 3.2, does occur.

4. Summary

As described in this paper, we verified by simulation that the enhanced field generated by the pseudo-optical cavity effect in a system consisting of a low-refractive-index layer—middle-refractive-index laye—high-refractive-index layer is applicable to metal nanoparticle (NP) arrays near the interface between the low-refractive-index layer and the middle-refractive-index layer to enhance enhanced IR absorption further. First, it was shown that the three-layer system with a vacuum layer—buffer layer—Si substrate layer functions as a pseudo-optical cavity and that it increases the infrared absorption of model molecules placed at the vacuum layer—buffer layer interface. Next, the IR absorption spectra of model molecules were simulated in a system with an array of Au NP layers at the vacuum layer–buffer layer interface to allow the enhanced field because of the pseudo-optical cavity to act on the NP layers. The enhancement factor in this system was the product of the enhancement factor because of the pseudo-optical cavity effect and the factor of the NP layer. Results clarified that a field enhanced because of the pseudo-optical cavity can be coupled to the enhanced field because of the NP layer. Finally, to obtain a more efficient optical cavity effect, a planar Au layer with reflectivity close to unity in the infrared region was set between the buffer layer and the Si substrate layer to simulate the infrared absorption spectra of model molecules between NPs. As expected, the addition of a planar Au layer provides greater IR absorption, thereby confirming that IR absorption can be enhanced further. This study demonstrates that enhanced infrared absorption

spectroscopy can have higher performance and more flexible tuning capabilities using simple manufacturing methods.

Acknowledgements

Author details

Daichi Mitobe and Yushi Suzuki*
Department of Mathematics and Physics, Graduate School of Science and Technology, Hirosaki, Japan

*Address all correspondence to: uc@hirosaki-u.ac.jp

IntechOpen

References

[1] Harrick NJ. Internal Reflection Spectroscopy. Interscience Publishers (a division of John Wiley & Sons). 1967

[2] Zhao D, Meng L, Gong H, Chen X, Chen Y, Yan M, et al. Ultra-narrow-band light dissipation by a stack of lamellar silver and alumina. Applied Physics Letters. 2014;**104**:221107. DOI: 10.1063/1.4881267

[3] Suzuki Y, Shimada S, Hatta A, Suëtaka W. Enhancement of the IR absorption of a thin film on gold in the Otto ATR configuration. Surface Science. 1989;**219**:L595-L600. DOI: 10.1016/0039-6028(89)90506-2

[4] Hartstein A, Kirtley JR, Tsang JC. Enhancement of the infrared absorption from molecular monolayers with thin metal overlayers. Physical Review Letters. 1980;**45**:201. DOI: 10.1103/PhysRevLett.45.201

[5] Hatta A, Suzuki Y, Suëtaka W. Infrared absorption enhancement of monolayer species on thin evaporated Ag films using a Kretschmann configuration. Applied Physics A: Solids and Surface. 1984;**35**:135-140. DOI: 10.1007/BF00616965

[6] Kellner R, Mizaikoff B, Jakusch M, Wanzenböck HD, Weissenbacher N. Surface-enhanced vibrational spectroscopy: A new tool in chemical IR sensing? Applied Spectroscopy. 1997;**51**:495-503

[7] Miyake H, Ye S, Osawa M. Electroless deposition of gold thin films on silicon for surface-enhanced infrared spectroelectrochemistry. Electrochemistry Communication. 2002;**4**:973-977. DOI: 10.1016/S1388-2481(02)00510-6

[8] Jensen TR, Van Duyne RP, Johnson SA, Maroni VA. Surface-enhanced infrared spectroscopy: A comparison of metal island films with discrete and nondiscrete surface plasmons. Applied Spectroscopy. 2000;**54**:371-377

[9] Cheruvalath A, Nampoori VPN, Thomas S. Oblique angle deposited silver islands on $Ge_{20}Se_{70}Te_{10}$ film substrate for surface-enhanced infrared spectroscopy. Sensors and Actuators B: Chemical. 2019;**287**:225-230. DOI: 10.1016/j.snb.2019.02.045

[10] Neubrech F, Pucci A, Cornelius TW, Karim S, García-Etxarri A, Aizpurua J. Resonant plasmonic and vibrational coupling in a tailored nanoantenna for infrared detection. Physical Review Letters. 2008;**101**:157403. DOI: 10.1103/PhysRevLett.101.157403

[11] Cubukcu E, Zhang S, Park YS, Bartal G, Zhang X. Split ring resonator sensors for infrared detection of single molecular monolayers. Applied Physics Letters. 2009;**95**:043113. DOI: 10.1063/1.3194154

[12] Chae J, Lahiri B, Kohoutek J, Holland G, Lezec H, Centrone A. Metal-dielectric-metal resonators with deep subwavelength dielectric layers increase the near-field SEIRA enhancement. Optics Express. 2015;**23**:25912-25922. DOI: 10.1364/OE.23.025912

[13] Chen K, Dao TD, Nagao T. Tunable nanoantennas for surface enhanced infrared absorption spectroscopy by colloidal lithography and post-fabrication etching. Scientific Reports. 2017;**7**:44069. DOI: 10.1038/srep44069

[14] Pandey AK, Sharma AK. Advancements in grating nanostructure based plasmonic sensors in last two decades: A review. IEEE Sensors Journal.

2021;**21**:12633-12644. DOI: 10.1109/ JSEN.2020.3045292

[15] Dhibi A. A comparative study of surface plasmon resonance sensors by using doped-silicon grating structure on doped silicon and aluminum film. Physica Scripta. 2019;**94**:105602. DOI: 10.1088/1402-4896/ab2c88

[16] Li Y, Liu Y, Liu Z, Tang Q, Shi L, Chen Q, et al. Grating-assisted ultra-narrow multispectral plasmonic resonances for sensing application. Applied Physics Express. 2019;**12**:072002. DOI: 10.7567/1882-0786/ab24af

[17] Sharma AK, Pandey AK. Design and analysis of plasmonic sensor in communication band with gold grating on nitride substrate. Superlattices and Microstructures. 2019;**130**:369-376. DOI: 10.1016/j.spmi.2019.05.006

[18] Pryce IM, Kelaita YA, Aydin K, Atwate HA. Compliant metamaterials for resonantly enhanced infrared absorption spectroscopy and refractive index sensing. ACS Nano. 2011;**5**:8167-8174. DOI: 10.1021/nn202815k

[19] Bibikova O, Haas J, López-Lorente ÁI, Popov A, Kinnunen M, Ryabchikov Y, et al. Surface enhanced infrared absorption spectroscopy based on gold nanostars and spherical nanoparticles. Analytica Chimica Acta. 2017;**990**:141-149. DOI: 10.1016/j.aca.2017.07.045

[20] Kundu J, Le F, Nordlander P, Halas N. J. Surface enhanced infrared absorption (SEIRA) spectroscopy on nanoshell aggregate substrates. Chemical Physics Letters. 2008:452:115-119. DOI: 10.1016/j. cplett.2007.12.042

[21] Suzuki Y, Kita K, Matsumoto N. The square columnar model in enhancement of an electromagnetic field. Applied

Physics A Materials Science & Processing. 2003;**77**:613-617. DOI: 10.1007/s00339-003-2127-3

[22] Osawa M. Dynamic processes in electrochemical reactions studied by surface-enhanced infrared absorption spectroscopy (SEIRAS). Bulletin of the Chemical Society of Japan. 1997;**70**:2861-2880. DOI: 10.1246/bcsj.70.2861

[23] Moharam MG, Gaylord TK. Rigorous coupled-wave analysis of planar-grating diffraction. Journal of the Optical Society of America. 1981;**71**:811-818. DOI: 10.1364/JOSA.71.000811

[24] Bao S, Zheng G, Ma Y. Total absorption for an ultrathin silicon grating within the low-loss mid-infrared window. Optical Materials. 2020;**108**:110431. DOI: 10.1016/j. optmat.2020.110431

[25] Chen F, Liu X, Tian Y, Zheng Y. Mechanically stretchable metamaterial with tunable mid-infrared optical properties. Optics Express. 2021;**29**:37368. DOI: 10.1364/OE.439767

[26] Suzuki Y, Ishigo Y, Tsushima M, Nakashima H, Shimada T. Simulation of enhanced infrared absorption spectra by rigorous coupled wave analysis. Materials Research Express. 2019;**6**:1050d7. DOI: 10.1088/2053-1591/ab432e

[27] Mitobe D, Suzuki Y, Shimada T. Local enhanced site in surface enhanced infrared absorption with gold nanoparticle array by Rigorous coupled-wave analysis. Journal of Physics Communications. 2020;**4**:115009. DOI: 10.1088/2399-6528/abc9d6

[28] Liu V, Fan S. S4: A free electromagnetic solver for layered periodic structures. Computer Physics Communications. 2012;**183**:2233-2244. DOI: 10.1016/j.cpc.2012.04.026

[29] Edwards DF, Ochoa E. Infrared refractive index of silicon. Applied Optics. 1980;**19**:4130-4131. DOI: 10.1364/AO.19.004130

[30] Olmon RL, Slovick B, Johnson TW, Shelton D, Oh SH, Boreman Glenn D, et al. Optical dielectric function of gold. Physical Review B. 2012;**86**:235147. DOI: 10.1103/PhysRevB.86.235147

[31] Debbrecht B, McElhiney M, Carey V, Cullen C, Mirotznik MS, BG DL. Cavity-based aluminum nanohole arrays with tunable infrared resonances. Optics Express. 2017;**25**:24501-24511. DOI: 10.1364/OE.25.024501

[32] Aslan E, Aslan E, Turkmen M, Saracoglu OG. Metamaterial plasmonic absorber for reducing the spectral shift between near- and far-field responses in surface-enhanced spectroscopy applications. Sensors and Actuators A: Physical. 2017;**267**:60-69. DOI: 10.1016/j.sna.2017.10.006

[33] Chen K, Dao TD, Ishii S, Aono M, Nagao T. Infrared aluminum metamaterial perfect absorbers for plasmon-enhanced infrared spectroscopy. Advanced Functional Materials. 2015;**25**:6637-6643. DOI: 10.1002/adfm.201501151

[34] Dao TD, Chenab K, Nagao T. Dual-band in situ molecular spectroscopy using single-sized Al-disk perfect absorbers. Nanoscale. 2019;**11**:9508-9517. DOI: 10.1039/C9NR00904C

[35] Aslan E, Aslan E, Turkmen M, Saracoglu OG. Experimental and numerical characterization of a mid-infrared plasmonic perfect absorber for dual-band enhanced vibrational spectroscopy. Optical Materials. 2017;**73**:213-222. DOI: 10.1016/j.optmat.2017.08.023

Edited by Safaa Najah Saud Al-Humairi

This book provides a comprehensive overview of gold nanoparticles (AuNPs) and their potential optical, physical, medical, and biological uses. Chapters discuss the synthesis and characterization of AuNPs, clinical applications of AuNPs, the usage of AuNPs as microbial fuel cells, the usefulness of optical exposure to AuNPs, and more.

IntechOpen